Tissue Engineering Models of Polycystic Kidney Disease

A thesis
submitted by

Wei-Che C. Ko

In partial fulfillment of the requirements
for the degree of

Master of Science (M.S.)

in

Biomedical Engineering

TUFTS UNIVERSITY

2012 May

Adviser: David L. Kaplan, Ph.D

Abstract

Autosomal Dominant Polycystic Kidney Disease (ADPKD) is a life-threatening monogenic disorder where innumerable cysts develop in the kidney, leading to renal failure. There is no known cure, and animal studies, while beneficial, often yield mixed results when translated to the human condition. Thus, new opportunities present itself for the study of human ADPKD by utilizing tissue engineering principles of disease modeling.

However, modeling cystic diseases *in vitro* presents a unique challenge as cyst morphogenesis, in addition to complex intercellular interactions, is also governed by synergistic spatial, mechanical and temporal effects. This thesis reports the development of kidney-like tissue structures for normal and diseased (cystic) states using commercially available human kidney cells. Gene silencing is used to simulate autosomal dominant polycystic kidney disease, as inactivating mutations in polycystins -1 and/or -2 are responsible for the disease *in vivo*. Our system utilizes extracellular-matrix molecules infused in slow degrading porous silk scaffolds, which provides a 3D microenvironment for proper cell polarization (ECM), while exhibiting structural robustness and tension (silk scaffold).

Our results indicate development of cyst-like structures in a 3D environment, while also demonstrating the respective normal and altered phenotypes concurrent with normal tissue and patient-derived ADPKD tissue. The structural and functional features of kidney-like tissue structures were further characterized based on distribution of E-cadherin, N-cadherin, transport phenomena of 6-carboxyfluorescein, and cell-matrix interactions through integrin signaling. Importantly, this 3D in vitro model may be further extended via perfusion reactor

for long term studies of ADPKD or other renal cystic diseases, and may have beneficial use as a therapeutic drug screening tool.

To my parents, Chih-Ming and Hsiu-Hui, and my little sister, Cynthia - for without their unending support, this work would not have been possible.

Acknowledgements

I would like to thank my thesis adviser David Kaplan, PhD, whose support and guidance from the beginning of my graduate studies at Tufts University has both enabled and inspired me to gain a deeper appreciation for the biomedical sciences. I am also grateful to the members of my thesis committee, Ronald Perrone, MD, and Qiaobing Xu, PhD, for their support and advice in the culmination of my graduate work.

I would like to thank Balajikarthick Subramanian, PhD, with whom I worked closely over the duration of my graduate work, and his guidance in the day-to-day laboratory has played an integral role in shaping my approach to biomedical research. I would also like to thank the other members of the Genitourinary System Minigroup, Teresa DesRochers, PhD, Michael House, MD, and undergraduates Erika Parisi and Rachel Lind, for helpful discussions. I also appreciate the help from Lab 162 for help in my early molecular biology assays: Keiji Numata, PhD, Guokui Qin, PhD, and Sreevidhya Tarrakad Krishnaji.

I would also like to acknowledge my colleagues in the Biomedical Engineering Department. In particular, the Office 141 girls: Lindsay Wray, Katherine Blanton, Evangelia Bellas, and Rebecca Scholl Hayden, and the 200 Boston Ave folks: Min Tang, PhD, Ethan Golden, DVM, Lee Tien, Shannon Smith, Rodrigo Jose, Roberto Elia, Christa Margossian, Kathleen Martinick, Amanda Baryshyan, Alexander Nectow, Alexander Mitropoulos, and Andrew Reeves. Though their discussions will be appreciated, more importantly, their friendships will be treasured.

Finally, I would like to thank the administrative staff: Milva Ricci, Keleigh Sanford, Carmen Preda, PhD, Martin Hunter, PhD, Nikos

Fourligas, PhD, and Bruce Panilaitis, PhD, along with the funding agencies: NIH P41 Tissue Engineering Resource Center, Genzyme Renal Innovations Program, and Hoffman-LaRoche, as their hard work and effort has been instrumental in facilitating lab research.

Contents

List of Figures

List of Tables

Chapter 1

Introduction

In ancient history, the kidneys were esteemed organs with allegorical connotations spanning multifarious cultures and time. They held their most prominence during the Bronze and Iron Ages, when great leaders such as Rameses of Egypt and the Hittites of Mesopotamia so greatly influenced the Middle World. Ancient Egyptian mummification practices called for careful preservation of internal organs as the dead were believed to rise again in the afterlife. While the kidney's importance in Ancient Egyptian culture is hotly contested, the Egyptians were indeed aware of the anatomic existence of the kidneys, which they called "*ggt*" (1). Often, kidneys were left in the body during the mummification process along with the heart, believed to be the center of one's existence. Thus, there may be a mythological role as to why the kidney was left in the body along with the most important organ, the heart (1). In the Hebrew Bible, the kidneys were believed to represent Man's true nature, since they were situated so deeply in the body, only privy to the eyes of God. Indeed, they were used as a metaphor for the core of a person, the area of most vulnerability (2).

It was only until the Greek and Roman eras, when Hippocrates and Plato extolled the brain (3) and Galen's early surveys identified the kidneys as an excretory organ (4), that the kidney lost prominence. Modern nephrology has given scientific explanation to the kidneys and its exquisite management of fluid homeostasis, but what is relevant for colloquial language are its functions for excretion; at first glance, a relatively unimportant task, and perhaps, one that has connotations of disgust. Perhaps the pre-Grecian cultures were actually more correct when they always linked the kidney to the heart (3), as science has provided us the intricate details in the link between the cardiovascular system

and renal. While often known only for urine production, the kidney plays integral roles in not only the renal system, but also cardiovascular and endocrine physiological systems.

Kidneys are tasked with filtration of the blood, of getting rid of waste products, and maintaining proper solute concentrations in the fluid that bathes all the cells in our body. Improper solute concentrations can lead to serious consequences. For instance, hypoosmotic or hyperosmotic extracellular concentrations can lead to cell swelling or shrinkage, respectively. This can manifest as headaches when one drinks too much water after running, as the cells in the brain swell slightly and activate pain receptors. Improper solute management can also result in visible swelling, or edema, in various locations of the body, such as in the abdominal wall, or in the lungs. Sodium and potassium, two major solutes of the body, are also integral to the electrical excitability of cells, such as myocardiocytes, cells of the heart muscle. Hyperkalemia, characterized by elevated potassium levels, can lead to heart arrhythmias. After all, lethal injection is based on intravenous administration of potassium chloride, which literally stops the heart.

Diseased kidneys also fail to excrete phosphates, which lead to calcification (calcium phosphate) in various tissues including blood vessels. Hypocalcemia can result, leading to decreased bone density and decreased muscle contraction including clinical manifestations in electrocardiophysiology. Electrical instabilities can lead to *torsades de pointes* (twisting points on the electrokardiogram), a type of ventricular fibrillation. In addition, a biosynthetic step for vitamin D production is normally performed in the kidneys, and thus diseased kidneys fail to produce vitamin D. As vitamin D is required for calcium absorption, calcium levels stay low. Kidneys are also responsible for erythropoetin (EPO) synthesis, which is necessary for production of new red blood cells. EPO is a necessary supplement for renal disease patients undergoing dialysis, and it is also an illicit performance enhancing drug used by elite athletes, most popularized by the Tour de France road bicycle championship.

The kidney also plays major roles in regulating blood pressure. As mentioned previously, the kidney regulates the solute concentration in the extraceullar fluid, which includes the blood and nephric filtrate. The kidney responds to changes in blood pressure by altering its renin secretion, which is part of the renin-angiotensin-aldosterone system. When blood volume is low (low blood pres-

sure), the kidney secretes renin, which produces angiotensin I. Angiotensin I is converted to angiotensin II by angiotensin-converting-enzyme, which stimulates aldosterone secretion from the adrenal glands. Aldosterone stimulates sodium reabsorption from the nephric filtrate back into the extracellular fluid compartment, and the resulting sodium reabsorption provides the necessary solute gradient for water reabsorption from the collecting duct. The net effect is an increase in extracellular and blood volume, thus raising blood pressure. Disruption of the renin-angiotensin-aldosterone system can lead to the loss of blood pressure maintenance, with very serious cardiovascular consequences. After all, heart disease was the number one cause of death in the United States in 2006 (5).

While a failing kidney's filtration responsibilities can largely be replaced by hemodialysis, there are major hurdles involved in clinical care, and also consequences in patient quality of life. Despite the efficiency of filtration, dialysis treatment must be custom tailored by a nephrologist. As mentioned previously, EPO, along with various other hormones, must be supplemented. Blood pressure medications and careful tuning of fluid must also be considered. Lastly, hemodialysis requires treatments several times a week, for several hours per session. There are obvious losses in quality of life. Despite the shortcomings of dialysis, the only other current treatment is renal transplantation. Renal transplantation is the optimal choice, since the kidney can replace filtration effects in addition to the endocrine effects. However, the kidney market is hardly teeming with ready donors. In addition, a life of immunosuppressive therapies follows, with chance of rejection, which can also lead to other immune system complications.

Advances in tissue engineering seek to ameliorate the problems of diseased tissues through various strategies such as organogenesis, bioartificial devices, or disease modeling. In principle, it would be possible to generate a kidney, or any other organ, through careful manipulation of growth signals applied at the correct times. Of course, the right conditions are exceedingly complex, and in the case of the kidney, perhaps one of the most complex in the body.

Bioartificial devices approach the problem by replacement with extracorporeal therapies. In the case of kidney disease management, a bioartificial kidney would similarly filter blood as hemodialysis, but functional tissue would also appropriately perform endocrine functions and solute homeostasis.

1. INTRODUCTION

Disease modeling is typically characterized by growing functional tissue mimics *in vitro*. If they are adequate models of *in vivo* conditions, then it is possible to assess molecular processes, and rapidly screen therapeutic drugs. In essence, disease modeling allows the investigator to clear logistical hurdles, for example, by imaging tissues that are difficult to access in the body, or by controlling the level of complexity of the tissue model. Indeed, the goal of this thesis is model development of kidney tubules in a 3D scaffold supported environment. While the primary metrics are modeling, there is still considerable overlap with the other previously described goals of kidney engineering, as various shared techniques are utilized.

Tissue engineering seeks to replicate how tissues and organs develop, and the core of the process is to control the growth signals applied to the individual cells that make up the organ. Growth factor hormones are certainly important growth signals, but spatial orientation and environmental interactions can also provide growth signals. Biomaterial scaffolds may be engineered to control location of individual cells or may be used in conjunction with bioreactors to introduce physical processes such as shear and pressure, with net results in the upregulation and downregulation of various genes.

This thesis seeks to develop a suitable model for normal kidney tissue, and upon the establishment of a model, to also demonstrate applications in modeling diseased kidney tissue. Autosomal Dominant Polycystic Kidney Disease (ADPKD), a member of the cystic kidney disease group, was chosen for modeling, and this thesis demonstrates the utility of disease models in the study of disease processes.

Chapter 2

Background

2.1 Kidney Development and Structure

2.1.1 Renal Anatomy

The kidney is a complex organ (Figure 2.1) characterized by branching networks of epithelial tissue, akin to the branching bronchiolar ducts of the lung or the mammary glands of the breast. As a common characteristic, these particular tissues and organs interface with the external environment through a single collection point, yet must maximize surface area as the functionally important characteristics occur at the cellular level. In development, the strategy used by these epithelial organs is called branching morphogenesis. And this is exactly what the kidney does: the millions of individual nephrons interface with the vasculature, as a parallel circuit, which maximizes the filtration of blood. The nephron's fluid exits at the collecting duct (at this point it is urine), which also receives urine from other adjacent nephrons. The collecting duct descends further through the kidney ultimately converging on other collecting ducts, which then empty at the renal papilla and into one of the six or seven minor calyces. The minor calyces receive urine from other collecting duct networks, and two or three minor calyces converge into a major calyx. Finally, the two or three major calyces in a kidney empty into the renal pelvis, which connects to the urinary bladder via a ureter. Thus, the kidney can be represented as a large branching network that provides maximum opportunity to filter blood, but waste products are shuttled along a system of decreasing branches that finally converge in a single location for excretion. Though one should note, it would be more correct to say that the kidney starts from the ureter, and branches its way up towards the

individual nephrons. Branching morphogenesis is a complex process, which can be described in detail, but first, it would be prudent to start at the beginning of kidney development.

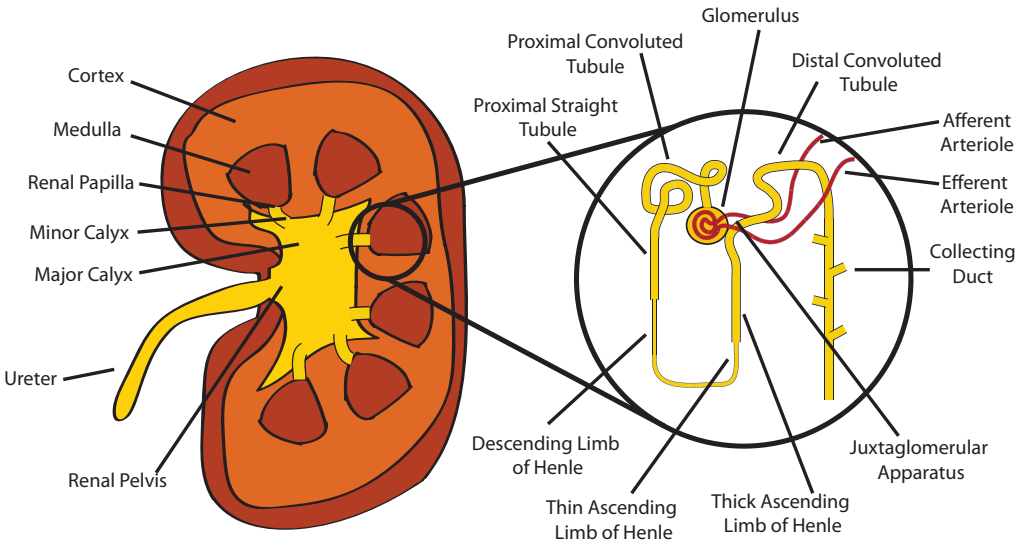

Figure 2.1: Kidney and Nephron - The kidney is composed of many parallel units of nephrons. Filtrate from blood is processed in the nephron tubules and exits as urine. Urine is shuttled to progressively larger channels in the kidney before finally exiting at the renal pelvis via the ureter.

2.1.2 Development by Induction

It is said that in development, there are three sets of kidneys: the pronephros, the mesonephros, and metanephros. The pronephros, arising at three weeks gestation, is essentially a pair of ducts extending along the mesoderm and opening into the cloaca. In humans, the pronephros does not serve excretory functions, but it is an important early structure in urinary system development. The mesonephros arises through induction from the pronephros, and at one end, the glomus and dorsal aorta pushes into the duct, forming a primitive glomerulus. At the other end, the pronephric duct becomes the mesonephric duct, also known as the Wolffian duct. In both males and females, the Wolffian duct becomes part of the bladder, while further reproductive system development extends the Wolffian duct system for males or regresses to vestigial structures for females. The mesonephros also atrophies as quickly as it develops, paving the way for metanephros development. The metanephric mesenchyme develops adjacent to the mesonephric duct, and interacts with the ureteric bud, a branch off

the mesonephric tubule. The ureteric bud (UB) and metanephric mesenchyme (MM) induce each other reciprocally in a branching tubule fashion, not unlike that of lung, vascular, or mammary gland development (6). The UB/MM interactions lead to the development of the paired kidneys and all the corresponding nephrons. At one end of the nephron, the collecting ducts correspond to the original ureteric bud, while the other renal tubules are of metanephric origin. At the other end of the nephron, the cells give rise to the glomerulus, interfacing the vasculature with the renal tubules.

Despite the elegance of the UB/MM interactions in forming the kidney, developmental defects are quite possible. In the instance of UB/MM interaction, the spatial location of both UB and MM is very important (Figure 2.2), if the cells are even slightly farther away so as to perturb intercellular communication, the mesonephric duct and metanephros will undergo apoptosis (6). Thus, the kidney may not even form, resulting in unilateral or bilateral renal agenesis. This can lead to clinical manifestations during fetal development such as the Potter sequence, which refers to the reduction of amniotic fluid secondary to lack of urine production. During gestation, the fetus continually swallows amniotic fluid and excretes urine via the metanephric kidneys, thus recycling and maintaining proper levels of amniotic fluid. In cases of kidney defects, amniotic fluid is lost, and the fetus is subject to pressure from the sac and maternal uterus, resulting in other developmental defects including organ atresias, improper lung development, and rarely, mermaid syndrome characterized by fused legs (7). The most common characteristic of Potter sequence, however, is the Potter facies characterized by parrot beak nose and a skinfold extending from the medial canthus across the cheek. Potter sequence fetuses usually result in miscarriage, and of those that are born, usually expire shortly due to pulmonary and renal failure.

The Potter sequence illustrates the importance of spatial effects, as well as temporal and mechanical effects in development, for not just the kidney, but all throughout the body. Tissue engineering seeks to study and manipulate these effects, and will be discussed further in following sections on tissue engineering.

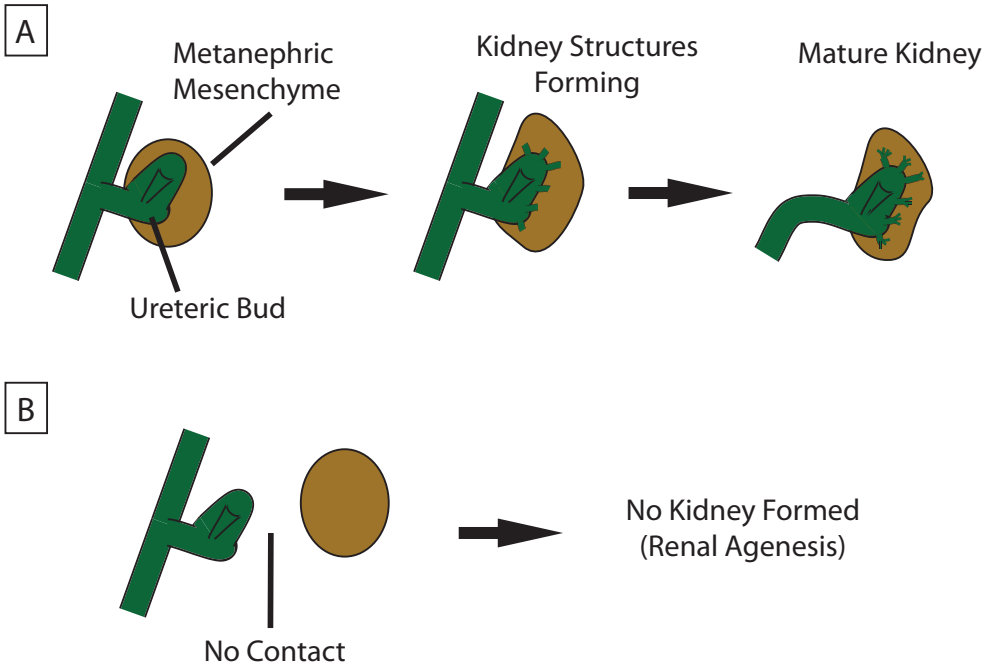

Figure 2.2: Induction in Kidney Development - **(A)** Ureteric Bud and Metanephric Mesenchyme induce each other in kidney development. **(B)** Aberrant signaling, such as that caused by spatial effects, lead to loss of induction and therefore, loss of kidney.

2.2 Kidney Physiology

2.2.1 Renal Vasculature and Filtration Membrane

The renal artery (one for each kidney) branches off from the aorta and enters the kidney at the hilus. Here, the renal artery branches into several segmental arteries, which branch several times further until forming the afferent arterioles. Each afferent arteriole ends in the glomerulus, a specialized capillary tuft that serves as the interface between the vascular system and the urinary system, and exits as an efferent arteriole. The efferent arteriole branches into capillaries that parallel the nephron's tubular segments, primarily to provide nutrients, and also plays an important role in urine concentration. The capillary ends drain into stellate veins, which anastomose several times with other veins, forming the renal vein at the kidney hilus and draining into the inferior vena cava. In net, the renal vasculature may be visualized as a parallel circuit, which in principle could independently modulate resistance (by vessel constriction or relaxation) across unique nephrons (Figure 2.3).

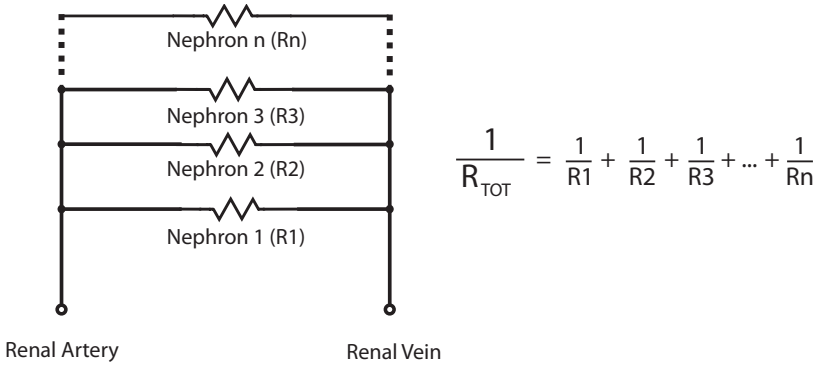

Figure 2.3: Kidney as a Parallel Circuit - The kidney vasculature may be represented as a parallel circuit. The renal artery enters the kidney and branches into progressively smaller vessels before ending at unique nephrons. The reverse occurs after the nephron, where vessels converge on progressively larger vessels before exiting the kidney as the renal vein. This strategy follows the same physics as parallel circuits, where total resistance decreases for each additional nephron

The glomerulus comprises several layers including specialized capillary endothelium, basement membrane, and podocytes. As blood flows through the glomerulus, the blood substances begin to equilibrate with the fluid in Bowman's space, on the opposite side of the barrier. Bowman's space and the glomerulus are enclosed by an epithelial structure, Bowman's capsule, and together form

the renal corpuscle. The fluid in Bowman's space is called filtrate, which after undergoing processing in the renal tubules, becomes urine. But why does urine not appear blood red if the blood and filtrate are equilibrating at the renal corpuscle? The answer lies in the fact that the glomerulus acts as a selectively permeable membrane. The fenestrated pores of the capillary endothelium, basement membrane, and the slit diaphragms of the podocytes act in concert to restrict the flow of bulky proteins across the membrane. Therefore the protein hemoglobin, which gives blood its red color, cannot pass into the filtrate. However, the molecule bilirubin, a breakdown product of hemoglobin, does pass into the filtrate and gives urine its distinct yellow color. Generally, small molecules can pass through uninhibited, so one can expect the filtrate in Bowman's space and blood to have similar concentrations of glucose, sodium, potassium, and other small solutes. The fluid component of blood will also pass through the membrane, and this can be roughly modeled by Starling's Equation:

$$J = P_c - P_i + \sigma(\pi_i - \pi_c)$$

- J is the net fluid movement between the capillary and Bowman's space
- P_c is capillary hydrostatic pressure
- P_i is Bowman's space hydrostatic pressure
- π_i is Bowman's space oncotic pressure
- π_c is capillary oncotic pressure
- σ is the reflection coefficient

Positive J indicates flow of fluid from the capillary into Bowman's space. Conversely, negative J indicates fluid flow from Bowman's space into the capillary. The hydrostatic pressures oppose each other, as do oncotic pressures driven by solute concentrations. The reflection coefficient has a value close to 1 in the glomerulus since the glomerular membrane normally restricts proteins movement, thus retaining the full osmotic effect of protein as a solute. The collective flux of all nephrons over a quantity of time is known as the Glomerular Filtration Rate, a metric for healthy renal function. Kidney diseases can reduce the collective glomerular filtration rate to pathological levels, thus precipitating the need for dialysis or kidney transplantation.

2.2.2 Filtrate Processing and the Production of Urine

Nephric filtrate proceeds from Bowman's space into the proximal tubules. The proximal tubules reabsorb a majority of the sodium in the filtrate by action of Na^+,K^+ ATPase, pumping sodium from the lumen of the tubule across and through the basement membrane. On the basolateral side, the peritubular capillaries carry away the solutes (and water that follows the osmotic gradient). 100% of glucose is also reabsorbed in the proximal tubules by the action of sodium-linked glucose transporters. However, if glucose concentrations in the blood, and thus nephric filtrate, exceed a threshold level, glucose may appear in the urine (glycosuria). While there are other causes to glycosuria, the most common occurrence is due to untreated diabetes mellitus.

Following the proximal tubules, filtrate passes into the loop of Henle, where a combination of sodium-potassium pumps, unique permeability characteristics, and countercurrent flow establish a gradient of increasing solute concentrations ranging from 300mOsm to 1200mOsm. This concentration gradient provides the potential for water reabsorption, and thus urine concentration, in the collecting ducts.

The next stop is the distal tubule, which does the fine-tuning for salt, potassium, calcium, and pH regulation. The distal tubule is sensitive to aldosterone, which controls sodium reabsorption and potassium secretion. The distal tubule also reabsorbs calcium in response to parathyroid hormone. Additionally, the distal tubule contacts the efferent arteriole at the juxtaglomerular apparatus and plays an endocrine role in regulating the cardiovascular system by the renin-angiotensin system.

After the distal tubule, filtrate travels into the collecting duct. The collecting duct, like the distal tubule, also reabsorbs sodium and secretes potassium in response to aldosterone. Similarly, acid-base homeostasis also occurs in response to acidosis and alkalosis. However, urine concentration is unique to the collecting duct. Antidiuretic hormone, also known as arginine vasopressin, is released from the posterior pituitary gland in the brain in response to increased plasma osmolality, or decreased plasma volume. Antidiuretic hormone's action on the collecting duct involves insertion of more aquaporins in the cell membrane, which allow the facilitated diffusion of water according to solute gradients. Recall that the loop of Henle has established a solute gradient of 300mOsm to 1200mOsm,

and aquaporins allow the flow of water out of the lumen of the collecting duct according to osmotic pressure, thus resulting in concentrated urine. After the collecting duct, the filtrate is otherwise urine, as there is no more processing that occurs. The urine travels to the renal papilla, into the calyces, renal pelvis, ureter, and finally into the bladder.

2.2.3 Antidiuresis in Detail

The apical insertion of aquaporin-2, the aquaporin relevant to collecting duct, begins with G protein coupled receptor activation of adenylate cyclase via arginine vasopressin receptor binding. Adenylate cyclase converts ATP to cyclic AMP (cAMP), which then activates protein kinase A (PKA). By an unknown mechanism, protein kinase A phosphorylates intracellular vesicles containing aquaporin-2, which then move along microtubules and actin filaments for insertion into the apical membrane (8).

Of note is that these messenger systems, cAMP and PKA, are very broad and utilized by many other cell processes, so disruption can have many unpredictable effects. For example, disturbed cAMP signaling is involved in certain cancers (9, 10). Thus, in the antidiuresis system, the cell's intracellular levels of cAMP are perfectly balanced so as to prevent adverse effects.

Of particular interest is the cystic fibrosis transmembrane conductance regulator (CFTR), the gene product which if mutated, is responsible for cystic fibrosis. CFTR transports chloride ions across cell membranes, which has an osmotic effect. CFTR is also dependent on cAMP stimulation (11). This may have relevance in the pathophysiology of Polycystic Kidney Disease (12), which will be discussed further in the PKD section.

2.3 Tissue Engineering

Tissue engineering is a multidisciplinary field that melds biology, medicine, and core engineering principles. Tissue engineering seeks to improve health and quality of life in the population by restoring tissue and organ functions. Tissue constructs may be grown artificially either in the patient or in the laboratory and subsequently transplanted. For example, artificial skin has not only been produced in the lab (13) but successfully used in surgery (14). This early tissue

construct was designed to satisfy several requirements of skin, including elasticity, moisture permeability, and as a physical barrier to bacterial entry. In recent years, more advanced tissues are undergoing extensive research as well, such as artery regeneration (15), or regeneration of the submucosal intestinal layer that is not only physiologically appropriate (16) but can also function *in vivo* (17). But perhaps the most sensational story was the human ear grown on the back of a mouse (18). Of course, it was not actually a functional ear for hearing use; the auditory components of the ear are far more complex. In actuality, cartilage precursors were seeded into a biodegradable polymer scaffold shaped like an ear. But it is still a complex problem, as tissue engineers must consider the cell type and the physical environment in which the tissue construct lies. While perhaps disappointing to some hoping to avoid hearing loss, this experiment still has excellent applications in plastic surgery, and of course, offers the tantalizing suggestion that one day, a functional ear or any other organ may be effectively recreated in the laboratory.

Tissue engineering also encompasses diagnostic applications, including imaging, toxicology, drug metabolism and therapeutic drug effects. Tissue constructs may also be used in non-clinical study of basic biological processes. For example, the lung on a chip (19), which involves cells of the alveolar-capillary interface, allows for imaging, toxicology, and study of lung physical phenomena. Importantly, the tissue must be representative of the physiological system, i.e. structurally and/or functionally. In order to achieve this, cells and tissue must be in the appropriate microenvironment, analogous to developmental biological processes.

2.3.1 The Cell and its Environment

Traditional cell culture is performed on flat plastic dishes or flat culture flasks, and is still in heavy use today. Cells are typically propagated on these flat surfaces for convenience, and many experiments are performed as well. For instance, cells extracted from a kidney or any other organ can be grown on tissue culture plates. While the cells are certainly relevant, and much scientific data can be gleaned, the investigator must also consider that the system is not entirely realistic. Cells cultured on 2D plastic do not recapitulate the *in vivo* microenvironment, and often do not express the same *in vivo* structural and

functional phenotype. After all, the human body is not a two-dimensional flat surface, but rather, three-dimensional.

Early efforts to address the problems of 2D cell culture led to the emergence of 3D cell culture models, where cells are cultured in ECM gels in order to improve expression of differentiated phenotypes and tissue organization (20). 3D gel cultures with reconstituted basement membrane were used extensively in the study of breast cancer tumorigenesis and metastatic invasion (21). The models also appear to be phenotypically relevant, as well-polarized glandular structure formed for normal cells, while transformed cells isolated from tumors exhibited cancer-like properties (22). It was also shown in the breast cancer model that known cancer signaling cascades, modulated by epidermal growth factor receptor, is only apparent in 3D culture and not 2D (23). In fact, stiffening the extracellular matrix, as *in vivo* tumors are observed to have stiff surrounding stroma, can promote neoplastic transformation of breast epithelial cells (24).

3D gel culture has been extended to Madin Darby Canine Kidney (MDCK) epithelial cells in cell morphogenesis experiments. On 2D tissue culture plate, MDCK appear as a sheet with cobblestone morphology, but in collagen gel, MDCK spontaneously form spherical cysts with lumens (25). By addition of hepatocyte growth factor, a major soluble factor secreted by fibroblasts, branching morphogenesis is observed (26). Other similar epithelial tissues that involve branching morphogenesis, such as lung alveoli or thyroid follicles are also easily cultured in 3D gel systems (25). Other groups have shown the viability of 3D culture of muscle (27) and neurons (28). By careful design of the 3D cell microenvironment, it is possible to direct better cell morphogenesis and also support proper cell phenotypes that are not seen in 2D cell culture.

Three-dimensional biomaterial scaffolds are also an integral part of tissue engineering, used in mimicking cellular microenvironments. Biomaterial scaffolds can be engineered to form the proper structure for induction of tissue formation (29), or they can encapsulate growth factors for controlled release to cells (30). A few examples of biomaterials used for scaffolding include: poly(lactic co-glycolic acid), polycaprolactone, hyaluronic acid, and silk fibroin (31, 32). These biomaterials may also be fit to different applications including films, fibers, hydrogels, or porous sponges. Common among biomaterials are their minimal immunogenicity and non-toxic properties. In the body, they pose minimal safety risks

as they are broken down to their constituent peptides or metabolites and subsequently excreted by physiological processes (33). Advancements in biomaterials include surface modifications such as RGD (arginine-glycine-aspartic acid) coupling to promote cell attachment, spreading, and differentiation (34).

2.3.2 Next generation Tissue Engineering

The evolution of tissue engineering is progressing at a rapid pace. Microfabrication techniques have paved the way for design of better shapes and structures, on the micrometer scale; these structures can better position cells and tissues for controlled morphology and function (35). In addition to using relevant cell types, ECM analogues, and biomaterial scaffolds, it is possible to also control physicochemical forces. Microfluidic cell-culture systems, by virtue of possessing small channels, have only laminar fluid flow, which is physiologically relevant. Gradients of membrane permeable chemicals can be applied at the single cell level in these laminar stream systems (36). It is also possible to integrate probes for visualization and quantitative analysis of relevant data such as cell structure, gene expression, and mechanical response (37).

Bioreactors can support control of mechanical forces in cell culture systems, such as stretch or compression for inducing tissue formation (38). Bioreactors can also be in used to improve nutrient delivery by overcoming mass transfer limitations. As tissue constructs must be of certain size (millimeter scale) for biomedical applications such as engraftment, mass transfer limitations must be addressed. Common bioreactors include spinner-flask reactors, where convective mixing reduces the concentration effect at the tissue surface; hollow fiber reactors, where media is perfused on the exterior surface of hollow tubes containing cells; and perfusion reactors where media is perfused directly through cell-seeded pores in a scaffold (39). Otherwise, mass transfer limitations lead to cell death in the inner core of the tissue construct, while cells on the surface thrive. Bioreactors that improve nutrient delivery can, in principle, sustain tissue constructs indefinitely.

2.3.3 Kidney Tissue Engineering

Early forays into kidney tissue engineering aimed to enhance life-saving dialysis measures. Extracorporeal therapies were designed to not only filter blood, but

2D Models	**3D Gel Systems**	**Tissue Engineered Systems**
Limited intercellular interactions	Better intercellular interactions	Better intercellular interactions
Altered morphology	*In vivo* like morphology	*In vivo* like morphology
Altered function	Limited function (fluid flow induced function not present)	Realistic functions of tissue
Limited time periods of culture (days to weeks)	Limited time periods of culture (days to weeks)	Sustainable cultures for long time frames (months)
No solute concentration gradient	Altered solute concentration gradient	Realistic solute concentration gradients by co-culture
No fluid flow induced stress	No fluid flow induced stress	Fluid flow induced stress

Table 2.1: Advantages of Tissue Engineered Systems

also provide endocrine functions such as vitamin D biosynthesis and production of renin and angiotensin (40). Further development on extracorporeal therapies led to the Renal Tubule Cell Assist Device, a hemofiltration cartridge lined with human kidney cells that filters blood and provides metabolic and endocrine functions (41).

Kidney tissue engineering has also seen advancements in *in vitro* diagnostics. Inspired by lab on a chip designs, Jang et al (42) designed a microfluidic device for the culture of mouse inner medullary collecting duct (IMCD) cells. IMCD cells are cultured in a flat channel where media contacts the basolateral surface and fluid is perfused on the apical surface in order to simulate in vivo fluidic shear stresses (Figure 2.4). They utilized this system to investigate aquaporin trafficking and cytoskeletal reorganization in response to shear stress (43). While IMCD cells are not cultured in a 3D tube simulating a duct, nevertheless, these early forays into kidney-on-chip designs hold great promise for assessing transport properties and other fluid flow phenomena.

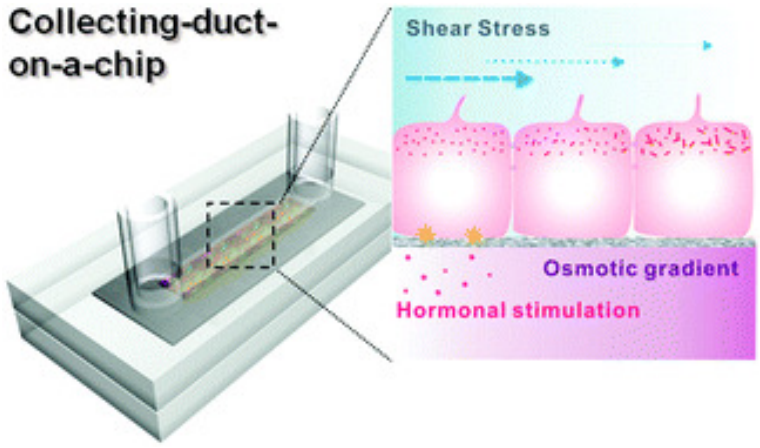

Figure 2.4: Collecting Duct on a Chip Design - A microfluidic device designed to assess the effect of fluid flow on mouse collecting duct cells. -*Jang et al,* ***Lab Chip*** *2010,* ***10****:36-42*

2.4 Modeling Cystic Kidney Diseases

Tisue engineered 3D tissue models provide valuable insights into disease progression. Cystic kidney disease group includes genetic diseases such as Autosomal Dominant Polycystic Kidney Disease (ADPKD), Autosomal Recessive Polycystic Kidney Disease (ARPKD), Medullary Cystic Kidney Disease (MCKD), and Nephronophthisis (NPH). Kidney cysts may also be associated with systemic diseases such as Von Hippel-Lindau and Tuberous Sclerosis, or acquired congenitally such as Medullary Sponge Kidney. In our tissue-engineered system, we chose to model the genetic disease ADPKD by perturbing the relevant gene involved and culturing the modified cells in a 3D microenvironment. As ARPKD, MCKD, and NPH are also monogenic disorders, in principle it would be straightforward to extend the tissue-engineered system to the study of these genetic diseases as well.

2.4.1 ADPKD Genetics

ADPKD is a genetic disease afflicting several hundred thousand people in the US alone. It is the most common monogenic kidney disorder. It is classified by inactivating mutations in *PKD1* or *PKD2*, the genes encoding the proteins polycystin-1 (PKD1) and polycystin-2 (PKD2) respectively (44). The resulting phenotype exhibits innumerable fluid-filled cysts throughout the kidney, which enlarge the kidney and can weigh up to 20 pounds in comparison to a normal

kidney weighing only a few pounds. The fluid filled cysts eventually collapse the renal parenchyma, inevitably leading to end stage renal disease.

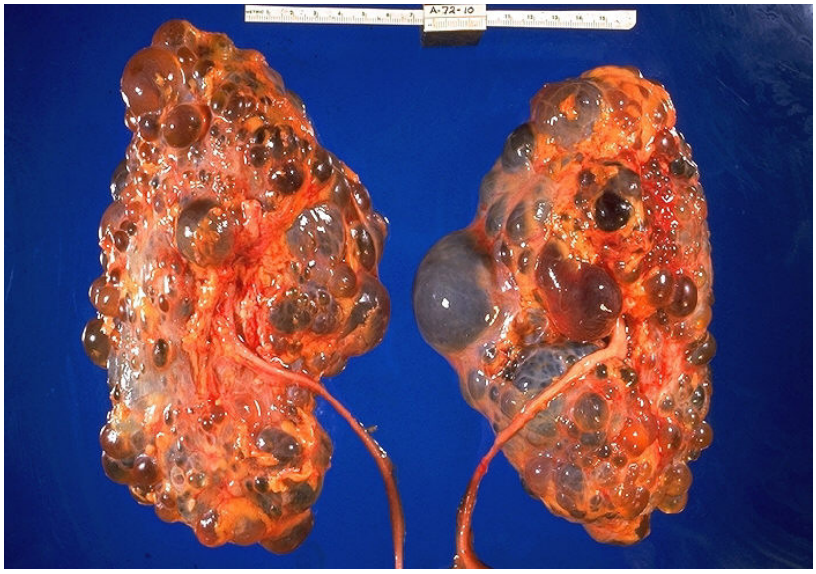

Figure 2.5: Gross pathology of polycystic kidneys - Both kidneys are greatly enlarged and show many fluid-filled cysts. *Figure credit Dr. Edwin P. Ewing, Jr. Public Health Image Library, Centers for Disease Control and Prevention, USA.*

PKD1 is mapped to the short arm of chromosome 16, specifically 16p13.3 (45). *PKD2* is mapped to the long arm of chromosome 4 at 4q22.1 (46).

Gene	Locus	Coding Sequence Length
PKD1	16p13.3	14138 bp
PKD2	4q22.1	5056 bp

Table 2.2: *PKD1* and *PKD2* Gene Summary - Overview of polycystin genes.

ADPKD is fully penetrant, which means that all individuals who inherit a mutated *PKD* gene will develop renal cysts. However, the severity of disease and age of onset of ESRD is quite variable, even among the same family (47). The variability of *PKD1* mutations is also quite large; deletions, insertions, missense and nonsense mutations have been observed (48). On the other hand, *PKD2* mutations are largely truncating mutations that would presumably lead to inactive PKD2 protein (49).

Interestingly, ADPKD is a focal disease. Despite carrying germline *PKD* mutations inherited from a parent, only a few renal cells actually develop into cysts. A two-hit hypothesis has been suggested for the explanation of the focal

behavior of ADPKD (50). The first hit is the mutated *PKD* gene that is passed down to offspring, who now possesses one wild type allele and one mutant allele. The second hit is a somatic inactivating mutation to the wild type allele, which then initiates cystogenesis. Since somatic mutations are relatively infrequent, this model conveniently explains the focal nature of ADPKD cysts. In addition, renal cysts are clonal, which suggests that the cyst develops from a single mutated cell that then proliferates and enlarges (50).

In addition to the two-hit hypothesis, haploinsufficiency may also play a role in cystogenesis. It was shown that some cysts possessed trans-heterozygous mutations with a germline *PKD1* mutation and a somatic *PKD2* mutation (51). Similarly, other cysts possessed germline *PKD2* mutations and somatic *PKD1* mutations (52).

2.4.2 ADPKD Polycystin Function

Polycystin-1 is an 11 transmembrane protein with a large extracellular N-terminal domain that is involved in cell-cell and cell-matrix interactions (53). Polycystin-1 was shown to localize to epithelial cell-cell contacts and is directly involved in intercellular adhesion (54). Polycystin-2 is a 6 transmembrane protein with intracellular N-terminal and C-terminal domains and also acts as a calcium ion channel (55). Polycystin-1 and -2 require each other for translocation and co-assembly at the plasma membrane (56). In particular, the coiled-coil motif of polycystin-1 interacts with the carboxy-terminal domain of polycystin-2 (57).

Polycystin-1 is also shown to undergo cleavage in both N- and C- terminal domains. N-terminal cleavage occurs at the G protein coupled receptor proteolytic site (GPS), which is necessary for cell survival (58); many ADPKD mutations abrogate C-terminal cleavage, PKD1-PKD2 binding, and subsequent activation of JAK-STAT signaling in cell cycle regulation (59). Two types of cytoplasmic C-terminal cleavages occur for polycystin-1. One cleavage results in a 35 kDa portion that accumulates in the nucleus (60), while another cleavage results in a 15 kDa portion that activates STAT6 transcription factor and p100 (61). Both arise in response to cessation of fluid flow, and interestingly, there is an elevation in STAT6, p100, and C-terminus tail in ADPKD cysts (61). The C-terminal cleavage also requires the presence of functional PKD2, or more specifically the calcium channel response associated with PKD2 (62). However, loss of PKD2 results in ADPKD, and it appears paradoxical that despite the loss of PKD2

and its role in mediating PKD1 C-terminal cleavage, there is still an increase in C-terminal tail in cysts. The mechanisms of ADPKD are still poorly understood and are an area of intensive research.

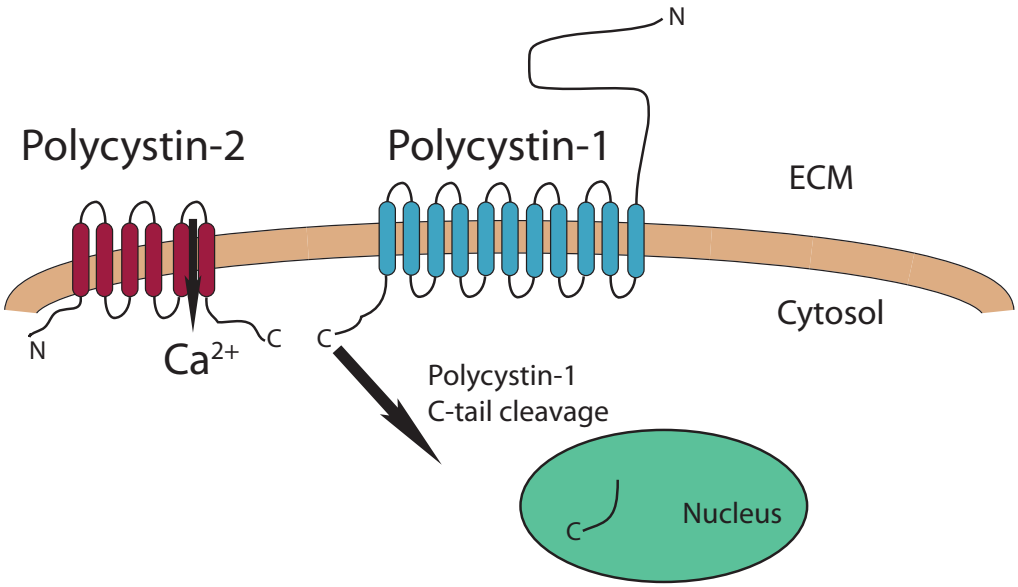

Figure 2.6: Polycystin-1 and -2 in the Membrane - Polycystin-1 and -2 interact with each other. Polycystin-1 is involved in cell-cell and cell-ECM interactions, while polycystin-2 functions as a selectively permeable Ca^{2+} channel. The C-terminal tail of polycystin-1 can be cleaved in the presence of polycystin-2, and the C-terminal tail translocates to the nucleus to initiate gene transcription.

2.4.3 ADPKD Signaling Pathways

The polycystins are also localized to the primary cilium (63, 64), a slender projection extending out from the apical surface of the cell. The primary cilium is typically a sensory organelle, and in the case of the kidney, the primary cilium transduces fluid shear stress into an intracellular Ca^{2+} response (65). This response is important in tissue morphogenesis and regulates lumen diameter in the vasculature (66). Polycystin-1 deficient cells still retain the ability to conduct Ca^{2+}, but lose the ability to sense fluid flow (67). Thus, it is possible that in ADPKD, damaged cilia continuously signal for high fluid flow rates, driving lumen expansion in order to accommodate the apparent increase in flow rate (67).

Several signaling pathways are also mediated by the polycystins including canonical and non-canonical Wnt signaling, mTOR pathway, JAK-STAT and

Id2, and G protein activation (68, 69). In the canonical Wnt pathway, polycystin-1 C-terminus tail normally inhibits β-catenin, thus preventing its transcriptional activity (70). Disruption in non-canonical Wnt pathway results in abnormalities in oriented cell division, and the elongation of renal tubules depends on the orientation of cells along the tubule axis (71). A related report shows that inversin, which modulates the non-canonical Wnt pathway, is disrupted in the cystic kidney disease nephronophthisis (72). Primary cilia are required for the maintenance of planar cell polarity (PCP), which is necessary for proper oriented cell division. However, cilia are disrupted by PKD mutations (68).

Normal polycystin-1 and -2 also activate STAT1 through JAK2, which induces p21 for cell cycle growth arrest (59). In parallel, polycystin-2 sequesters Id2, thus preventing p21 repression by Id2 (73). It appears that Id2 also plays roles in proliferation and epithelial-mesenchymal transition (EMT) through transforming growth factor-β (74). Further evidence of EMT is noted in ADPKD patient-derived cells. The PKD1/PKD2/E-cadherin/β-catenin complex is disrupted, membrane E-cadherin is depleted, and consequently, mesenchymal-associated N-cadherin is upregulated to stabilize β-catenin (75).

Polycystin-1 and -2 are also involved in G protein signaling, with activation of ERK and JNK pathways coalescing in AP-1 transcriptional activation, which plays roles in proliferation, differentiation, and survival (76). The JNK pathway, as shown in *Drosophila*, plays roles in planar polarity (77) and epithelial adhesion (78). Thus polycystin mutations could also affect planar cell polarity and epithelial dedifferentiation through aberrant G protein signaling.

Mammalian target of rapamycin (mTOR) is also linked to the polycystin signaling pathway. mTOR is regulated by *TSC2*, the gene involved in tuberous sclerosis. *PKD1* and *TSC2* are related as they are localized next to each other on chromosome 16p13.3 (53). In addition, polycystin-1 requires tuberin, the gene product of *TSC2*, to localize to the plasma membrane (79), while tuberin is stabilized at the membrane by polycystin-1 (80). As polycystin-1 and tuberin require each other for membrane localization and stability, the loss of one or the other activates the mTOR pathway and drives cyst expansion. Indeed, inhibition of mTOR reverses cystogenesis (81). mTOR is only one of many corrupted signaling pathways in ADPKD. The other signaling pathways described are all disrupted upon loss of PKD1 or PKD2, and it is thought that cystogenesis occurs due to misregulation of these signaling pathways.

Signaling Molecule	Effect on Signaling Pathway	Global Effect
Activated β-catenin	Activated Wnt pathway	Gene expression
Aberrant primary cilia	Disrupted non-canonical Wnt pathway	Loss of planar cell polarity
Loss of JAK-STAT	Activated p21	Cell proliferation
Activated Id2	Activated p21	Cell proliferation and EMT
Altered G proteins	Loss of AP-1 activation and JNK pathway	Loss of epithelial adhesion
Loss of tuberin	Activated mTOR pathway	Cyst expansion

Table 2.3: ADPKD Signaling Pathways - Altered pathways upon the loss of Polycystin-1 and/or Polycystin-2.

2.4.4 ADPKD Proliferation and Cyst Expansion

Due to the aberrant signaling pathways, there is net cell proliferation. Indeed, ADPKD cyst derived cells are associated with increased proliferation (82, 83). However, the role of polycystins and its effects on cell cycle regulation are still unclear. It was also shown that *Pkd1* inactivation of both alleles in developing mouse kidney resulted in extensive cystogenesis (84), but *Pkd1* inactivation of both alleles in mature mouse kidney resulted only in few focal cysts (85). It is not merely a switch in *PKD1* expression that drives cystogenesis, but also other gene expression occurring at different stages of development. Indeed, postnatal kidneys are still undergoing tubule elongation and maturation with very active cell proliferation (84). It is still unclear what exactly triggers the rapid cyst expansion in adult kidneys.

Cyclic adenosine monophosphate (cAMP) is elevated in ADPKD cyst derived cells (Hanaoka 2000). cAMP drives cell proliferation in cyst derived cells through the ERK signaling pathway (86). cAMP was shown to drive proliferation in *in vitro* cell cultures of cyst derived cells, but had no proliferative effect on normal cells (87). It is thought that cAMP drives fluid secretion into the lumen by activating the cystic fibrosis transmembrane receptor (CFTR) (88). The probable mechanism involves CFTR conducting chloride ions into the lumen, which drives net fluid movement into the lumen. This expands the cyst both by

engorgement with fluid and also drives cell proliferation due to the hydrostatic force exerted on the apical surface of the cyst. Antidiuretic hormone, also known as arginine vasopressin, stimulates cAMP production. In ADPKD kidneys, antidiuretic hormone elevates cAMP, driving cystogenesis, and in animal models, blocking antidiuretic hormone ameliorates the disease (89).

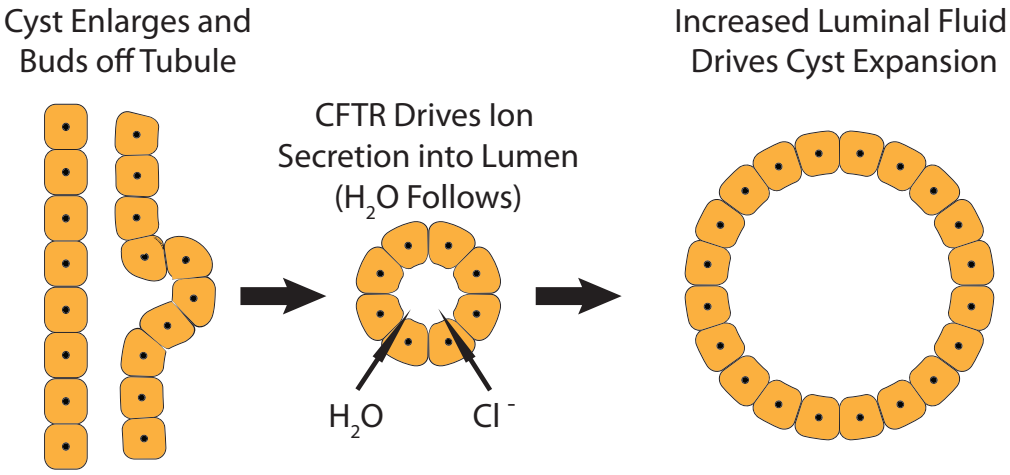

Figure 2.7: cAMP and CFTR Drives Cyst Expansion - ADPKD cyst buds off a dilating tubule into the interstitial space in the kidney. Cyclic AMP is upregulated in ADPKD, which drives the cystic fibrosis transmembrane receptor. This conducts chloride ions into the lumen, which generates a solute gradient for fluid movement into the lumen. Increased fluid in the lumen drives cyst expansion.

ECM mediated effects may also drive cystogenesis, as polycystin-1 is important in cell-cell and cell-ECM signaling. In ADPKD, β-4-integrin receptor and laminin 5 ECM ligand are aberrantly expressed (90). When cultured *in vitro*, ADPKD cyst derived cells are stimulated by exogenous laminin-5, while inhibited by blocking of endogenous laminin-5 (91). Indeed, PKD1 and PKD2 interact to regulate ECM secretion and assembly, and the altered matrix may play a role in ADPKD (92). The ECM exerts its effects through the integrin receptors, in a signaling cascade called integrin signaling that ultimately regulates proliferation, survival, and cytoskeletal rearrangements (93).

2.4.5 Genotype-Phenotype and Clinical Manifestations of ADPKD

While mutations in *PKD1* or *PKD2* both lead to the ADPKD phenotype, genetic analysis shows that patients with *PKD1* mutations reach end-stage renal disease 20 years earlier, on average, than patients with *PKD2* mutations (94). A cyst

interferes with urine flow since the cyst is formed by separating from its tubular origin. This impediment is amplified if the cyst occurs further down the branching collecting system, such as the medullary nephrons, as a solitary medullary cyst would impede the urine flow from several upstream cortical nephrons. For a sense of magnitude, a 400μM cyst in the cortex would block 32 adjacent tubules, while a cyst of the same size blocking inner medulla collecting ducts could potentially impede urine flow from ∼16,800 upstream tubules (95). In addition, as cysts expand, compression of the renal parenchyma occurs, reducing overall blood flow and urine formation. Thus, cyst expansion and total number of cysts is responsible for renal failure, and *PKD1* mutations are correlated to both greater number and larger cysts than *PKD2* mutations (96).

As cyst volume expands, the total size of the kidney also enlarges as a function of cyst number and volume. The CRISP cohort study was established to track disease progression by total kidney enlargement along with cyst enlargement measured by magnetic resonance imaging (97). Indeed, total kidney and cyst volumes increase in most ADPKD patients, and larger kidneys are associated with decline in kidney function (98). Interestingly, the rate of cyst growth is relatively consistent; the growth rate may be modeled by exponential growth. From JJ Grantham's model (99), individual cyst volume ($V_i(t)$) may be modeled by:

$$V_i(t) = V_0 U(t_i) e^{k(t-t_i)}$$

and the total cyst volume (TCV) as the sum:

$$TCV = \sum_{i=1}^{n} V_0 U(t_i) e^{k(t-t_i)}$$

where:

- t_i is the time of initiation for cyst i
- U is the unit step function $U(t) = 0$ if $t<0$, $U(t) = 1$ if $t\geq 0$
- k is constant growth rate of total cysts

Finally, Total Kidney Volume $(TKV) = TCV + NCV$, where NCV is non-cyst volume comprising normal renal parenchyma, not expected to expand. For validation, both individual cyst growth and total cyst volume match the CRISP cohort data (99).

Importantly, this model also corroborates the observation that despite a larger average annual increase in kidney volume for patients with *PKD1* mutations than those with *PKD2* mutations (74.9ml vs 32ml respectively), the rate of change is similar (∼5%) (96, 99). This suggests that *PKD1* mutations do not trigger a more severe phenotype such as faster proliferation or increased inflammation and fibrosis than *PKD2* mutations, but rather, patients with *PKD1* mutations have earlier cyst formation.

It is unclear what drives the initiation of cyst formation, but recent data suggests a role for gene dosage and incomplete penetrance (100). Typically, a mutant *PKD1* or *PKD2* allele exists along with a normal allele, and cystic phenotype occurs upon somatic mutation of the normal allele, accordingly named the two-hit hypothesis (101, 102). In less typical cases, often associated with consanguinity, homozygous mutant alleles, or mutant alleles in trans with inactivating mutations can result in early onset disease or in utero onset (100). It is suggested that the disease phenotype results from a below-threshold level of functional protein. Thus, gene dosage appears to be important, and cyst formation occurs when somatic mutations cause functional protein levels to fall below a critical level.

Germline *PKD1* with somatic *PKD2* mutations, as well as germline *PKD2* with somatic *PKD1* mutations, have also been documented in a small subset of cysts (∼10%) from ADPKD patients (51, 52). Gene dosage may also play a critical role in these cases of cystogenesis in trans-heterozygotes. As PKD1 and PKD2 are known to interact and function as a complex (57), it is likely that mutant PKD1 complexed with wild type PKD2, as well as wild type PKD1 complexed with mutant PKD2 lead to compromised function of the polycystin complex. In the case of trans-heterozygotes, the model speculated by *Koptides et al* provide for structures derived from permutations of wild type and mutant alleles (51). In addition, mutant proteins of the complex possibly exert a dominant negative effect on the wild type proteins of the same polycystin complex. Thus, there are only few complexes comprising only wild type polycystins; presumably, these few wild type polycystin complexes are below threshold level for normal renal tubular development and instead initiate cystogenesis. Indeed, mouse models for trans-heterozygous inactivation of *PKD1* and *PKD2* may help elucidate the mechanisms of gene dosing (103). It is speculated that the threshold is modified by hypomorphic alleles in either gene, as reduced dosage in conjunction with a

mutation resulting in reduced dosage in the corresponding partner polycystin protein initiates cyst formation.

While hypomorphic or loss of PKD1 or PKD2 both result in ADPKD phenotype, cyst formation tends to occur earlier for *PKD1* mutants. It is likely that this results from the fact that *PKD1* is more easily mutated than *PKD2*. Indeed, the coding region of *PKD1* is much larger than that of *PKD2*, at 12.9 kb compared to 3 kb, and in addition, the *PKD1* region is rich in CpG nucleotides which are prone to mutation (48). Cytosine nucleobases are often methylated in somatic tissues for the regulation of gene transcription, but spontaneous deamination can occur by attack of H_2O; the more stable keto form of the resulting tautomer is the same structure as another nucleobase, thymine. While the cell has mechanisms for mutation repair, sometimes mutations escape correction. If a mutation on *PKD1* or *PKD2* alleles result in a missense mutation at a conserved amino acid residue, protein function could be adversely affected.

While truncating or frameshift mutations abrogate protein function and intuitively suggest disease presentation, in-frame missense mutations are far less clear. For missense mutations, the polycystins may still be translated, but with potential alterations in signaling, membrane translocation, endoplasmic reticulum and golgi processing, or other various effects. Clinical data suggest that mutations located closer to the 5' region of *PKD1* result in more severe clinical manifestations than those closer to the 3' region (104). 5' mutations would indicate protein errors towards the N-terminal tail, which are the domains responsible for ECM and cell-cell interactions. In addition, patients with 5' mutations are also more prone to intracranial aneurysms and hemorrhage and other vascular events (105). Particularly, the 5225delAG mutation was identified in three pedigrees (105), along with previous identification in two families with aneurysms (106). Importantly, the 5225delAG mutation is a mutation occurring between the N-terminus and the Receptor-Egg-Jelly (REJ) region of PKD1, and it is suggested that mutations to this region of the gene corresponding to extracellular portion of the protein, rather than specific mutations, are responsible for the more severe phenotype.

However, correlation of mutation location to phenotype is complicated by mutations that still result in partially functional polycystin-1, or potential mosaicism which would not be detected in typical mutation screening (104). Other complicating factors include multiple mutations in associated genes that play a

role in ADPKD cystogenesis, such as *TSC2* tuberous sclerosis or mTOR pathway genes (81), or *CFTR* cystic fibrosis transmembrane receptor (107). Mutations of genes in broader contexts of cilia trafficking, such as kinesin II motor subunit *KIF3A* result in cyst development (108), as do other genes such as cilia-associated Meckel Syndrome *MKS1* and *MKS3* (109, 110) and Bardet Biedl Syndrome *BBS* genes (111).

Despite the intricacies involved in *PKD1* and *PKD2* gene analysis, there is also great headway made in correlations of geneotype to phenotypic presentation. In fact, Mayo Clinic and PKD Foundation have established an ADPKD mutation database (112), collating specific mutations and correlating to degree of pathogenicity. While most mutations are unique, a few mutations such as 5014delAG, a frameshift mutation that leads to early truncation, and Q2556X, a nonsense mutation, were observed in separate family pedigrees in a molecular genetics analysis of the CRISP cohort (113). This study is a step towards improved prognostic tools for correlating genetic background to a tangible phenotype of renal enlargement. Meanwhile, the Critical Path Institute Polycystic Kidney Disease Outcomes Consortium is seeking to qualify kidney volume as a FDA approved biomarker (114). Thus, improved prognostic tools would also be supported by earlier treatment.

The CRISP cohort not only provides evidence for correlation of kidney volume with ADPKD, but measurements of vital signs in the study have also inspired other cohort studies such as HALT PKD. In the CRISP study, hypertensive ADPKD patients showed greater increase in kidney volume, and so the HALT PKD study aims to show a causal role for hypertension in kidney growth using angiotensin converting enzyme inhibitors and/or angiotensin II receptor antagonists to block the renin-angiotensin-aldosterone system (RAAS), lowering blood pressure (115). HALT PKD study is still ongoing as of the time of this writing, thus, there are no reports of results after intervention. Current published reports assess baseline parameters, and not only show association of blood pressure to kidney volume, but have also identified other novel factors such as height, birth weight, gender, serum potassium, urinary albumin, aldosterone, among others (116). As an addition to the HALT PKD study, magnetic resonance imaging was used to assess left ventricular hypertrophy (LVH) of the heart correlated to baseline blood pressures of the HALT population (117), as LVH contributes to cardiovascular morbidity ultimately leading to mortality in

the context of ADPKD (118). RAAS blockade as part of the HALT PKD study could potentially decrease LVH in the hypertensive ADPKD population, thus potentially decreasing cardiovascular mortality (117). The CRISP and HALT PKD cohort studies have thus generated a variety of useful and relevant data which serve to increase our knowledge of the disease and also to inspire new avenues of study. As more and more clinical data is collected in the imminent future, much of our efforts must also go towards decoding data and extracting relevant information. It is indeed a worthy endeavor, as comprehensive knowledge of disease etiology and pathogenesis will formulate appropriate treatment plans. Improvements in technology such as single molecule DNA sequencing through nanowire-nanopore sensors (119) and scalable DNA sequencing ion chip sensors (120) promise to bring rapid and low-cost sequencing. Affordable and accessible DNA sequencing combined with a comprehensive genetic database and well characterized phenotypes can provide a powerful prognostic tool for researchers, clinicians, and most importantly, patients.

2.4.6 Current models of ADPKD

Animal models have enhanced our understanding of polycystic kidney disease. There are several mouse models of ADPKD arising from spontaneous mutations or engineered mutations including juvenile congenital polycystic kidney (*jcpk*); juvenile cystic kidney (*jck*); and polycystic kidney disease (*pcy*) (121). These mouse strains were not chosen for mutations in *Pkd1* and *Pkd2*, as the polycystins were yet to be identified as the causal agents of ADPKD. Instead, they were chosen as model organisms due to the occurrence of renal cysts and transmission patterns.

The *jcpk* mouse has a mutation in *Bicc1*, located on mouse chromosome 10 (122). *Jcpk* is characterized by severe cystic lesions and extrarenal abnormalities in homozygous animals with death in a few days. On the other hand, heterozygotes only begin to exhibit symptoms of disease around 10 months (123).

The *jck* mouse develops early focal cysts, but further cystogenesis progresses slowly (124). *Jck* transmission is recessive and is due to a mutation in *Nek8* on mouse chromosome 11 (125). In humans, mutations in *NEK8* are associated with the cystic disease nephronophthisis (126). However, the gene product Nek8 also interacts with the signaling pathways of the polycystins and thus may share common pathways in cystogenesis (127).

The *pcy* mouse is characterized by slow progressive renal cysts and occasional cerebral aneurysms (121). *Pcy* is mapped to mouse chromosome 9 (128), and this region is syntenic with human chromosome 3q21-22 gene *NPHP3* involved in nephronophthisis (129).

While these mouse models cystic disease phenotype does not arise due to polycystin mutations, they have been very well characterized. They are still used as models for cyst mechanisms and therapeutic treatments; although a shift to *in vivo* studies using *Pkd1* and *Pkd2* targeted mutations (130) might be more relevant to ADPKD.

On another front, *in vitro* models are also used for better understanding of the ADPKD cystogenesis process. In the MDCK cyst model, increased expression of PKD1 is protective against apoptosis and MDCK fail to undergo cyst cavitation, instead forming branching tubules (131). Other model systems utilize ADPKD patient derived cells. Exogenous addition of cyclic AMP and epidermal growth factor were shown to promote proliferation and cyst expansion of patient derived cells in collagen gel (87). Cells derived from *Pkd1* gene knockout mice also display ciliary and other structural abnormalities *in vitro* (132). These knockout cells were also extended to long-term 3D culture using collagen/Matrigel, silk scaffold, and perfusion bioreactor (133). The model system was validated by cadherin distribution (structural features) and by organic anion transport (functional features). Our lab has also utilized lentivirus mediated gene silencing in mouse cells in order to assess integrin signaling in *Pkd1* silencing conditions (*manuscript in review*).

2.4.7 Emerging Therapeutics for ADPKD

As many signal transduction pathways of ADPKD have been elucidated, there are several potential targets for therapeutic treatment. As mTOR pathway is upregulated in ADPKD and probably contributes to the proliferative and cystic phenotype, an mTOR inhibitor would be a good candidate therapeutic. Indeed, the inhibition of mTOR in ADPKD mouse models reversed cyst progression (81). However, human trials using sirolimus, an mTOR inhibitor, did not halt cystic kidney growth (134).

The action of antidiuretic hormone (vasopressin) on ADPKD kidney activates cAMP production, which drives cyst proliferation and activates the CFTR

channel for cyst expansion (88). In this signal cascade, there are several targets for therapy. Tolvaptan, a V2 vasopressin receptor antagonist, has been shown to slow cyst progression in ADPKD mouse models (135). The downstream CFTR channel activity could also be inhibited. Indeed, thiazolidinone, a small molecule CFTR inhibitor, slows cyst expansion in MDCK models and ADPKD mouse models (136). An intriguing therapy involves drinking water so as to lower circulating plasma levels of antidiuretic hormone. In ADPKD murine models, increased water consumption so that urine osmolality fell below that of plasma slowed the progression of PKD (137).

Other therapies involve targeting the downstream effects of the various signaling pathways such as proliferation. Roscovitine, a cyclin-dependent kinase inhibitor, slows the cell cycle. When used in *jck* mouse, cystic disease was effectively arrested (138).

While many of the proposed therapies work well in murine models, often hopes are tempered by disappointing results from human clinical trials. Tissue engineered *in vitro* models seeks to provide a platform not only for basic understanding, but also drug screening, aiming to bridge the gap between animal studies and the clinic.

Aberrant Pathway	**Candidate Drug**	**Mechanism of Action**
mTOR activation	Sirolimus	mTOR inhibitor
Cell cycle activity	Roscovitine	Cyclin-dependent kinase inhibitor
CFTR activation	Thiazolidinone	CFTR inhibitor
cAMP production stimulated by vasopressin	Tolvaptan	Vasopressin receptor antagonist
Vasopressin activity	Drink more water	Lower vasopressin secretion

Table 2.4: Emerging Drug Therapeutics - Pathways altered in ADPKD, the candidate drugs, and their mechanisms of action.

Chapter 3

Objectives

The goal of the study is to develop and validate a novel 3D human kidney tissue system under sustained culture for the study of disease progression over time. Human renal cortex epithelial cells will be modified by lentivirus silencing to recapitulate the ADPKD condition, and cultured in a 3D tissue engineered system where structural and functional outcomes can be assessed. Our hypothesis is that loss of polycystin-1 and/or polycystin-2 expression by gene silencing is reflected by phenotypic changes similar to that of human ADPKD tissues.

3.1 Objective 1: Establish Diseased Cells

Normal epithelial cells isolated from the human kidney cortex will be modified by lentivirus gene delivery of shRNA specific for *PKD1* or *PKD2*, as loss of either gene is responsible for ADPKD. Silencing efficiciency will be confirmed with quantitative RT-PCR of *PKD1* and *PKD2* mRNA and Western blot for PKD1 and PKD2 proteins.

3.2 Objective 2: Establish 3D Culture Conditions for human PKD

Primary human kidney cells will be used as control tissue, while constitutively silenced cells for *PKD1* and *PKD2* will be used for diseased tissue. Porous silk biomaterial scaffolds will be used to support modified and unmodified kidney cells in an ECM gel. The ECM gel provides an appropriate chemical environment for cell morphogenesis, while silk scaffold provides structural integrity and

prevents excessive gel contraction which can adversely affect cystogenesis. Concentration of matrix molecules will be varied along with silk scaffold geometries in order to optimize cyst formation.

3.3 Objective 3: Validate Tissue Engineered Model

3D tissue engineered constructs will be validated by comparing structural and functional features to *in vivo* human tissue samples. Structural metrics include polarized cell phenotypes, cystic phenotype, cadherin complexes, while functional metrics include organic anion transport and secretory properties.

3.4 Objective 4: Mapping Signaling Pathways

Signaling mechanisms of diseased tissue engineered constructs will also be evaluated. Effectors of cystogenesis such as proliferation, apoptosis, cell cycle aberrations, integrin signaling, and abnormal matrix deposition will be assessed with relevant assays.

Chapter 4

Materials & Methods

4.1 Cell Culture

Human Renal Cortical Epithelial cells (HRCE) (Lonza, Walkersville, MD) were maintained in Lonza Renal Epithelial Basal Media and Lonza proprietary REGM BulletKit, which contains the following supplements: fetal bovine serum, human transferrin, hydrocortisone, insulin, triiodothyronine, epinephrine, epidermal growth factor (EGF), interferon-γ, and antibiotics gentamicin and amphotericin-B.

4.2 RNA Interference

4.2.1 *PKD1* shRNA Oligo Design

shRNA sequences targeting *PKD1* mRNA were cloned into LentiLox plasmid (pLL3.7) (Addgene, Cambridge, MA). shRNA sequences were designed by Primer-BLAST (NCBI, NIH, USA) and also from a validated sequence (139). Complementary sense and antisense oligos were synthesized with incorporation of hairpin loops such that expression of sense strand leads to formation of shRNA (140). The oligos were also designed to fit into specific base pairs left open after restriction digest of plasmid vector.

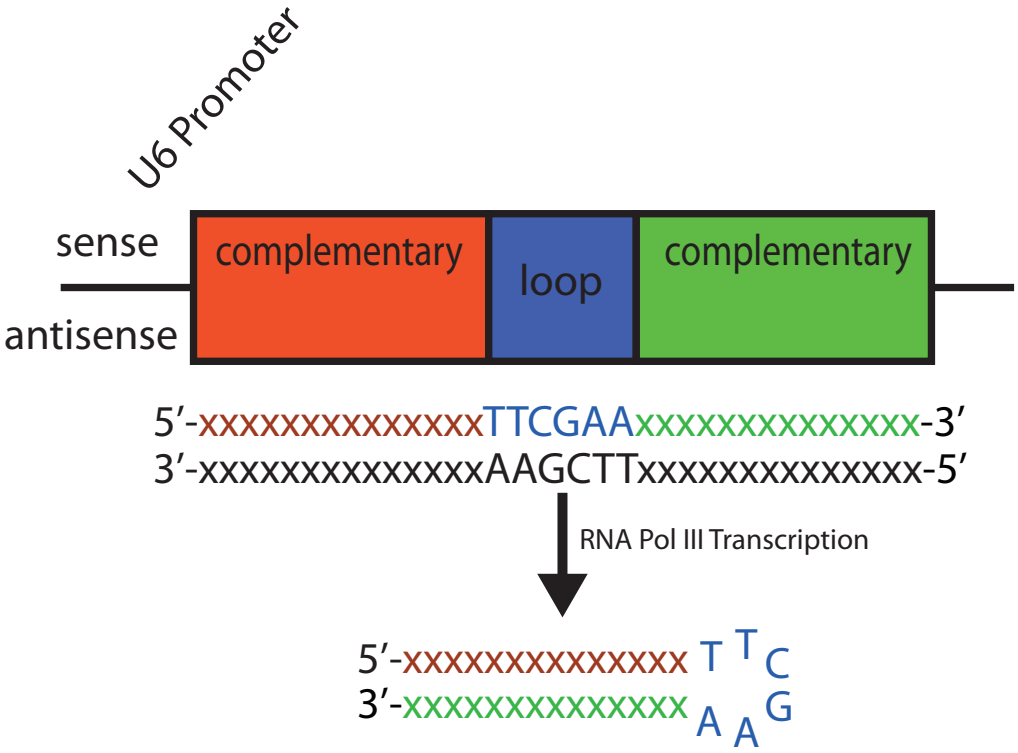

Figure 4.1: shRNA Loop Formation and Expression - Expression of the sense strand results in hairpin loop structure due to intra-strand complementary base pairing. shRNA is processed by the cell to target specific mRNA transcripts for degradation.

Primers were synthesized as follows (specific complementary siRNA sequences are italicized):

- Primer-BLAST *PKD1* Sequence 1 Sense 5' T*GCTCAACTATACGCTGCTG TTCAAGAGA CAGCAGCGTATAGTTGAGC* TTTTTTC 3'
- Primer-BLAST *PKD1* Sequence 1 Antisense 5' TCGAGAAAAAA *GCTCAACTATACGCTGCTG TCTCTTGAA AGCAGCGTATAGTTGAGC*A 3'
- Validated *PKD1* Sequence 2 Sense 5' TG*CCACGTGAGCAACGTCACC TTCAAGAGA GGTGACGTTGCTCACGTGG*C TTTTTTC 3'
- Validated *PKD1* Sequence 2 Antisense 5' TCGAGAAAAAAG *CCACGTGAGCAACGTCACC TCTCTTGAA GGTGACGTTGCTCACGTGG*CA 3'

Oligo pairs were mixed in DNA ligase buffer (New England Biolabs, Ipswich, MA) and brought to 95°C and allowed to slowly cool to room temperature. Annealed oligo products were electrophoresed in 3% agarose gel and visualized with ethidium bromide staining. Complementary inter-strand base pairing (thermodynamic product) result in 50bp length reflected on gel. Intra-strand base pairing (kinetic product) is also expected, since the oligos are self-complementary as well, and this is indicated by 25bp length on gel. The 50bp inter-strand products were extracted and purified using a Qiagen Gel Extraction Kit (Qiagen, Valencia, CA).

4.2.2 *PKD1* Plasmid Construct

The LentiLox 3.7 (pLL) plasmid was used as the vector backbone. LentiLox 3.7 is an engineered plasmid for lentivirus shRNA applications. As a plasmid, pLL can be expanded in bacteria cultures, and confers ampicillin resistance to bacteria for selection purposes. But it is the sequence between the long terminal repeats (LTRs) that is relevant for RNA interference. There is a multiple cloning site available (XhoI and HpaI) for insertion of shRNA sequence. The U6 promoter preceding the multiple cloning site expresses shRNA transcript for targeted silencing. The eukaryotic CMV promoter drives EGFP (green fluorescent protein) expression which is used to select transduced cells.

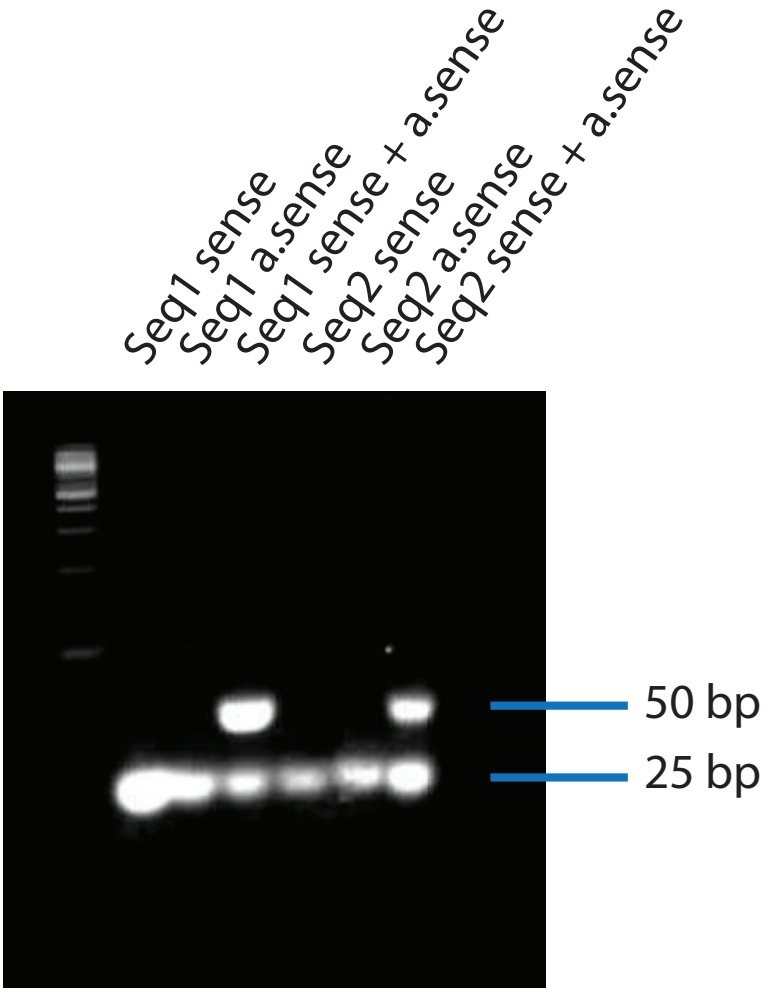

Figure 4.2: shRNA Oligos on DNA Gel - Sense and anti-sense strands were annealed to form complementary strands for the sequence pairs. Sense only and anti-sense only oligos were also run on agarose gel electrophoresis as controls for intra-strand base pairing. Inter-strand base pairing results in 50bp product. The 25bp product represents intra-strand pairing of oligos. 3% agarose gel was used for better resolution of short length nucleic acids.

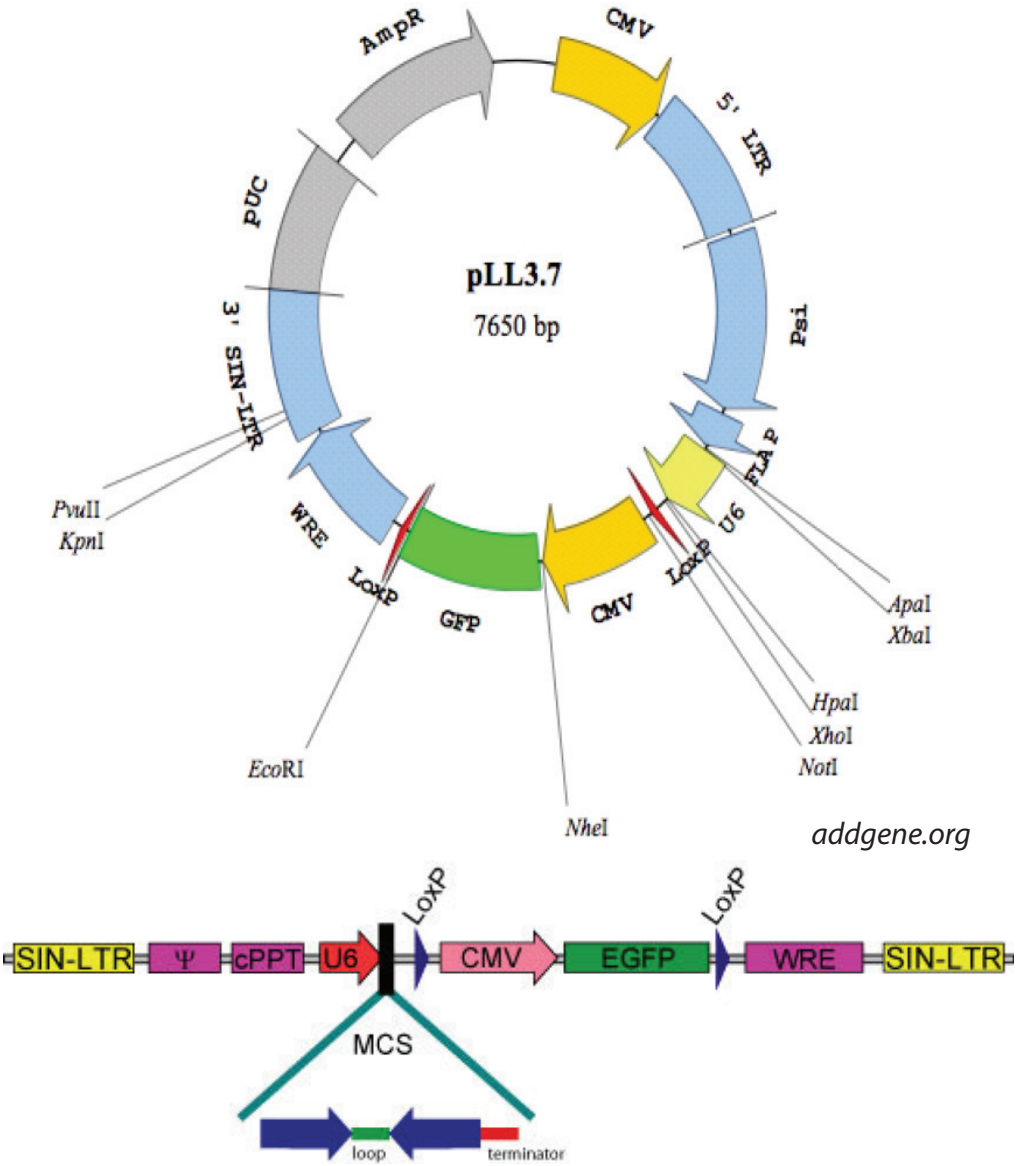

Figure 4.3: LentiLox Plasmid Map - LentiLox is a 7.6kb Plasmid that possesses eukaryotic promoter CMV for use in eukaryotic cells, U6 promoter for shRNA expression, and Ampicillin resistance for propogation in bacterial culture. LentiLox also has a Multiple Cloning Site for restriction enzyme digestion and subsequent insertion of engineered DNA.

pLL was linearized by restriction enzyme digestion with XhoI and HpaI (New England Biolabs, Ipswich, MA) and electrophoresed in 0.7% agarose gel. The linearized vector was purified with a Qiagen Gel Extraction Kit.

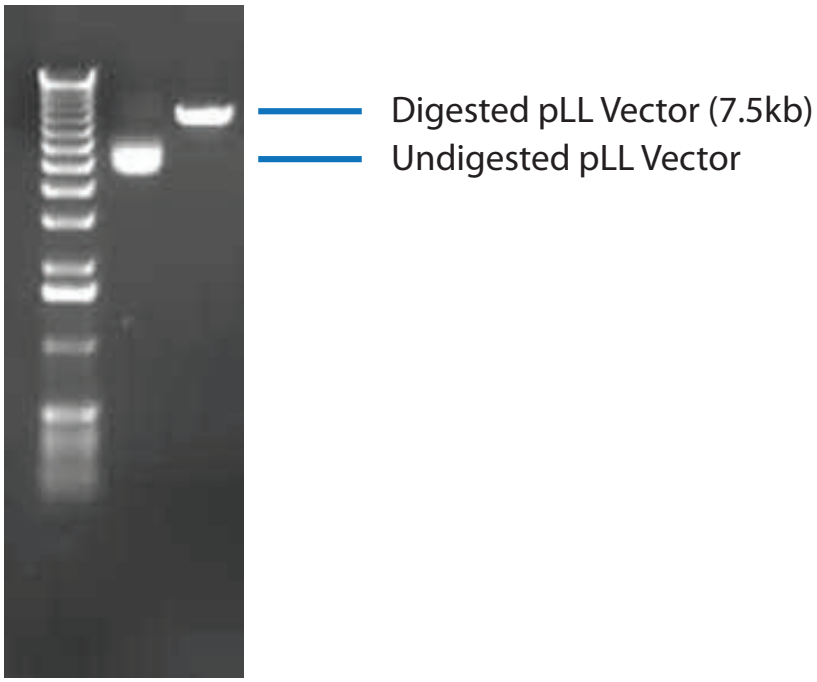

Figure 4.4: Preparation of LentiLox Vector for Ligation - LentiLox plasmid was cut with restriction enzymes XhoI and HpaI, resulting in a linear strand of DNA around 7.5kb. The sequence in between the restriction enzymes is minimal in length and has likely run off the gel. Uncut lentilox plasmid was run as a control, which runs faster in gel electrophoresis due to its circular nature.

The purified sense-antisense product was then mixed with the purified linear LentiLox vector along with exogenous T4 DNA ligase (New England Biolabs, Ipswich, MA). Product DNA was designed to fit into the open vector, but the binding is reversible without DNA ligase. Ligase seals the DNA together by restoring phosphodiester bonds.

The ligated plasmid constructs were then electroporated into DH5α competent bacterial cells (Invitrogen, Carlsbad, CA). Competent cells can be transformed with plasmid and replicate the extrachromosomal plasmid in each cell division. Transformed cells were streaked on Luria-Bertani Agar (Invitrogen, Carlsbad, CA). Individual colonies were picked and expanded in 3mL Luria-Bertani Broth (Invitrogen, Carlsbad, CA) and plasmid DNA was purified by Qiagen MiniPrep Kit (Qiagen, Valencia, CA). Plasmid DNA was cut with re-

striction enzymes XbaI and NotI (New England Biolabs, Ipswich, MA) and electrophoresed. XbaI and NotI result in a 450bp sequence which also includes the region in which shRNA oligos are ligated. Thus, shRNA plasmids with successful oligo ligation are expected to have a 50bp band shift compared to no oligo ligation, resulting in a 500bp sequence.

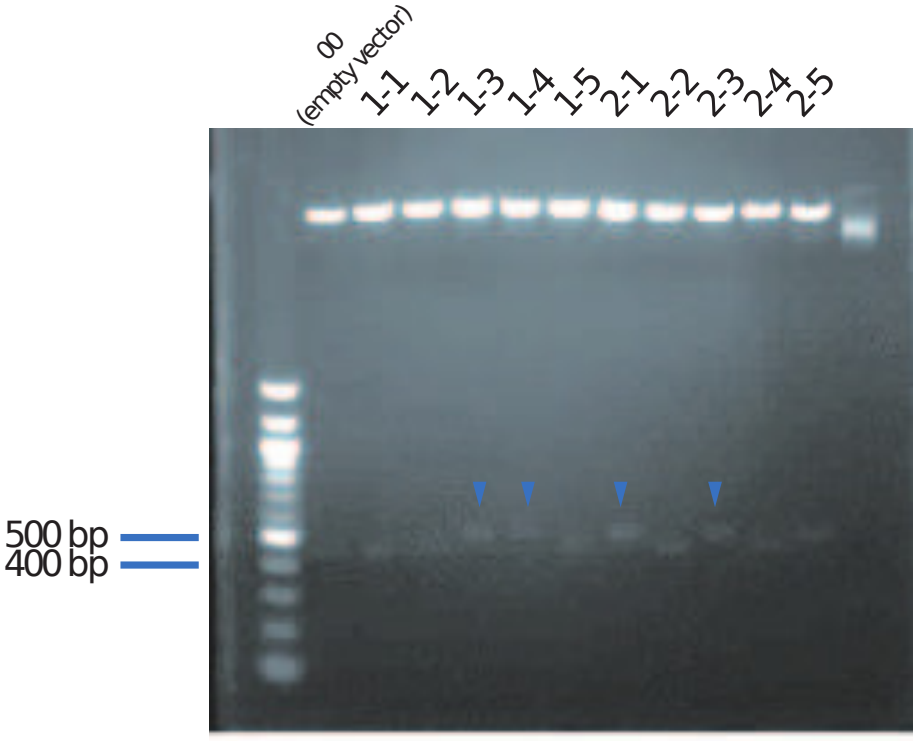

Figure 4.5: Ligated shRNA Plasmids on DNA Gel - Following ligation, plasmids were cut with XbaI and NotI, resulting in 450bp or 500bp sequences. 450bp sequences represent empty vector or plasmids that did not undergo successful ligation of shRNA oligos (shRNA oligos are approximately 50bp in length). 500bp sequences, as indicated by 1-3, 1-4, 2-1, and 2-3 represent plasmids that successfully underwent ligation of shRNA oligos.

Plasmids 1-3, 1-4, 2-1, and 2-3 were sequenced with the sequencing primer 5'cagtgcaggggaaagaatagtagac3', which sequences into pLL FLAP region, in order to confirm ligation of shRNA oligos. 1-3 and 2-1 were designated as *PKD*1 seq1 and *PKD1* seq2 respectively, and used for virus production. *PKD1* seq1 and *PKD1* seq2 plasmids were expanded in DH5α and 250mL Luria-Bertani Broth for large scale preparation and purification using a Qiagen MaxiPrep Kit (Qiagen, Valencia, CA). Purified plasma DNA concentration was determined by NanoDrop Instrument (Thermo Scientific, Waltham, MA).

4.2.3 *PKD1* shRNA Lentivirus Production and Infection

shRNA plasmid was mixed with VSV-G Env plasmid, RSV-REV plasmid, and MDLg/pRRE plasmid (Addgene, Cambridge, MA). Together, these compose the third generation lentivirus packaging system (141). The third generation packaging system uses a pseudotyped viral envelope, based on vesicular stomatitis virus, which allows broad infection of mammalian cells. RSV-REV and MDLg/pRRE separate elements of HIV viral replication (e.g. gag, pol, rev and rev response element) onto different plasmids in order to increase biosafety. Lipofectamine 2000 (Invitrogen, Carlsbad, CA) was added to form liposomes containing the plasmids. Liposomes containing packaging plasmids and empty vector pLL3.7 were also prepared as a control. The liposomes were added to HEK293FT cells (Invitrogen, Carlsbad, CA) for transient transfection of the plasmids. HEK293FT cells assemble a virus particle containing viral proteins from the packaging plasmids and an RNA transcript containing the shRNA sequences. The RNA transcript has self-inactivating long-terminal repeats, which allow integration into host genomes, but are engineered such that the complete viral genome cannot be transcribed for generating new infectious particles. Thus, generated virus can only infect cells once.

Viruses produced from HEK293FT were collected in the cell media and concentrated by ultracentrifugation in a SW-32 Ti rotor (Beckman Coulter, Brea, CA) at 28,000 rpm, 5 hours, 4°C. Virus particles were quantified by p24 ELISA (Zeptometrix, Buffalo, NY). The p24 ELISA is based on production of the viral antigen p24. Colorimetric readings of samples were fitted to a standard curve of known p24 concentrations as supplied by kit. p24 concentration was converted to transducing units (TU), one virus particle per cell. HRCE were infected with lentivirus at 50% confluency, and at a multiplicity of infection (MOI) of 5 for 24 hours before media was changed. MOI is a ratio of infectious particles to number of cells. In principle, MOI of 5 equates to 5 TU per cell. However, infection follows a Poisson distribution, as some cells will absorb more than 5 TU, while others absorb less.

4.2.4 Selection of *PKD1* Silenced Cells

After infection of HRCE cells with virus 00, virus 1-3 (*PKD1* seq1) and virus 2-1 (*PKD1* seq2), all cells expressed green fluorescent protein (GFP), which emits

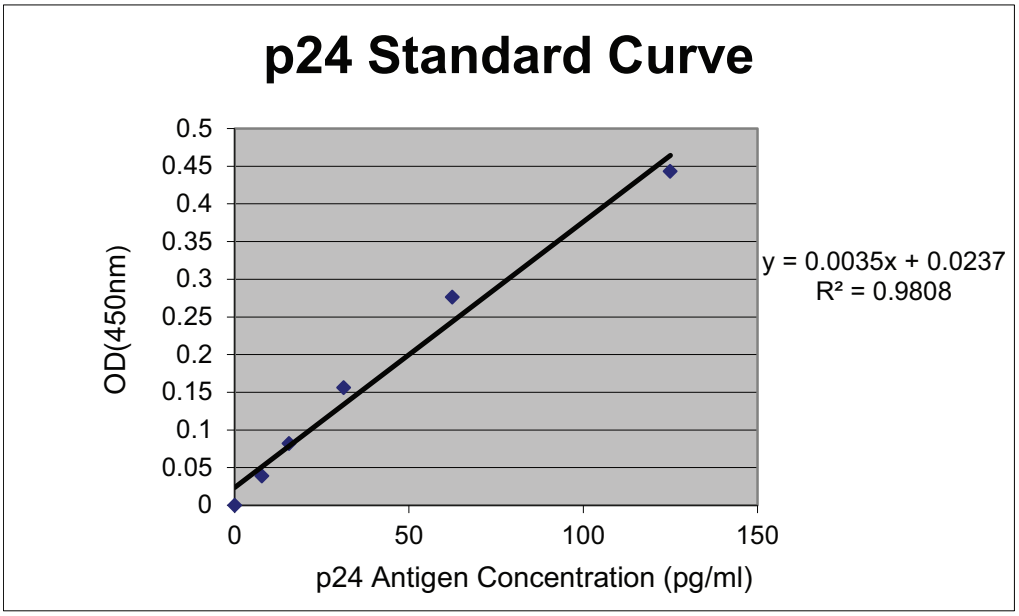

Virus	TU/mL
00 (empty vector)	5311429
1-3	11957143
2-1	7048571

Figure 4.6: Quantifying Viral Titer with p24 Antigen ELISA - A standard curve is produced with known concentrations of p24. The concentration of virus (Transducing Units/mL) is determined for control virus 00, virus produced from plasmid 1-3 and 2-1.

green color (maximal emission 520nm) upon excitation with blue light (maximal excitation 480nm). As engineered in the LentiLox plasmid, GFP expression is driven by the cytomegalovirus (CMV) promoter, a constitutive expression cassette in mammalian cells. PKD1 seq1 and PKD1 seq2 express the shRNA sequence, while empty vector has no sense shRNA strand to express. GFP expression was used to select cells that were infected, which also indicates the cells that express shRNA.

GFP positive cells were selected by flow cytometry. In flow cytometry, individual cells are pulsed with a laser and the resulting scatter of light is collected by detectors. One detector in line with the laser collects forward scatter (FSC), which is related to cell size, while a perpendicular detector collects side scatter (SSC), which is related to cell granularity. These data are used to select subpopulations of cells, and in flow cytometry, FSC and SSC data are used to distinguish single cells from debris or cell clumps. The laser also excites fluorophores, and as electrons return to the ground state, longer wavelengths of light specific to the fluorophore are emitted. These are detected by four photomultiplier tubes that are have bandpass filters for specific wavelengths. FL-1 corresponds to 525nm, FL-2 to 575nm, FL-3 to 620nm, and FL-4 to 675nm. The photomultiplier tubes amplify current produced by light emission, and strong signals correspond to strong expression of fluorophore. Frequently, FL-1 is used for GFP fluorophores and FL-2 is used for phycoerythrin (PE). However, there is some spectral overlap between GFP and PE which must be considered in analysis. FL-1 detects the maximal emission of GFP, and while FL-2 detects less intensity than FL-1, FL-2 detection of GFP still scales linearly.

For sorting of cells, uninfected HRCE were analyzed to detect the range of autofluorescence as detected by FL-1 (Figure 4.7). Cells expressing GFP are represented by FL-1 data beyond autofluorescence, and these cells were collected with the sorting function of flow cytometry. Strong GFP expression suggests cells transduced with multiple viral particles, and thus strong shRNA expression. Empty vector GFP-only cells (00), PKD1 seq1 (1-3), and PKD1 seq2 (2-1) were collected. Sorted cells were plated on tissue culture plastic, and GFP expression was visualized with excitation by blue light.

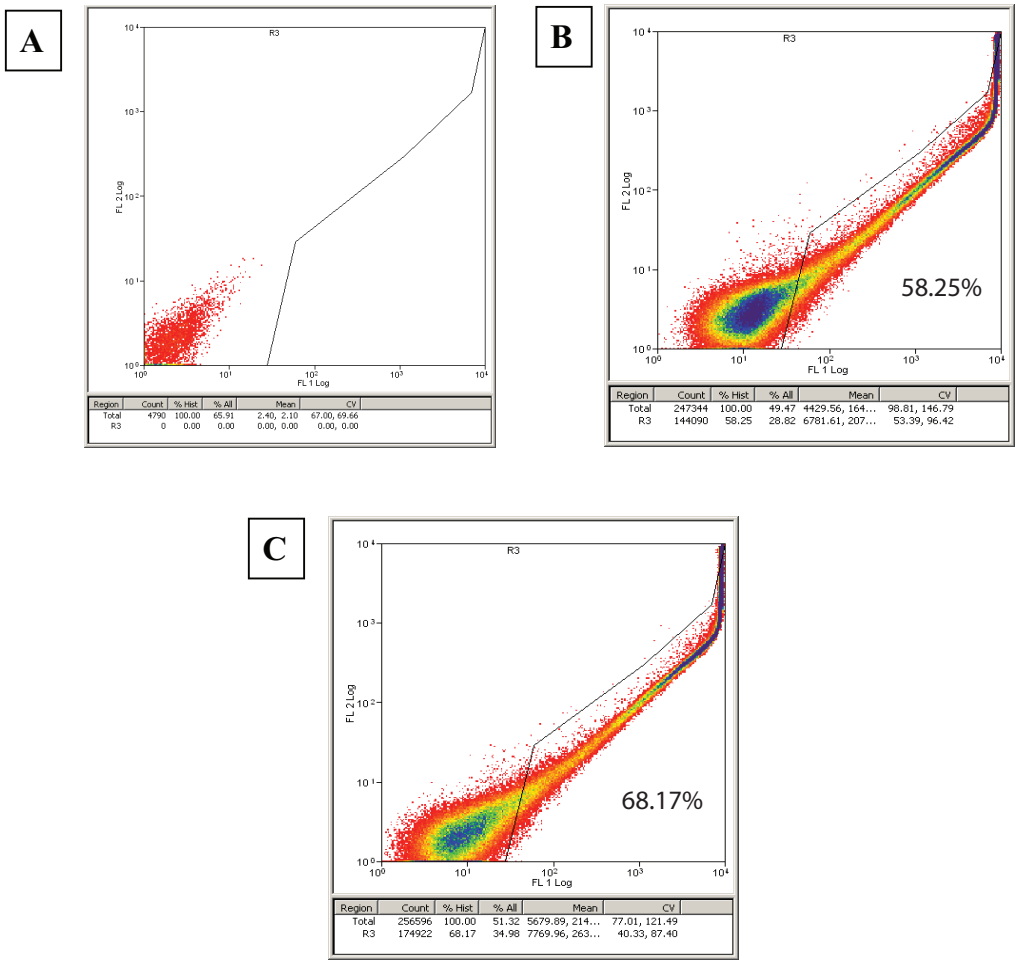

Figure 4.7: Flow cytometry data for FL1 (green) vs FL2 (red) detectors - Expression of GFP has spectral overlap with the red detector (FL2) such that not only is there detection on FL2, but FL2 levels also scale with FL1 intensity. **(A)** Unstained control outputs autofluorescence readings, along with a gate for cell sorting beyond the autofluorescence levels. **(B)** Control vector cells expressing only GFP, along with the gate collecting cells expressing GFP. **(C)** PKD1 Silenced cells expressing GFP along with the same gate as in unstained and control.

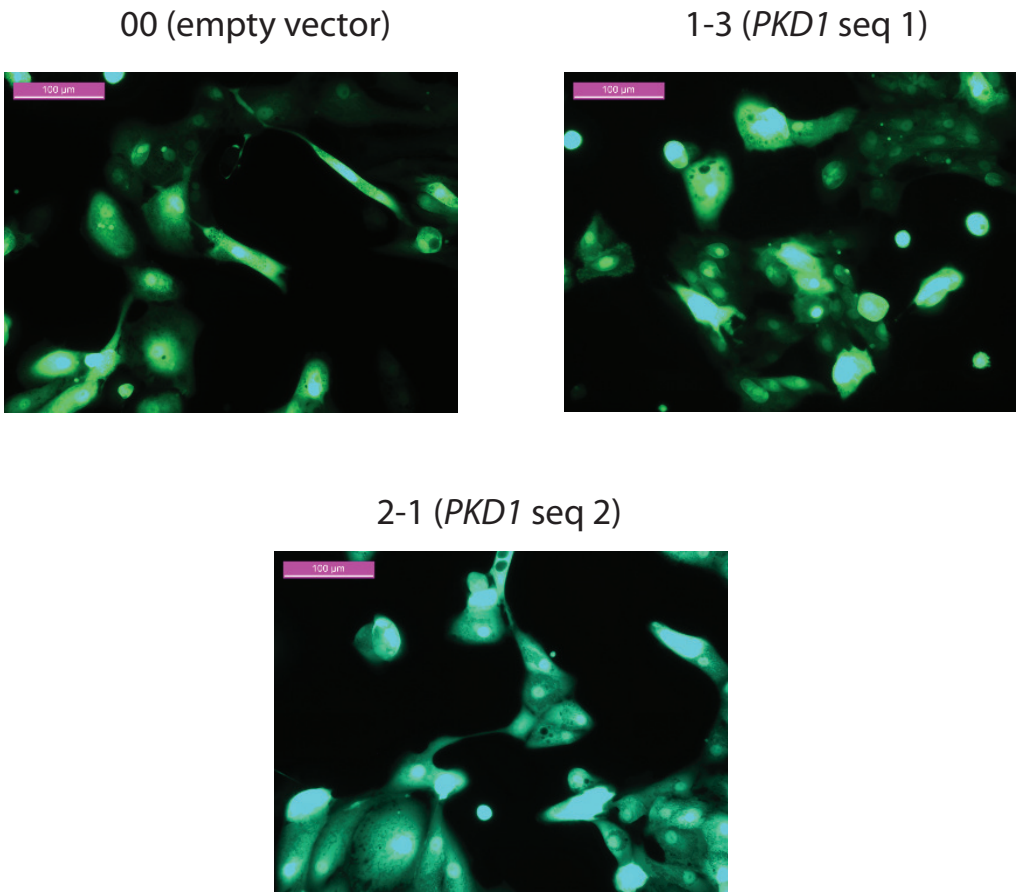

Figure 4.8: GFP Expressing Cells - Monolayer culture of cells following flow cytometry GFP selection

4.2.5 *PKD2* shRNA

PKD2 shRNA lentiviral particles were available from commercial sources. Two different validated sequences were ordered: NM_00 0297.2-1553s1c1, designated as Sequence 1, and NM_000297.2-2552s1c1, designated as Sequence 2 (Sigma-Aldrich, St. Louis, MO) along with empty vector virus particles SHC001V (Sigma-Aldrich, St. Louis, MO).

The *PKD2* shRNA lentiviral particles are based on the pLKO plasmid, which is also an engineered lentivirus plasmid. Similar to LentiLox, pLKO also has eukaryotic promoters for eukaryotic selection and shRNA expression, Multiple Cloning Site for oligo insertion, and antibiotic resistance for bacterial expansion. pLKO confers puromycin resistance to eukaryotic cells for selection by antibiotic.

HRCE were infected with lentivirus at 50% confluency, and at a multiplicity of infection (MOI) of 5 for 24 hours before media was changed. The *PKD2* lentiviral particles are based on the pLKO vector, which expresses an enzyme to inactivate puromycin, thus conferring puromycin resistance. Puromycin (Sigma-Aldrich, St. Louis, MO) was added to the culture media at a concentration of 10μg/mL and used as a selection agent for 48 hours.

4.3 Real-time Polymerase Chain Reaction

4.3.1 RNA Preparation

Cells were lysed and purified with Ambion RNAqueous kit (Ambion, Austin, TX). RNA was electrophoresed in 1.5% agarose gel to confirm quality of RNA. Large ribosomal RNAs 18s and 28s can be visualized on agarose gel, where 28s band intensity is twice that of 18s. As the polymerase chain reaction (PCR) amplifies nucleic acids, it is important to determine if there is any degradation of RNA during sample preparation.

RNA was then reverse transcribed with High Capacity cDNA Reverse Transcription Kit (Applied Biosystems, Foster City, CA) using thermal cycler settings of 25C for 10 min, 37C for 120min, and 85C for 5 min. Enzyme reverse transcriptase proceeds along RNA strand and adds complementary deoxy-ribonucleotides (dNTPs) to form complementary DNA (cDNA) strand. Thermal cycler settings allow random primer annealing at 25°C, extension of cDNA nucleotides by reverse transcriptase at 37°C, and reverse transcriptase inactivation at 85°C.

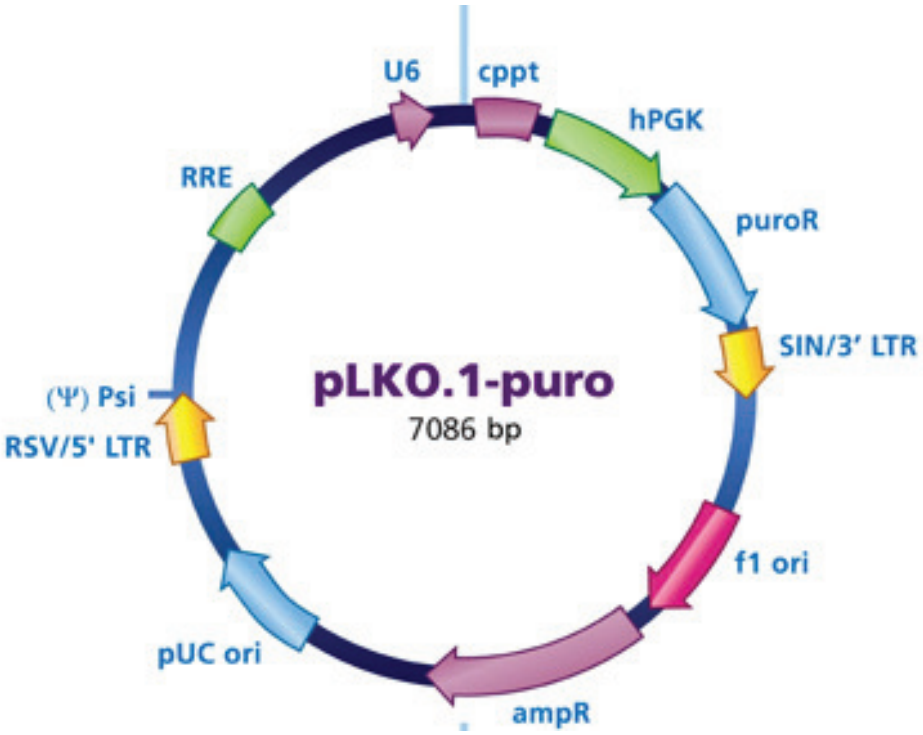

Figure 4.9: pLKO Plasmid Map - LentiLox is a 7.0kb Plasmid that possesses eukaryotic promoter CMV for use in eukaryotic cells, U6 promoter for shRNA expression, and Ampicillin resistance for propogation in bacterial culture. pLKO also has a Multiple Cloning Site (not shown in figure) for restriction enzyme digestion and insertion of engineered DNA. pLKO plasmid confers puromycin resistance to eukaryotic cells (indicated by puroR following CMV promoter). Puromycin, rather than GFP, is the selection agent for pLKO based lentivirus.

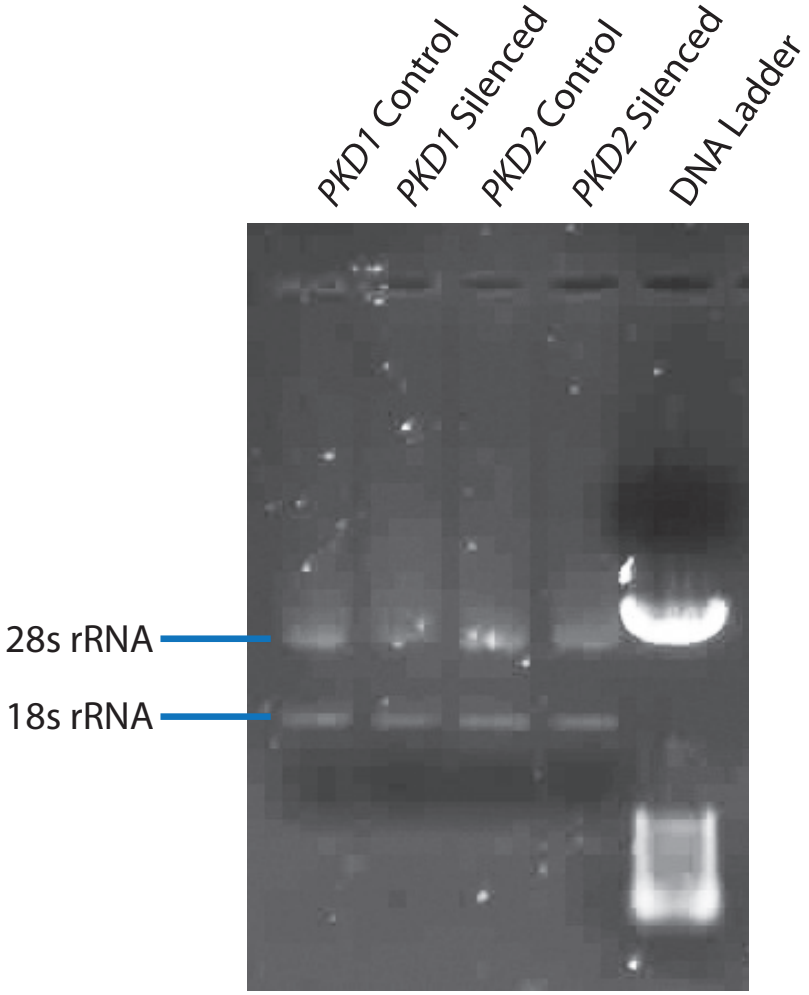

Figure 4.10: RNA Gel to Confirm RNA Quality - 18s and 28s ribosomal RNA as visualized on agarose gel. 18s and 28s are 1:1 molar ratio and 28s RNA is approximately twice as long as 18s RNA. Thus, 28s band fluoresces at twice the intensity of 18s under UV excitation. If the 28s band intensity were the same or less than 18s band intensity, then degradation of RNA would be indicated.

4.3.2 PCR Analysis

cDNA samples were assayed in real-time PCR machine Mx3000P (Agilent Technologies, Santa Clara, CA). Like traditional PCR, real-time PCR also expands DNA with DNA denaturation step, primer annealing step, and DNA extension step. As an added feature, real-time PCR also quantifies DNA by detection of fluorescence that scales linearly with DNA.

In the SYBR Green system, the fluorescent dye SYBR Green intercalates in double helix DNA and emits green light upon excitation with blue light. Thus, PCR machine can detect SYBR Green amount at the end of the extension step, which quantifies total double helix DNA, an amount that doubles every cycle. However, SYBR Green binds indiscriminately; all double stranded DNA will fluoresce, including primer dimers. Thus, melting curve analysis is used to determine primer dimer expansion.

The TaqMan system utilizes probes that fit within regions specified by the PCR primers. The probe is conjugated with a fluorophore and a quencher that abrogates fluorescence when in proximity of the fluorophore. However, when Taq polymerase extends DNA bases during extension step, Taq exonuclease activity cleaves the fluorophore off the probe, and the fluorophore is then free to fluoresce. Fluorescence detection also scales linearly with DNA amount, and the TaqMan system also offers better specificity since the probe is designed to fit within the primer regions.

Glyceraldehyde 3-Phosphate Dehydrogenase (GAPDH) was detected with TaqMan probe: Hs02758991_g1 (Applied Biosystems, Foster City, CA).

PKD1 and *PKD2* primers were designed with Primer-BLAST (NCBI, NIH, USA) and QuantiTect SYBR Green Kit (Qiagen, Valencia, CA) was used to quantify DNA.

Primer Target	**Primer Sequence**	**Product Length**
PKD1	fwd 5'-GCCTACAGCACGGGGCATGTGT-3' rev 5'-CAGCGTGGAGGCCTGAGAACGT-3'	250 bp
PKD2	fwd 5'-CCCCGAAATGGAACCGCTTGG-3' rev 5'-TGCCCTGGTTCCTCGGTCCA-3'	186 bp

Table 4.1: qRT-PCR Primer Design

4.4 Immunoblotting

Cells were lysed in a Radio Immuno-precipitation Assay (RIPA) lysis buffer (Pierce Biotechnology, Rockford, IL) with Halt^{TM}protease and Phosphatase inhibitors (Pierce Biotechnology, Rockford, IL) and the total cell proteins were collected by centrifugation at 14,000 rpm for 15 min. Protein was quantified using Bradford Reagent (Bio-Rad, Hercules, CA), a colorimetric assay where samples are compared to a standard curve of known protein concentrations.

Western blot was used to assess relative protein amounts in control and silenced cells. Western blot is based on primary antibody binding to specific epitopes of proteins. A secondary antibody raised against the host animal of the primary antibody is then applied, which binds to the primary antibody. The secondary antibody is also conjugated to an enzyme, horseradish peroxidase, which oxidizes luminol substrate to excited 3-aminophthlate. Excited 3-aminophthlate emits light as it returns to the ground state 3-aminophthlate, and this light is captured on radiographic film, which is then fixed and developed.

Equal amounts of protein samples were electrophoresed in 4-12% Bis-Tris gel (Invitrogen, Carlsbad, CA) and transferred to a poly-vinylidenefluoride (PVDF) membrane (Invitrogen, Carlsbad, CA). Probing with primary antibodies for PKD1 (sc130554-1:1000), Integrin-1 (sc8978-1:2000) (Santa Cruz Biotechnology Inc, Santa Cruz, CA) and with antibodies for PKD2 (ab90648-1:2000), laminin (ab11575-1:2000), collagen IV (ab6586-1:1000) and CyclinD1(ab16663-1:400) (Abcam Inc, Cambridge MA) were performed in 3% skimmed milk. Glyceraldehyde 3-Phosphate dehydrogenase (GAPDH) (ab9484-1:2500) and CyclinE (ab2959-1:5000) (Abcam Inc, Cambridge MA) were probed in 5% bovine serum albumin (BSA). Secondary antibodies conjugated with horse radish peroxidase (HRP), (Goat Anti-rabbit HRP sc2004 or Goat Anti-mouse HRP sc2005) (Santa Cruz Biotechnology, Santa Cruz, CA) were used according to the primary antibody host. PKD1 blotting was developed using ECL Advance reagents while other proteins were developed using ECL plus reagents (GE Healthcare Biosciences, Piscataway, NJ).

4.5 3D Culture

4.5.1 Scaffold Preparation

Aqueous silk scaffolds were prepared from silk fibroin solution extracted from *Bombyx mori* silkworm cocoons as we have described previously (133). Silk solution was prepared by first boiling silk cocoons to remove sericin component, and isolate fibroin fibers, the structural core of silk. Fibroin was then dissolved into solution with chaotropic agent lithium bromide over several hours in a 60°C oven. Fibroin solution was dialyzed in water with Slide-A-Lyzer dialysis casettes (Pierce Biotechnology, Rockford, IL) to achieve 8-10% fibroin concentration and remove lithium and bromide ions. 1mL of 8-10% fibroin was placed in a plastic cylinder and 500μM diameter NaCl (Sigma-Aldrich, St. Louis, MO) was sifted into the solution and allowed to salt-leach over three days to form porous scaffolds. Scaffolds were then rinsed with ddH_2O, and cut to size 6mm x 2 mm (diameter x height) with a 6mm biopsy punch and surgical knife.

4.5.2 Tissue Engineered Constructs

Tissue engineered constructs were developed by mixing cells with a 1:1 (vol/vol) mix of collagen type I (1 mg/mL) and Matrigel^{TM}(BD Biosciences, Rockville, MD) to a final concentration of 2x10^6 cells/mL. The gel mix was then added to the scaffolds. The pores of the scaffolds were filled with the cell-matrix mix and allowed to gel for 30 min at 37°C. Cells were maintained in static culture conditions with media changes every two days. Culture media was supplemented with cyclic AMP elevating agent 50μM cAMP Sp-isomer (EMD Chemicals, Gibbstown, NJ). Although not performed in this thesis work, tissue engineered constructs in scaffold could be extended with perfusion culture reactor as shown previously (133) for long-term culture.

4.5.3 Human ADPKD Tissue

Human ADPKD tissue was generously donated from an anonymous kidney transplant recipient who underwent nephrectomy to remove ADPKD kidneys. Kidney tissue samples were generously prepared by Jillian Grau, MD (Lehigh Valley Health Network, Allentown, PA). Human tissue protocol was approved by Tufts University Institutional Review Board, Study #1101012.

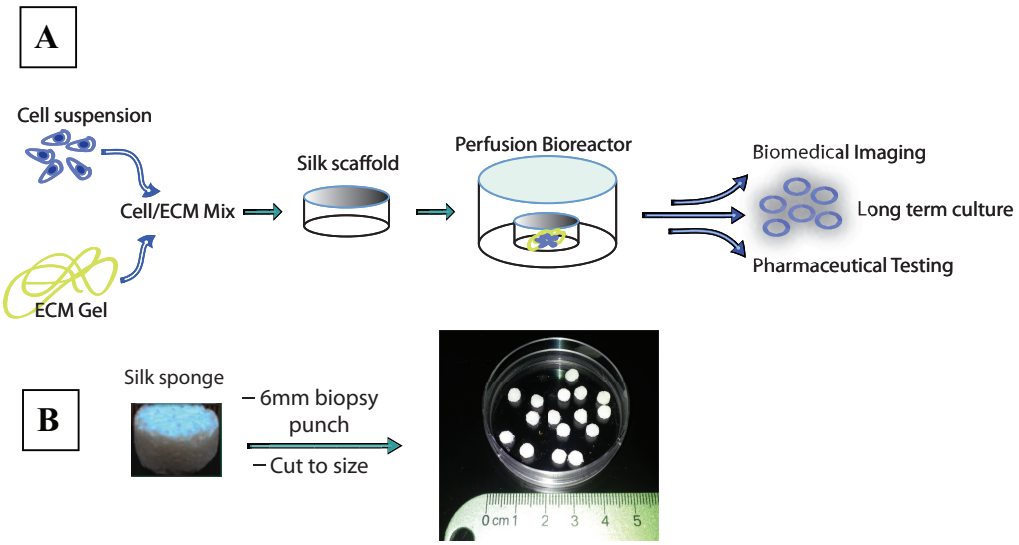

Figure 4.11: Tissue Engineered Kidney Schematic - **(A)** Cells were mixed with collagen type I and Matrigel^{TM}mix and seeded to silk scaffold. Tissue constructs were cultured in static media, and could be expanded with perfusion culture. Downstream applications include biomedical imaging and pharmaceutical analysis. **(B)** Silk sponge scaffold prepared as described. Scaffolds used for tissue engineered constructs were 6mm x 2mm (diameter x height).

4.6 Histology and Confocal Imaging

4.6.1 Sample Preparation

Tissue engineered constructs were fixed in formalin at 14 days culture. ADPKD kidney tissue was also fixed in formalin. Fixed tissues were encased in paraffin, which involves progressively dehydrating steps of ethanol, since paraffin is immiscible with water, a major constituent of tissue. Ethanol dehydration steps include 70%, 95%, and 100% ethanol soak, followed by two xylene washes to clear ethanol. Molten paraffin was applied, which infiltrates tissue and scaffold, and then embedded on tissue cassette as a paraffin block. Paraffin blocks were then cut to 5μM thick sections with a Leica Microtome (Leica Microsystems, Wetzlar, Germany) and mounted on microscope slides.

Paraffin sections were deparraffinized by reverse order of paraffin embedding, which includes xylene wash followed by progressively re-hydrating concentrations of ethanol and water. Slides were stained with Hematoxylin and Eosin (H&E), where Hematoxylin binds to the histone nucleoproteins in the nucleus as a blue dye, and eosin stains the cytoplasm red. For immunofluorescence, paraffin sec-

tions were deparaffinized as before and antigen retrieval was performed with Antigen Unmasking Solution (Vector Laboratories, Burlingame, CA) by boiling slides for 30 min. After antigen retrieval, sections were blocked with 5% bovine serum albumin (BSA) supplemented with 10% serum from the secondary antibody host, in Dulbeccos Phosphate Buffered Saline (DPBS) (Invitrogen, Carlsbad, CA).

4.6.2 Antibody-dependent Fluorescence Imaging

E-cadherin was probed with rabbit polyclonal IgG (ab53033-1:50) (Abcam, Cambridge, MA) and goat polyclonal to rabbit IgG-Cy5 conjugate (ab6564-1:100) (Abcam, Cambridge, MA). N-cadherin was probed with mouse monoclonal IgG (ab66025-1:50) (Abcam, Cambridge, MA) and goat polyclonal to mouse IgG-FITC conjugate (ab6785-1:100) (Abcam, Cambridge, MA). For acetylated alpha-tubulin, anti-sera from clone (6-11B-1) (T6793-1:25) (Sigma-Aldrich, St.Louis, MO) and goat polyclonal mouse IgG-Cy5 (ab6563-1:50) (Abcam, Cambridge, MA) were used. Slides were counterstained for the nucleus using 4, 6- Diamidino-2-phenylindole (DAPI) (Invitrogen, Carlsbad, CA) and mounted with Fluoroguard Antifade reagent (Bio-Rad, Hercules, CA).

Cells were viewed with an Ar/Kr laser (488 nm) or helium neon laser (633 nm) in conjunction with a confocal laser scan head in a Leica Confocal Microscope (Leica Microsystems, Wetzlar, Germany). DAPI was visualized with multiphoton laser at (770nm) where collision of two-photon excites at half the wavelength, which corresponds to the excitation wavelength of DAPI at 388nm). A series of photomultiplier tubes with adjustable bandpass filters isolate the emission wavelengths of the fluorophores for analysis. Digital images were collected with a 20x objective lens.

4.7 Proliferation Assay

Proliferation rate of the cells were measured by Alamar Blue assay (Invitrogen, Carlsbad, CA). Alamar Blue assay is based on the oxidation of nonfluorescent blue dye resazurin to fluorescent pink dye resorufin. Resazurin is reduced by cytochrome c oxidase, the final step in the electron transport chain that reduces molecular oxygen to water. Thus, electron transport chain is not halted by

interference at an intermediate stage, and resazurin is only converted by actively respiring cells, which indicates cell proliferation and viability.

Equal number of cells were plated in 6cm culture dish with full media, followed by incubation in a full media plus Alamar Blue dye for 3 hr. Sample aliquots were collected and fluorescence was measured. Sample aliquots were collected at semiconfluent culture condition and ended when cells reached confluence. Cells were then switched to dye free media for further proliferation and the procedure was repeated at the next time point of analysis at 24 hour intervals. Samples collected 12 hours after plating were used as 0 hour time point in the analysis.

4.8 Apoptosis Assay

Apoptosis was measured by Annexin V PE binding assay (BD Pharmingen, San Diego, CA). Annexin V binds strongly to phosphatidylserine, a membrane phospholipid that is flipped to the outer leaflet and exposed to the extracellular milieu in the early stages of apoptosis. Annexin V conjugated with phycoerythin (PE), a fluorescent marker, can be detected with flow cytometry. Equal number of cells were trypsinized and collected two days after plating in full media. Cells were then incubated with Annexin V-PE and kit supplied binding buffer.

In another assay, three sets of equal number of cells were plated in full media. Media was changed to serum-free media such that one set of cells was cultured for 48 hours in serum free media, the second set of cells was cultured for 24 hours in serum free media, and the third set of cells was continuously cultured in full media.

For both experiments, samples were run in a BD FACSCalibur flow cytometer (BD Biosciences, San Jose, CA) and the results were analyzed using Flow Jo software (Treestar, Ashland, OR).

4.9 Cell Cycle Analysis

Cells were trypsinized and collected every five hours over a 25 hour interval. Cells were fixed in 70% ice cold ethanol and stored at -20°C overnight. Cells were then washed in PBS and re-suspended in a DNA staining solution (2.5 μg/mL propidium iodide and 1 mg/mL RNase A in PBS) for 1hr at 4°C. Samples were

run in a BD FACSCalibur flow cytometer (BD Biosciences, San Jose, CA) and the results were analyzed using Flow Jo software (Treestar, Ashland, OR).

The principle of cell cycle analysis involves fixing cells over the course of the cell cycle. Cell cycle involves Interphase, which replicates DNA, and Mitosis, which divides the cell in two. Flow cytometry detects the relative amounts of DNA per cell by propidium iodide staining detected by FL2 detector, and indicates how many cells are in G0-G1 phase, at 1X DNA concentration; how many cells are in G2 phase, where DNA has completely replicated and is 2X DNA concentration; and how many cells are in S phase, where DNA content is synthesized and thus intermediate between 1X and 2X. The G2 peak cannot be differentiated from Mitosis, as the flow cytometry analysis reflects purely DNA content per cell, and Mitosis phase also has 2X DNA content until cleavage is complete.

Flow cytometry settings were determined as follows. FSC and SSC voltages were set to confirm relative homogeneity of cell size to cell granularity in FSC vs SSC plot. FL2 voltage and gain were adjusted until G0-G1 peak had a value of 200 on FL2-A histogram and G2-M peak had a value of 400 on FL2-A. FL2-A represents the area of fluorescent intensity as a cell is excited by laser and passes by a detector. FL2-A was set under linear amplification settings to better resolve the G2-M peak at twice the value of G0-G1 peak, whereas logarithmic amplification would compress the peaks together in analysis. FL2-W, a measure of the pulse width, or width of the cell that passes by the detector, was set to between 200 and 600. The graph of FL2-A vs FL2-W show a majority of cells at FL2-W value of 200, and FL2-A values from 200 to 400, which indicates cells of the same size varying from 1X to 2X DNA content. These are the cells of interest and were gated appropriately. Other cells are seen at FL2-W value of 400 along with FL2-A value of 400, which indicates probable double cell aggregate of G0-G1 phase cells, hence twice the DNA content, but also twice the pulse width. FL2-W greater than 400 indicates even larger aggregates of cells, while values much smaller than 200 for both FL2-W and FL2-A are likely cell debris. Following appropriate gating of single cells, counts of FL2-A were acquired to determine the peaks, and thus cell cycle phase of the samples over 25 hour time period.

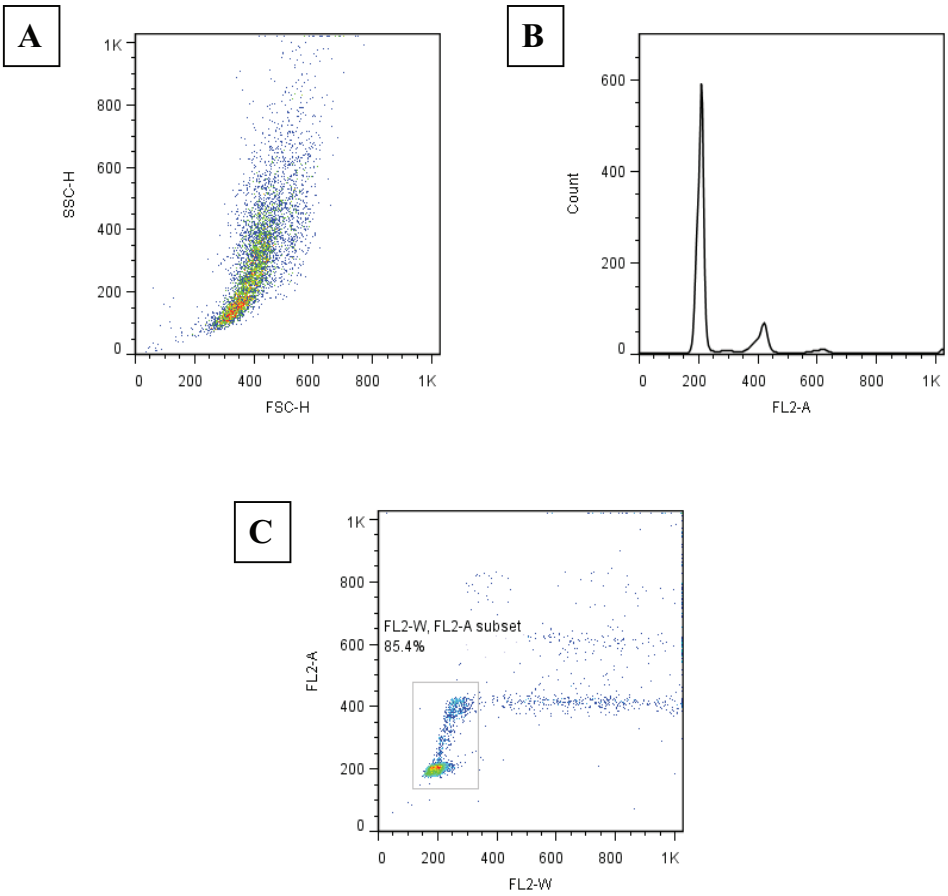

Figure 4.12: Flow Cytometry Settings for Cell Cycle Analysis - **(A)** Forward Scatter (FSC) vs Side Scatter (SSC) show homogeneity of the sample population in regard to cell size and granularity. **(B)** FL2 detects propidium iodide fluorescence. FL2-A voltages were adjusted prior to gating and exclusion of cell aggregates. The majority of cells were in two peaks, the G0-G1 peak at 200 and G2-M peak at 400, which is twice the DNA content, and S phase which is intermediate in DNA content. Some counts above 400 are due to cell aggregates and will not appear after aggregate exclusion. **(C)** FL2-A vs FL2-W were adjusted to exclude cell aggregates. Cells were gated at 200 pulse width (FL2-W) and FL2-A ranging from 200 to 400 indicates DNA content ranging from 1X to 2X in single cells.

4.10 Transport Assay

In preparation for transport assay, scaffolds were incubated with CellMask DeepRed plasma membrane stain (Invitrogen, Carlsbad, CA) which is a lipophilic probe that anchors in the plasma membrane for indicating cell borders in live cell imaging. While not completed for this thesis work, transport assay protocol includes incubating scaffolds in phenol red free basal media followed by addition of 6-carboxyfluorescein diacetate succinimidyl ester (CFDA-SE) (Sigma-Aldrich, St. Louis, MO). CFDA-SE diffuses into cells by virtue of its acetate groups, and is cleaved in the cell by endogenous esterases to release the fluorescent dye carboxyfluorescein, thus localizing fluorescence within the cell. Organic anion transport of carboxyfluorescein out of the cell can be inhibited with probenecid (Invitrogen, Carlsbad, CA). Following uptake, scaffolds would be washed in PBS and imaged with confocal microscopy.

Chapter 5

Results and Discussion

5.1 Confirmation of *PKD1* and *PKD2* Silencing

As *PKD1* and *PKD2* mRNA transcripts are degraded by RNA interference, we can confirm silencing by assessing RNA transcript expression levels along with protein expression levels. Following are data of transcript expression by quantitative Polymerase Chain Reaction (qPCR) and protein expression by Western blot.

5.1.1 *PKD1* and *PKD2* mRNA Transcript Expression

Total RNA was extracted from cells and undergoes reverse transcription with random primers to form complementary DNA (cDNA), as described in methods chapter. RNA is the product of gene transcription, and is generated by RNA polymerases reading a DNA strand that is complementary to the RNA transcript product. In other words, RNA polymerase reads the antisense strand to generate the RNA equivalent to the sense strand of a gene. For the cDNA to exist, the RNA template must exist in the cell, and RNA is only formed from gene transcription. We utilized qPCR and quantified the relative amounts of cDNA complementary *PKD1* and *PKD2* transcripts, which are representative of the number of RNA transcripts. Primers specific for short (approximately 200bp) regions of *PKD1* and *PKD2* transcripts were used. Under silencing conditions, fewer RNA transcripts are expected, as these transcripts are degraded by shRNA, and this is reflected by higher cycle counts in qPCR data.

However, the resulting figures are not definitive, as silencing efficiency is expected to be much greater. It is quite possible that the primers, as they

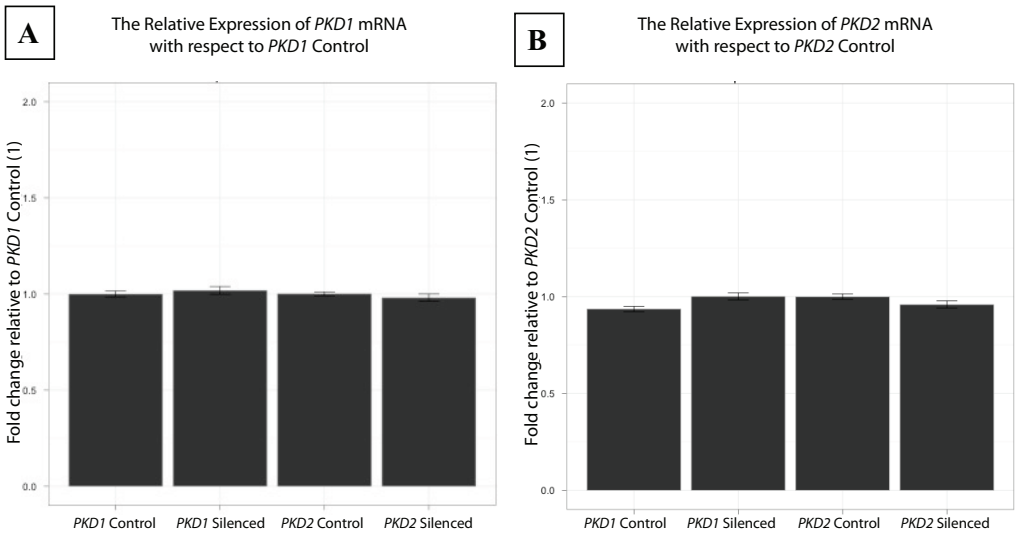

Figure 5.1: Relative Expression of *PKD1* and *PKD2* Control and Silenced mRNA - qPCR graphs of relative expression of *PKD1* and *PKD2* mRNA for control and silenced cells. Fold change was determined with respect to *PKD1* Control **(A)** and *PKD2* Control **(B)**, which are set at 1.0 each. Loading control is GAPDH expression. Error bars represent $p<0.05$

were designed by the bioinformatics tool BLAST, were inefficient. It is difficult to measure fold change in silencing applications, because after siRNA binding and degradation of a transcript, there may still be leftover mRNA of significant length. While degraded mRNA is unsuitable for ribosomal translation, it is possible for a qPCR primer to bind onto residual mRNA, as the RNA need only be at least long enough and continuous to contain the forward and reverse primer binding sites (roughly 200bp for our primers). And as long as the binding sites are intact, qPCR will amplify those targets. Melting curve analysis was also performed to confirm that only one amplicon was amplified, thus barring any misleading results from primers associating promiscuously with other targets.

However, we are ultimately concerned with the protein level, rather than the transcript level, as it is the loss of polycystin-1 or -2 protein function that drives cystic events, and we confirm silencing via Western blot.

5.1.2 PKD1 and PKD2 Protein Expression

Silencing of *PKD1* and *PKD2* was also supported by Western blot protein analysis. Figure 5.2 shows a slight reduction in band intensity for PKD1 in *PKD1* Silenced cells. PKD1 protein was detected at approximiately 460kDa. *PKD2*

silencing was more efficient, as there was no band visualized in *PKD2* Silenced cells for PKD2 protein. PKD2 protein was detected at approximately 110kDa.

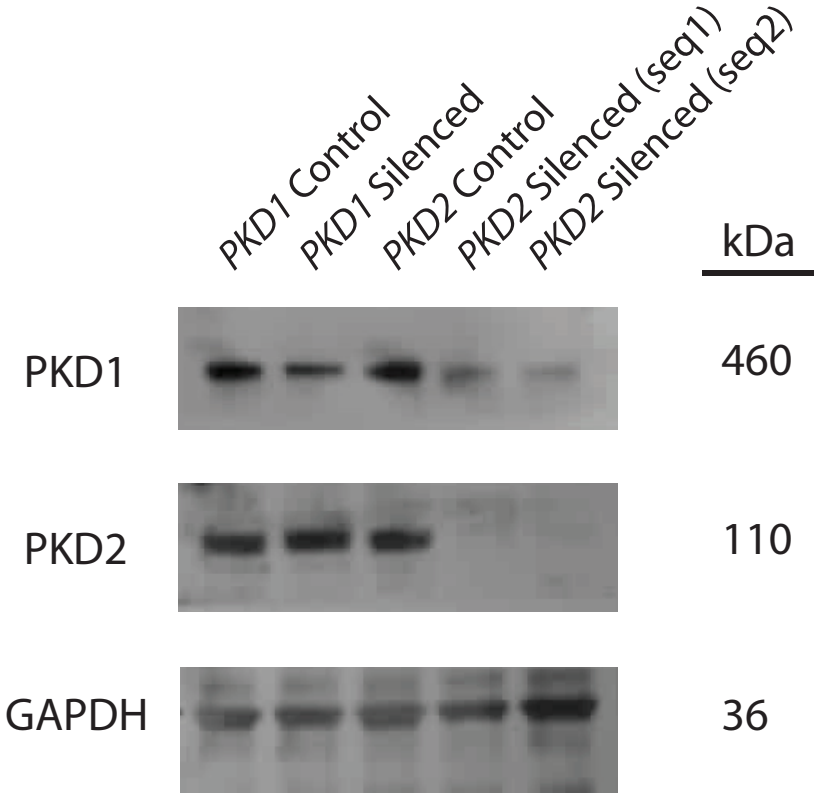

Figure 5.2: Knockdown Analysis for Polycystin-1 and Polycystin-2 - Total cell lysates were collected from the normal and transduced cells and blotted for PKD1 and PKD2. PKD1 expression was reduced in *PKD1* silencing conditions and PKD2 expression was reduced in *PKD2* silencing conditions.

Interestingly, the silencing of *PKD2* led to a reduction of PKD1 protein. *PKD1* silencing did not appear to affect PKD2 protein expression; however, the efficacy of *PKD1* silencing was also limited in comparison to *PKD2* silencing. It has been demonstrated that PKD1 and PKD2 interact with one another as part of a complex (57), and so the loss of either of the polycystins could adversely affect the other. It was also demonstrated in HEK293T cells that interaction between the C-termini of PKD1 and PKD2 led to increase in PKD1 but not PKD2 (142). Thus it is possible that PKD2 plays roles in stabilizing PKD1, and the loss of PKD2 with concomitant loss of PKD1 is further indirect evidence of its stabilizing role.

5.2 Proliferative Abnormalities Following *PKD1* and *PKD2* Silencing

Proliferation is an important aspect of the PKD phenotype, as discussed in background sections. Cyst derived cells have been shown to proliferate faster than normal HRCE cells (87). Thus, assessing the proliferative capacity of silenced cells was relevant. However, we observed the opposite; both *PKD1* and *PKD2* Silenced cells proliferated slower than their respective control cells.

5.2.1 AlamarBlue Cell Viability Experiment for *PKD1* and *PKD2* Silenced Cells

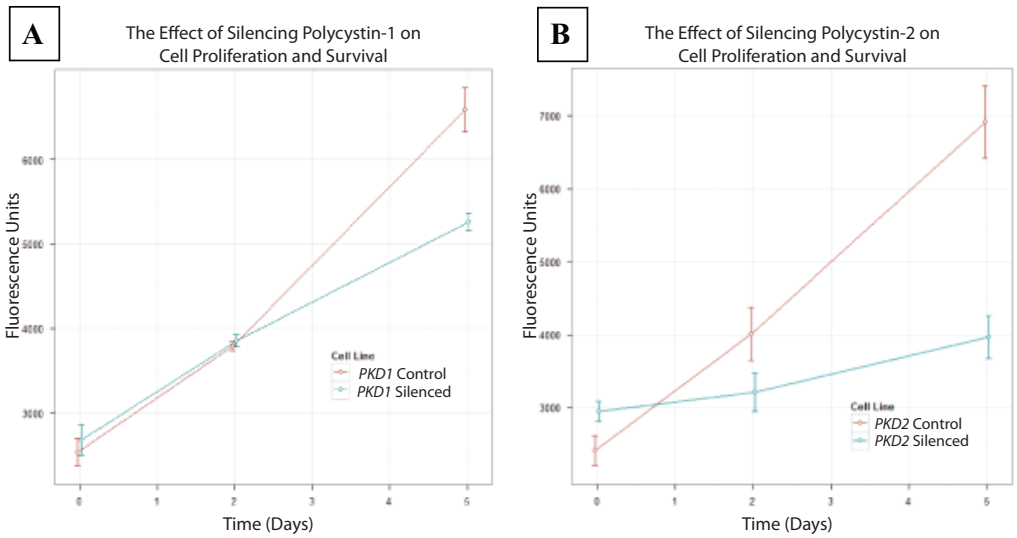

Figure 5.3: Cell Viability of *PKD1* and *PKD2* Control and Silenced Cells - Alamar Blue assay for **(A)** *PKD1* Control vs *PKD1* Silenced and **(B)** *PKD2* Control vs *PKD2* Silenced. Loss of Polycystins -1 and -2 resulted in slower proliferation or loss of cell viability over the course of several days. Error bars reflect ($p<0.05$)

AlamarBlue cell viability indicator is based on a reduction reaction of non-fluorescent resazurin to fluorescent resorufin in cell cytosol. Lower fluorescence readings for *PKD1* and *PKD2* Silenced cells in comparison to Control cells indicate net fewer cells at the end of five days. Interestingly, *PKD2* Silenced cells had a markedly reduced fluorescence reading at the end of the experiment than *PKD1* Silenced cells, which could be related to the limited degree of *PKD1* Silencing. Fewer cells suggest a slower proliferation rate and/or a greater amount

of apoptosis for silenced cells. Silencing for immortalized cell lines such MDCK indicate a large increase in proliferation along with increased apoptosis (143). However, in experiments on immortalized cell lines, the increased proliferative capacity of silenced cells overcomes the cell death mediated by apoptosis to net a greater amount of cells than control cells (133, 143). Then, for our case of net loss of cells in the silencing condition, we are left to wonder whether there is faster proliferation, but an even greater amount of apoptosis.

5.2.2 Apoptosis mediated by *PKD1* and *PKD2* Silencing

We noted increased apoptosis for silenced cells as shown in Figure 5.4 and Figure 5.5. Early in apoptosis, phosphatidylserine, which is normally contained on the inner leaflet of the plasma membrane, is flipped to the outer leaflet and thus exposed to the extracellular milieu. Annexin V is a protein that has very strong binding affinity for phosphatidylserine, and so Annexin V conjugated with a fluorescent tag may be used in flow cytometry to detect apoptotic cells (144, 145).

We utilized Annexin V conjugated to phycoerythin (PE), which is maximally detected by the FL2 detector on flow cytometry instrumentation. For *PKD2* Control and Silenced cells, the experiment was rather straightforward, as the cells do not express any other fluorescent colors. The same gate was applied to control and silenced cells, which show a greater percentage of apoptotic cells in the silenced condition.

PKD1 Control and Silenced cells were more difficult to analyze by flow cytometry, as instrument compensation was required. *PKD1* Control and Silenced cells constitutively express GFP, which is maximally detected by the FL1 detector, but its emission spectra also falls into the detection range of the FL2 detector, contributing to higher FL2 readings. Thus, compensation was required in order to reduce the influence of GFP on FL2, which necessitates the use of more unstained controls. The figure provided for *PKD1* Control and Silenced cells are considered preliminary data, and multiple unstained controls for correct compensation settings must be utilized in future apoptosis assays.

An alternative apoptosis experiment was performed for *PKD2* Control and Silenced cells. The level of apoptosis after serum starvation was compared, with the hypothesis that silenced cells were more sensitive than control cells to apoptosis-inducing conditions.

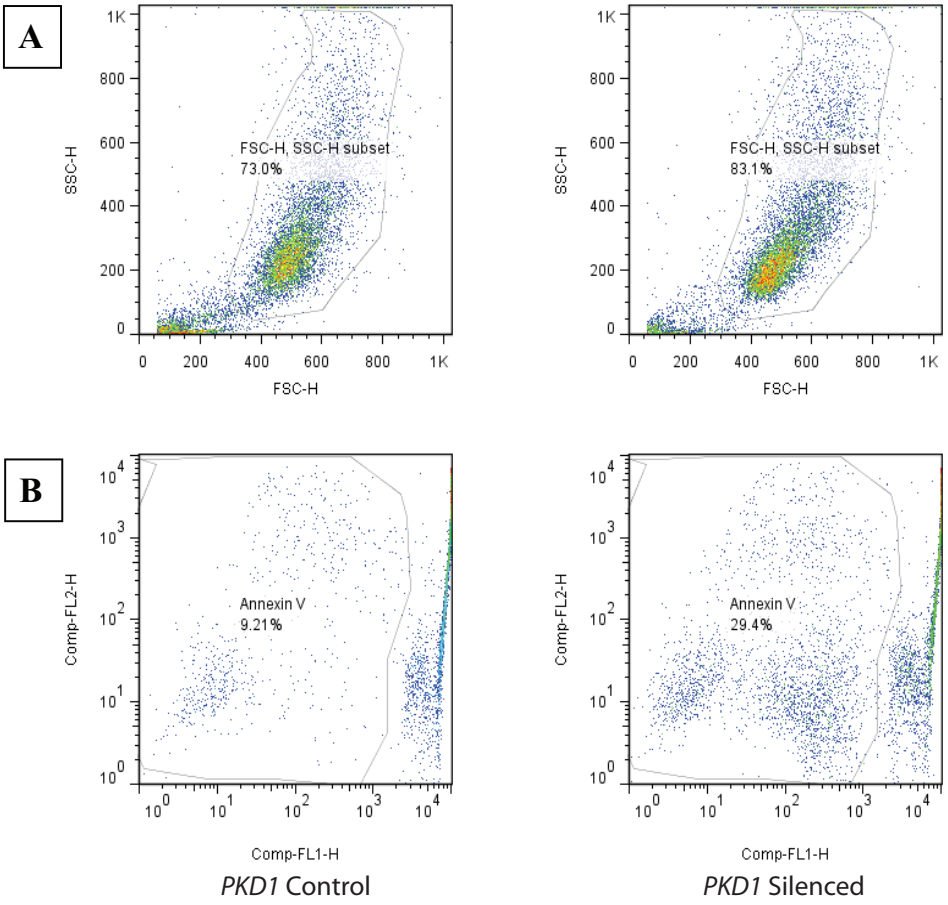

Figure 5.4: Apoptotic Markers in *PKD1* Control and Silenced Cells - (A) FACS gating for single cells. Forward Scatter (FSC) vs Side Scatter (SSC) confirm homogeneity of the sample population in regard to cell size and granularity and was used to exclude cell debris. **(B)** *PKD1* Control and *PKD1* Silenced cells stained with apoptotic marker Annexin V. Annexin V was detected by the FL2 detector. FL2-H was compensated for the spectral overlap with GFP by reducing the influence of FL1. X-axis is the level of GFP detection by FL1, which was subtracted from FL2 until the contribution of FL1 to FL2 was below threshold, thus the remaining FL2 detection correspond to Annexin V-PE detection above influence of FL1. However, unstained and single stain controls, which were not prepared for this assay, are necessary for accurate compensation settings. Preliminary data as shown suggest increase in apoptosis in *PKD1* Silenced condition. Cells were cultured for five days before flow cytometry.

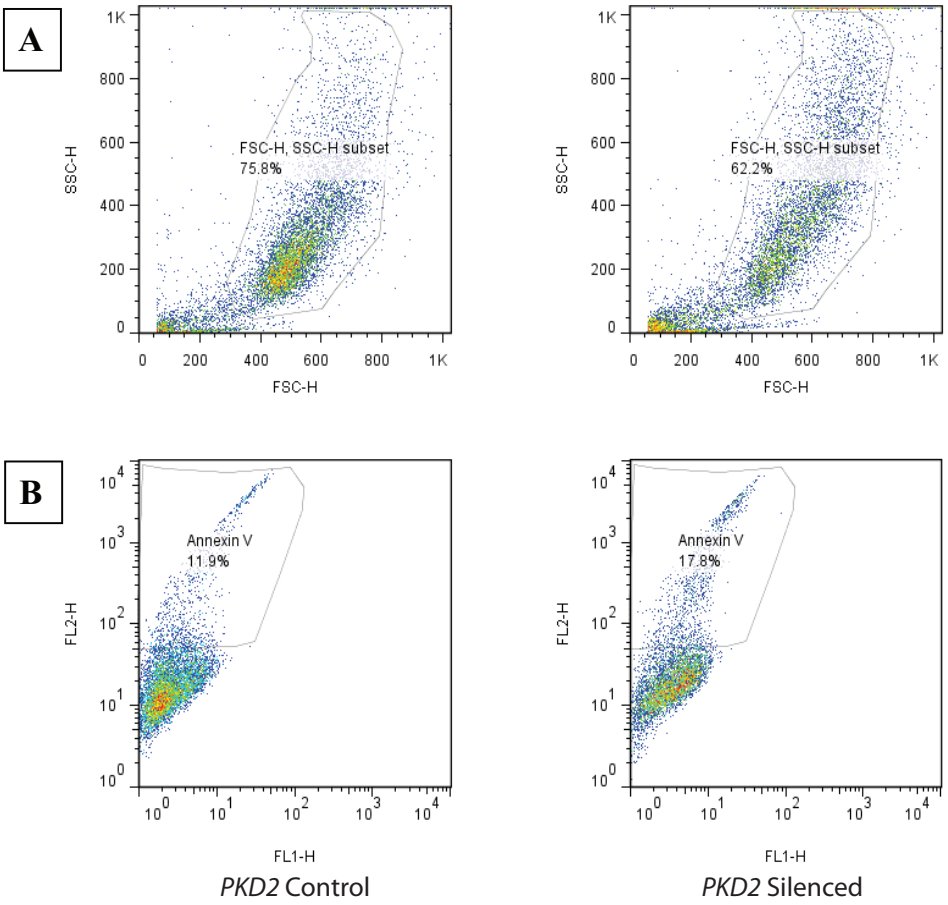

Figure 5.5: Apoptotic Markers in *PKD2* Control and Silenced Cells - **(A)** FACS gating for single cells. Forward Scatter (FSC) vs Side Scatter (SSC) confirm homogeneity of the sample population in regard to cell size and granularity and was used to exclude cell debris. **(B)** *PKD2* Control and *PKD2* Silenced cells stained with apoptotic marker Annexin V. Annexin V was detected by the FL2 detector as shown on Y-axis. No compensation was required, as *PKD2* cells do not express GFP. Apoptotic cells were indicated in the upper left quadrant, as cells were of higher FL2 level for the same FL1 level, which was utilized as a control axis in flow cytometry. Unstained control was not prepared for this assay, but it would be beneficial for determining the basal FL2 detection levels for accurate exclusion of non-apoptotic cells. Preliminary data as shown suggest increase in apoptosis in *PKD2* Silenced condition. Cells were cultured for five days before flow cytometry.

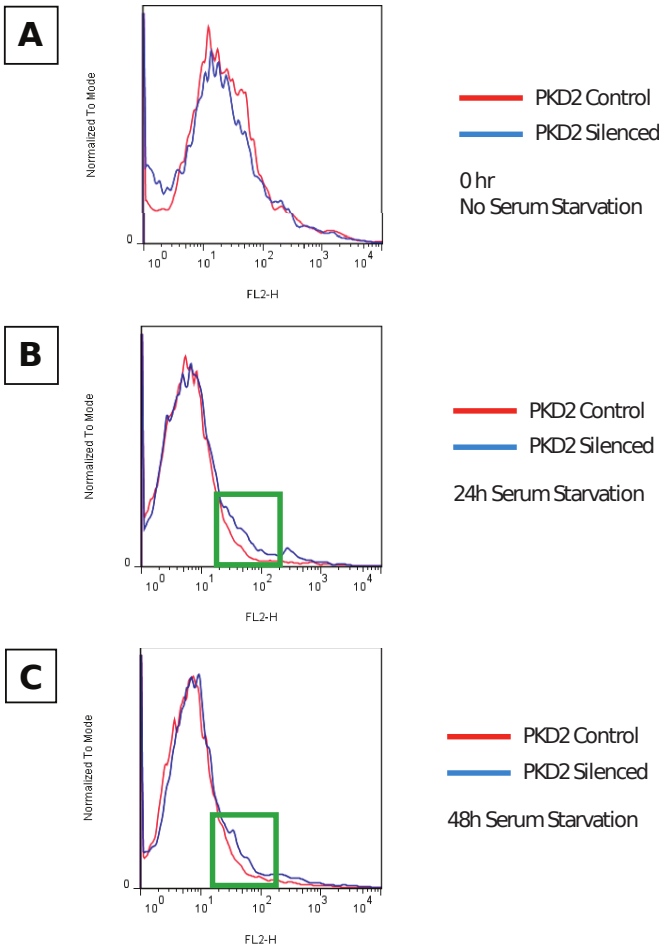

Figure 5.6: Increased Susceptibility to Apoptosis in Silenced Cells - Apoptosis of *PKD2* Control (Red) and Silenced (Blue) over serum starvation durations of **(A)** 0hr, **(B)** 24hr, and **(C)** 48hr. Apoptosis was slightly increased for Silenced cells after 24hr and 48hr serum starvation as measured by the area above background staining as indicated by the Green Box. Cells were cultured for three days before flow cytometry, thus, the 48hr time point corresponds to a change to serum free media on day 1; 24hr serum starvation corresponds to serum free media on day 2; and 0hr corresponds to no media changes for the duration of the experiment. X-axis is maximal level of FL2 detection per cell of phycoerythin conjugated to Annexin V, which corresponds to apoptosis marker. Y-axis is the relative quantity of cells for each FL2-H level. X-axis is on logarithmic scale.

Figure 5.6 shows a slight increase of apoptosis for *PKD2* Silenced cells in comparison to Control cells under serum starving conditions. This is seen as the area under the curve beyond a threshold; the background fluorescence of non-apoptotic cells, which is seen mostly below 10^1 FL2 fluorescence height. Unfortunately, the experiment contained an experimental error. From the time of cell plating, media was not changed for the 0hr (non-serum starvation) time point. For the serum starvation conditions, media was changed between time of cell plating and the switch to serum-free media. Since media was not changed for the 0hr time point, there was a greater quantity of apoptotic cells as a consequence of the damage sustained during cell passaging, rather than media conditions, and these apoptotic cells were reflected in the experiment, which resulted in a higher FL2-H reading. However, it appears that the dead cells were relatively consistent for both Control and Silenced cells, suggesting that there were no differences in apoptosis over short culture periods of three days in growth media. Silenced cells appear to be more susceptible to apoptosis under serum-free conditions, which may suggest a degree of fragility conferred by the loss of polycystin-2. Under full media conditions, apoptosis is seemingly not a major factor for under three days, but apoptosis may be significant over longer culture periods. Thus, the observed lower proliferation for silenced cells, as discussed in previous sections, is likely due to cell cycle abnormalities rather than high rates of apoptosis.

5.3 The Cell Cycle and Aberrant Signal Transduction

We hypothesized that loss of polycystins -1 and -2 are linked to cell cycle aberrations, as the previous sections indicated lower proliferation for silenced cells, but was likely not due to increased apoptosis. The following sections include the cell cycle profile for *PKD2* Control and Silenced cells over a 25 hour time period. Aberrant signal transduction from the extracellular matrix lead to a signaling cascade that affects the cell cycle proteins, which lead to disruption of the cell cycle.

5.3.1 Cell Cycle Analysis

The cell cycle profile (Figure 5.7) indicates the relative amount of cells in particular phases of the cell cycle. *PKD2* Silenced cells show fewer cells in S-phase

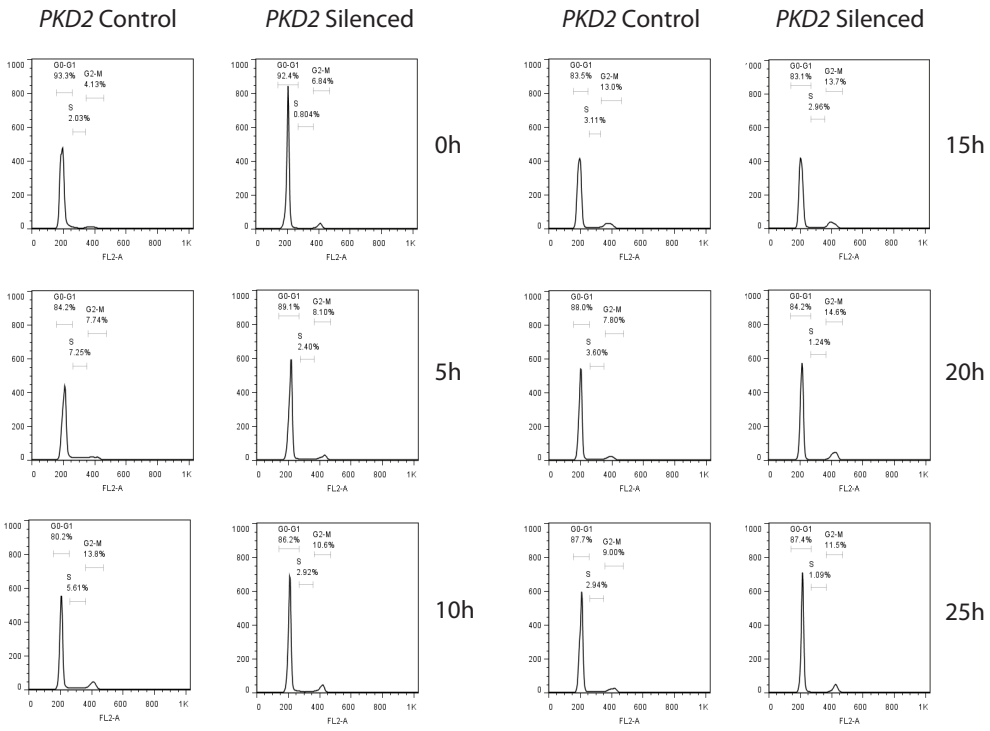

Figure 5.7: Cell Cycle Profile by FACS Analysis for *PKD2* Control and Silenced Cells - **(A)** *PKD2* Control and **(B)** *PKD2* Silenced cells were collected every five hours over a 25 hour time period and stained for propidium iodide, a DNA stain. *PKD2* Silenced cells indicate a cell cycle block at cell cycle checkpoints G1-S and G2-Mitosis phase transitions.

than *PKD2* Control. Silenced cells also show more cells in G1 phase and G2 phase. Taken together, this data suggests that silenced cells were blocked at the G1-S phase transition, moved quickly through S phase, and were blocked again at the G2-Mitosis transition.

Generally, cell cycle transitions are controlled by proteins that sense DNA damage and do not allow progress into S phase or mitosis lest aberrant cell progeny are produced. For example, p53, which is influenced by p21, controls both G1 to S transition and G2 to mitosis (146). Retinoblastoma also delays G1 to S transition by inhibiting the transcription factor E2F, unless there is high expression of cyclin D, which upon forming the cyclin D/cyclin-dependent-kinase complex, deactivates retinoblastoma thus allowing S phase transition (147). As described in background sections, the p21 pathways are also influenced by polycystin-1 and -2 (59, 73). There are several other proteins involved in cell cycle control, but p53 and retinoblastoma are the major players and are also the proteins perturbed in cell immortalization techniques.

5.3.2 Analysis of Cell Cycle Proteins

As the cell cycle is disturbed, it is prudent to also assess the relevant proteins. As was mentioned previously, cyclin D is responsible for forming a complex with its affiliated cyclin-dependent kinase (CDK) in order to inactivate the retinoblastoma suppressor protein. E2F transcription factor then leads to the expression of cyclin E which is also required for the G1-S transition (147).

As shown in Figure 5.8, in *PKD2* Silenced cells, cyclin D expression is increased, which is in agreement with current literature. However, cyclin E expression appears to be the same for both control and silenced cells. This suggests that despite cyclin D overexpression, which likely leads to inactivation of retinoblastoma, there are other factors such as p53 preventing silenced cells from a faster-than-normal transition into S phase. Future experiments detailing the full cell cycle profile of cyclin expression would be very informative, as well as experiments assessing the tumor suppressor proteins.

While the proliferation results we have obtained do not correlate to literature involving cyst-derived cells, it is possible that the low proliferation phenotype is reflective of early cystic events. In our experimental design, our data is collected only after few passages post-knockdown, while ADPKD cyst-derived cells are

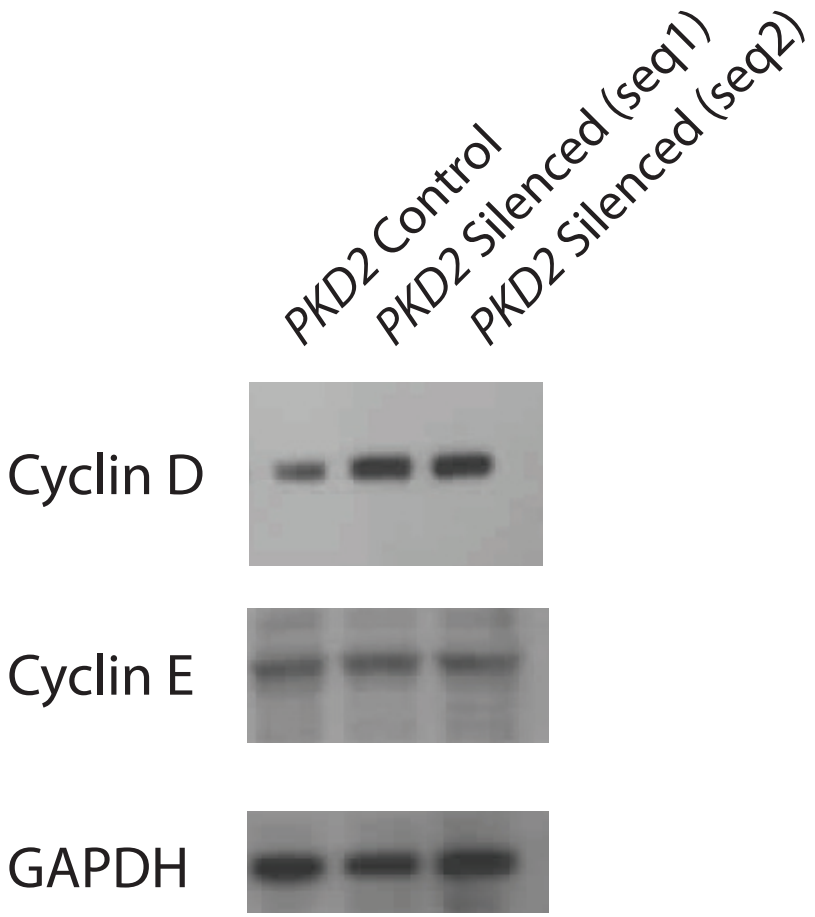

Figure 5.8: Analysis of Cell Cycle Proteins Cyclin D and Cyclin E - Cyclin D and Cyclin E for *PKD2* Control and Silenced cells. Total cell lysates were collected and blotted for Cyclin D, Cyclin E, and GAPDH (loading control). Cyclin D was increased in silenced cells, while there were no noticeable differences for cyclin E.

harvested typically after the many years that a patient has lived before undergoing a transplant and nephrectomy. Thus, it is possible that loss of polycystin leads to chromosomal aberrations which are detected by the cell and the various tumor suppressor genes delay cell cycle transitions. In addition, p53 delay could attribute to the apoptotic phenotype we observed, as normally cells that do not correct DNA errors eventually undergo apoptosis (148). For a future experiment, we could immortalize the silenced cells with the SV40 large T antigen which disrupts the tumor suppressor genes and assess proliferation. If proliferation increased, it would suggest that only after a mutation of p53 and associated proteins does the proliferative phenotype exhibit. It is possible that in human ADPKD, over time, the cyst-lining epithelia have undergone mutations for the tumor suppressor genes. Indeed, aneuploidy is observed in renal biopsies of ADPKD kidneys (139), which is suggestive of a loss of tumor suppressor genes, as cells are allowed to proliferate despite having chromosomal aberrations.

5.3.3 Extracellular Matrix Mediated Effects

It is also important to look at the cell in its extracellular milieu. Polycystin-1 is thought to engage in cell-cell and cell-ECM communication, and pericystic ECM anomalities have been observed in ADPKD (44). In addition, we have previously shown evidence for an extant autocrine loop signaling in *Pkd1* silenced mouse IMCD cells where cells secrete abnormal matrix proteins (collagen IV and laminin) that interact with the integrin receptor subunit protein Integrin-β1. These ECM and integrin-β1 aberrations drive the proliferative and cystic phenotype, and are reversed upon silencing integrin-β1 (*manuscript in review*).

As shown in Figure 5.9, collagen IV and laminin were slightly increased for total cell lysates of *PKD1* and *PKD2* Silenced cells. We also observed that the integrin-β1 receptor is also overexpressed in *PKD2* Silenced cells in comparison to *PKD2* Control. Both ECM ligand and ECM receptor upregulation is in agreement with our previous work with *Pkd1* silenced mouse cells. While only *PKD2* cells were shown for integrin-β1 blot, recall that silencing *PKD2* also led to reduction of PKD1 expression. Integrin-β1 is upstream of proliferation signal transduction pathways including Ras/Raf/MAPK and PI3K/Akt/mTOR (149). It is possible that the proliferative phenotype following loss of polycystins is due to autocrine loop signaling where abnormal matrix secretions drive integrin-β1 mediated pathways. However, in our case of early silencing of HRCE cells,

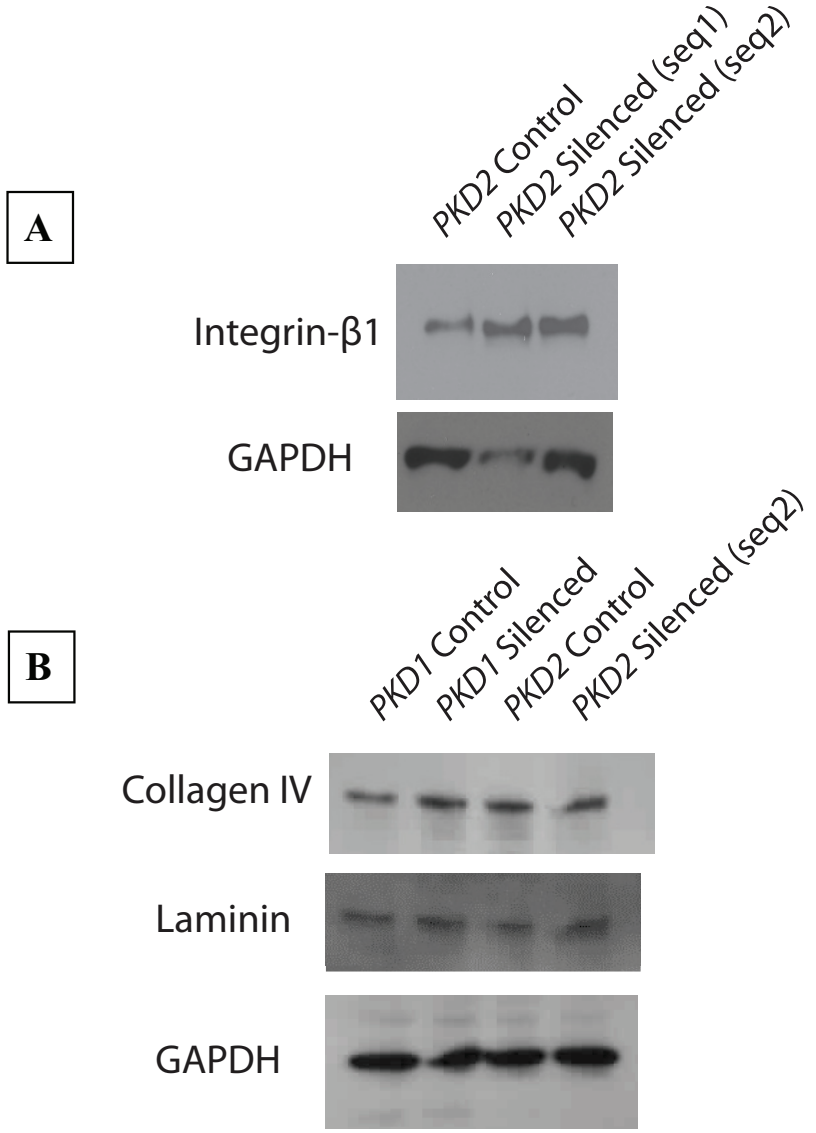

Figure 5.9: Analysis of Abnormal ECM Receptor and ECM Ligands - **(A)** ECM receptor integrin-β1 was increased for *PKD2* Silenced cells. Total cell lysates were collected and blotted for integrin-β1 and GAPDH (loading control). **(B)** Collagen IV and laminin, ECM ligands for integrin-β1 receptor, were slightly increased in *PKD1* and *PKD2* Silenced cells. Total cell lysates were collected and blotted for collagen IV, laminin, and GAPDH (loading control).

perhaps proliferation is checked by other cell cycle regulators, despite the up-regulation of integrin-β1. Future experiments would include integrin-β1 blot for *PKD1* Silenced cells. Additionally, the matrix proteins could also be assessed by immunohistochemistry of 3D tissue constructs.

5.4 Characterizing Cell Lines

As HRCE are a heterogeneous cell population, it is important to characterize the cells with which we work. The use of lectin stains can tell what tubular origin cells are, based on sugar residue expression unique to proximal or distal tubule cells. We also observe how HRCE behave in a 3D gel microenvironment and assess structure by confocal microscopy.

5.4.1 A Heterogeneous Cell Population

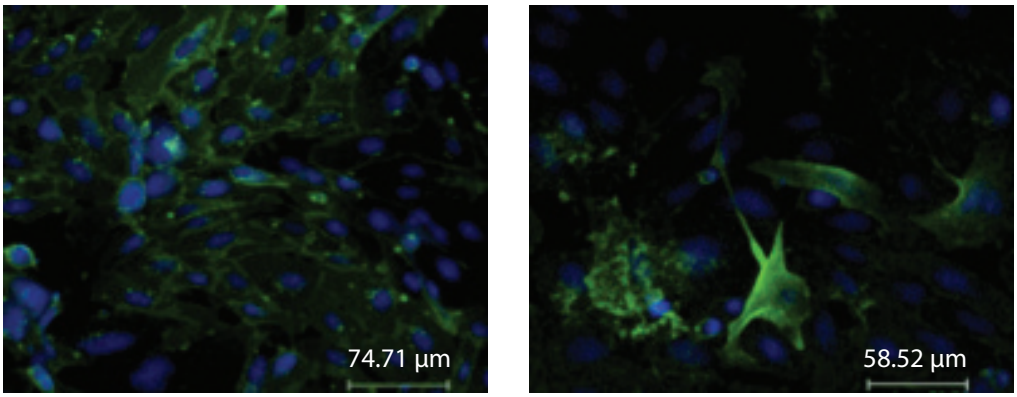

Figure 5.10: Identification of Tubular Origin in HRCE - PHA-E lectin and PNA lectin distinguished proximal tubule and distal tubule origin cells in the heterogeneous HRCE cell population.

Proximal tubule origin cells are identified with more frequency than distal tubule origin (Figure 5.10). This may have implications in cystogenesis *in vitro*, as discussed in background, tubule development begins from the distal end.

5.4.2 Cystogenesis in 3D Microenvironment

As shown in Figure 5.11, HRCE formed cystic structures when cultured in a gel matrix, such as Matrigel and/or collagen type I. Cyst formation was spontaneous

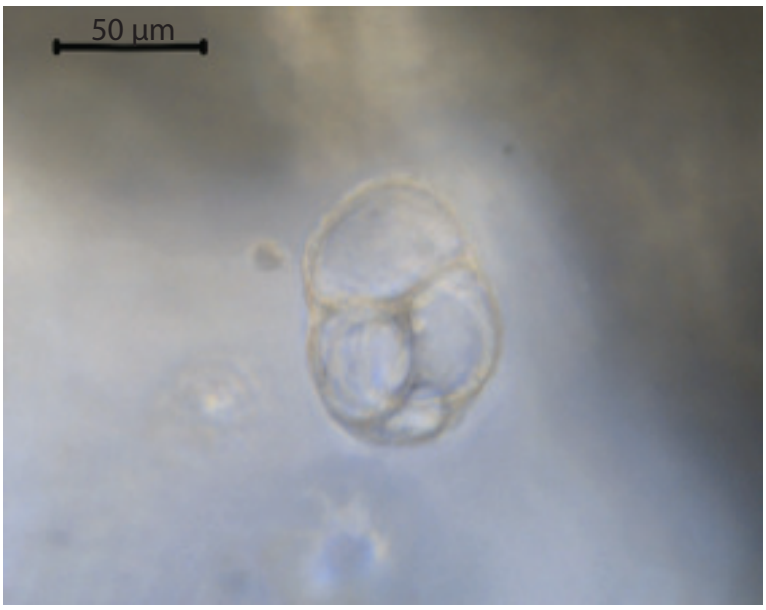

Figure 5.11: Cyst Formation of HRCE in Gel Matrix - HRCE were infused in a mix of collagen I and Matrigel and cultured for five days in growth media. Cyst-like structures formed with lumen development.

with the defined growth media. The cysts probably formed from cells of distal tubule origin, but it would be useful to also confirm with lectin stains as a future experiment.

After fixation, cystic structures were stained with dyes and viewed under confocal laser microscopy, which offers a greater resolution (Figure 5.12). Confocal laser microscopy also allows for a broader range of fluorescent dyes.

The formation of cystic structures is useful for comparison between control and silenced cells, and *in vitro* cysts compared to tissue samples. Nuclear stains may offer insight into the Planar Cell Polarity pathway by observing nuclear orientation (71). Actin may be used to observe polarity differences and cytoskeletal abnormalities (150). Confocal laser microscopy can also image in a stack in the Z direction, which in the case of the HRCE cyst, provides evidence of depth in 3D culture, and that the cyst is not merely on the surface of the gel.

5.5 Tissue Engineered 3D Tissue Constructs of ADPKD

In our efforts to model ADPKD, it is important to generate relevant tissue constructs similar to the *in vivo* condition. To do so, we generated an *in vitro* cyst

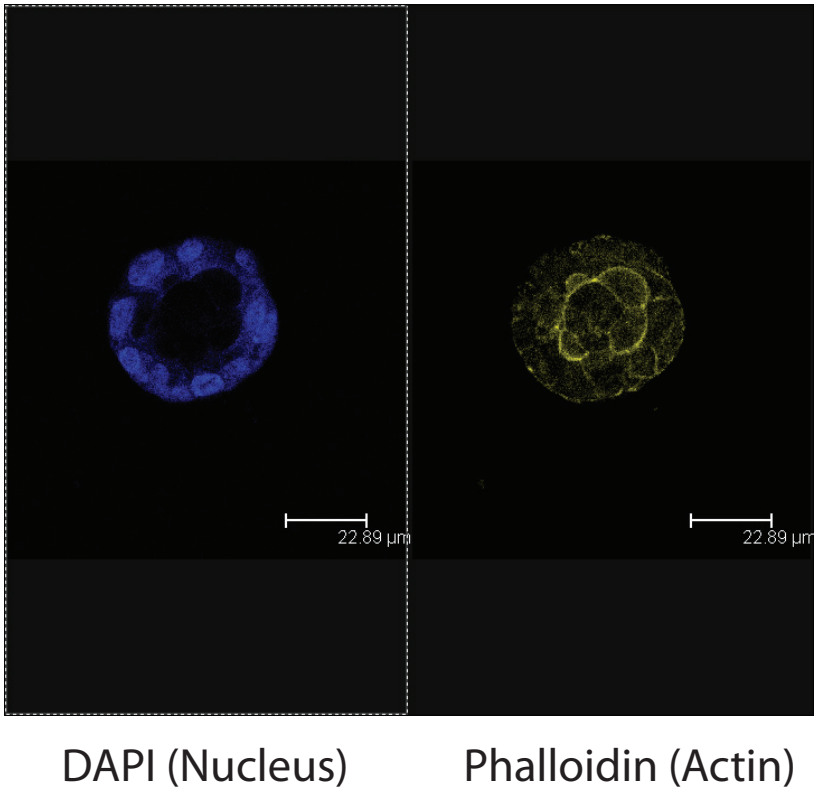

Figure 5.12: Structural Assessment of HRCE Cyst - Confocal image of HRCE cyst with DAPI stain for nucleus and Phalloidin stain for F-actin. Actin is useful for assessing the overall cytoskeletal organization of the construct. There is strong actin polarization towards the lumen. Cells were cultured in collagen and Matrigel for fourteen days, fixed, stained and imaged under confocal microscopy.

representative of an ADPKD cyst by culture of silenced cells in 3D gel and scaffold. For confirmation, structural markers were compared to ADPKD tissue. It is also relevant to assess functional outcomes, such as transport phenomena of tissue engineered constructs in comparison to known ADPKD transport functions.

5.5.1 Short-term Culture in Gel and Scaffold

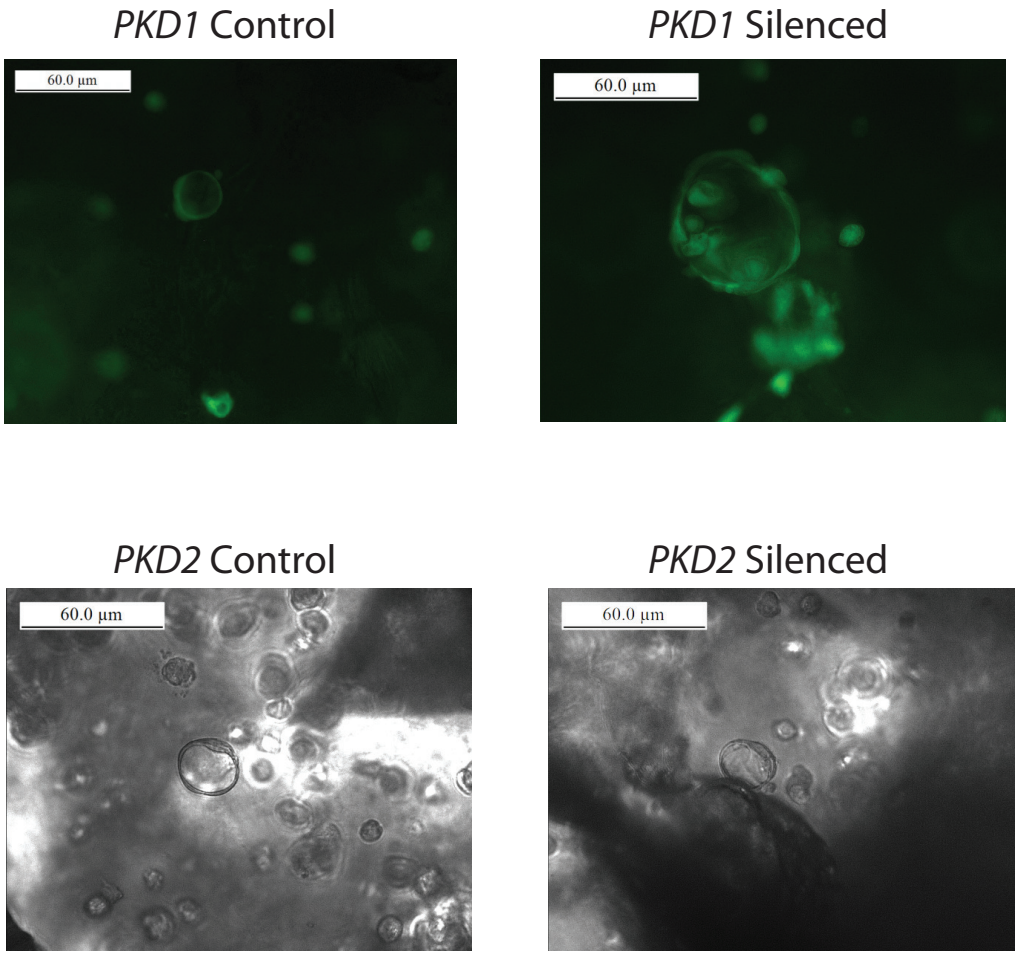

Figure 5.13: Cyst Formation of *PKD1* and *PKD2* Control and Silenced Cells in Gel Matrix - Cystic structures developed at day 5 for *PKD1* and *PKD2* Control and Silenced cells. Human cells displayed heterogeneity in structure formation. Cells were infused in collagen I and Matrigel and seeded to silk scaffold. Cells were cultured in defined growth media supplemented with cyclic AMP.

As shown in Figure 5.13, *PKD1* and *PKD2* Control and Silenced cells were infused in collagen type I and Matrigel, and seeded in silk scaffold. Cells under-

went morphogenesis to form cyst-like structures. Cells have rounded borders and clear lumen formation, although structures were very heterogeneous as HRCE are a heterogeneous cell population. With growth media supplemented with cyclic AMP, improved spherical cyst-like structures formed in collagen gel. However, as was previously shown in MDCK cells, supplementation with hepatocyte growth factor led to branching tubulogenesis instead of the spherical cyst structures (26). Thus by modulating the extracellular matrix and associated growth factors, such as by growth factor supplementation or addition of paracrine secreting cells (e.g. fibroblasts), one can control structure formation. While the role of silk scaffold in this system was to prevent excessive gel contraction, future directions may include using the scaffold to transduce controlled forces to effect growth outcomes. Silk scaffold also supports perfusion bioreactor for long term culture.

5.5.2 Analysis of ADPKD Structural Markers

As shown in previous sections, scaffolds containing tissue engineered constructs can be imaged by confocal laser microscopy. Antibodies to structural markers along with other specific probes can be used on whole scaffolds or scaffold sections mounted on microscope slides. From a technical standpoint, scaffolds are easier to handle; the user can avoid compressing and tearing a gel-only culture of tissue engineered constructs in preparation for paraffin embedding.

Future work is planned for imaging the tissue engineered constructs with antibodies to structural markers such as E-cadherin and N-cadherin. As discussed in the background section; E-cadherin is associated with epithelial tissues and is seen in normal kidney. On the other hand, ADPKD kidneys exhibit a dedifferentiated phenotype and increases expression of mesenchymal-associated N-cadherin. These structural markers are also shown for human ADPKD tissue in Figure 5.14. As was previously demonstrated with tissue engineered mouse model, *PKD1* and *PKD2* Control and Silenced constructs are expected to exhibit similar phenotypes to human normal kidney and ADPKD kidney, respectively.

Other important structural markers may be assessed with the tissue engineered system, such as cilia. As cilia display shortened length in ADPKD kidneys, tissue engineered constructs are also expected to reflect cilia abnormalities. Previously we have demonstrated feasibility to detect primary cilia in MDCK cysts grown in collagen gel (Figure 5.15). Future experiments include assessing primary cilium length for the tissue engineered human kidney constructs and

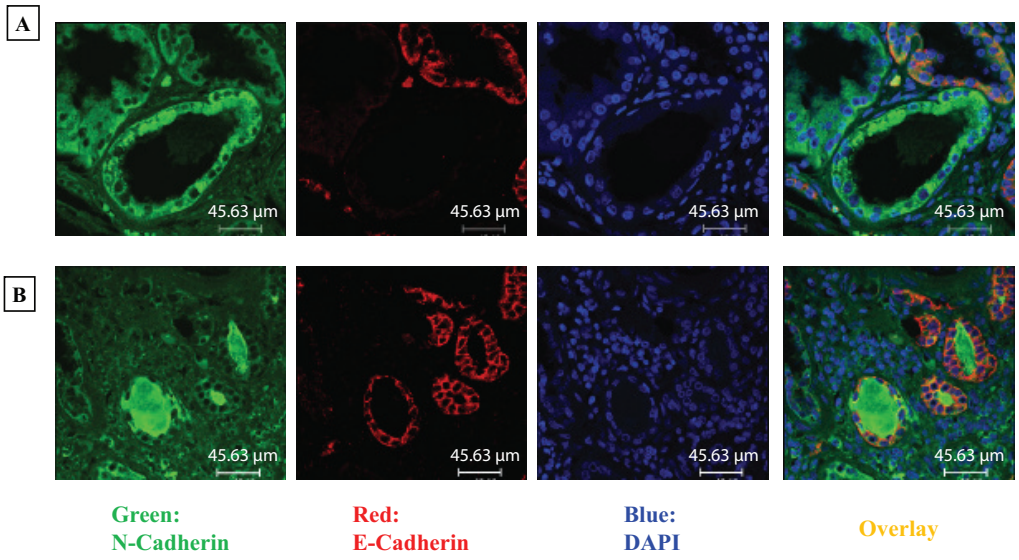

Figure 5.14: Structural Markers in Human ADPKD Tissue - (A) Structural markers for dilated tubule in ADPKD Kidney. N-cadherin expression was upregulated, while E-cadherin expression was downregulated in ADPKD tubule exhibiting cystic dilatation morphology. **(B)** Structural markers for tubules in ADPKD Kidney. Tubules exhibiting normal-like morphology retained high E-cadherin expression and lower N-cadherin expression.

comparing to normal and ADPKD kidneys. However, in addition to assessing cilia length, cilia functionality should also be confirmed in future experiments.

5.5.3 Live Imaging and Functional Assays

Tissue engineered constructs can also be assayed under live culture conditions. Functional assays such as organic anion transport can only be performed when cells are live. As a demonstration, the cell membrane was stained under live cell conditions.

Figure 5.16 demonstrate that cells can be imaged under live conditions with a non-destructive plasma membrane stain. Future experiments include using 6-carboxyfluorescein diacetate succinimidyl ester to assess organic anion transport along with probenecid, an organic anion transport inhibitor. Potentially, we can assess other transporters associated with the kidney tubules in tissue engineered constructs and compare control and silenced conditions along with expected outcomes in normal and ADPKD kidneys.

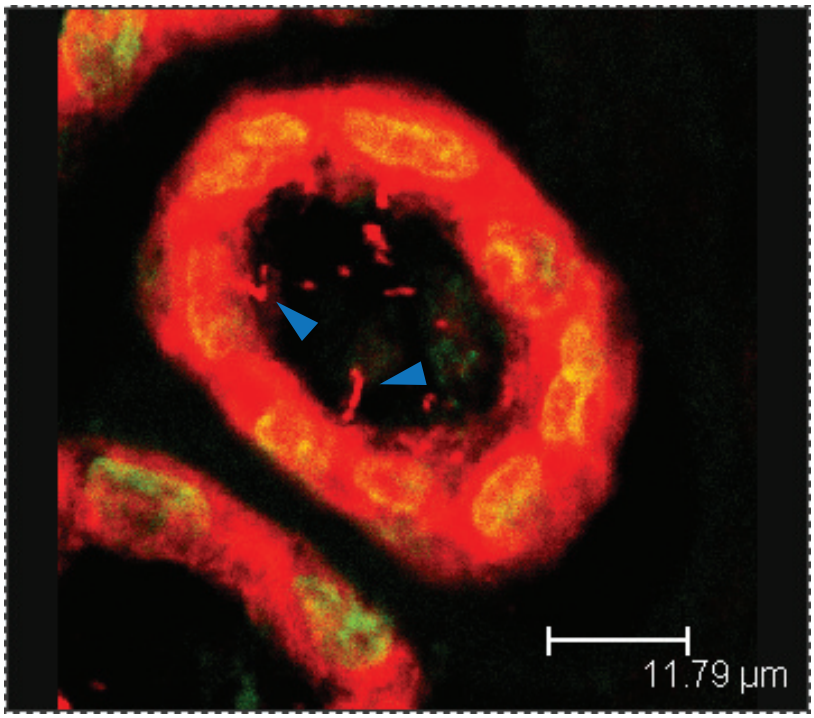

Figure 5.15: Primary Cilia in Tissue Engineered MDCK Cyst - Primary cilia detected in MDCK cyst grown in collagen gel. Cystic structures in human tissue engineered constructs are also expected to express cilia. Tissue Engineered MDCK cysts were sectioned and stained with acetylated α-tubulin.

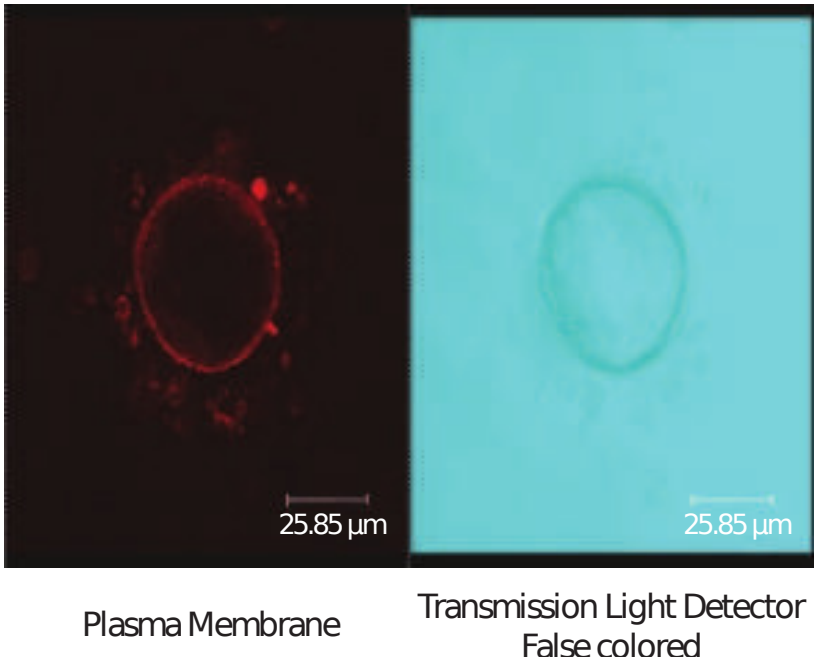

Figure 5.16: Live Imaging of HRCE Cyst - Tissue engineered construct within silk scaffold was stained for the plasma membrane under live cell conditions. Other assays requiring live cells may be applied with the clarity of cell boundaries.

Chapter 6

Conclusions and Future Directions

Tissue engineering principles can enhance many facets of traditional kidney research by surmounting many technical challenges. *In vitro* cell culture began as merely 2d experiments in tissue culture flasks, but engineering has allowed for more advanced studies. Defining the matrix chemically and/or structurally (151) has provided a more realistic extracellular milieu for cell morphogenesis. Advancements in the field of biomaterials have further improved the ability to control the cell microenvironment, such as with mechanical (38) or electrical stimulation (152). In our system, silk plays an important role in controlling the cell microenvironment for cystogenesis. Porous silk sponges hold the collagen and Matrigel mix in place, preventing excessive gel contraction and the associated contractile forces on cyst formation.

Tissue engineering is also scalable. The kidney tissue engineering project we have presented is rudimentary; it requires only the parenchymal cells infused in a gel matrix, supported by a silk fibroin scaffold. But simplicity is not necessarily a drawback; this design allows the user to tightly control competing factors in analysis, as such is often the case *in vivo*. With greater understanding of a simple model system, it becomes feasible to isolate the effects of adding additional layers of complexity to the model system. In the kidney project, we can add paracrine secreting stromal cells, i.e. fibroblasts. Or perhaps future advancements could include vasa recta, glomerulus, or other functional components of the nephron. The tissue engineered kidney system could also integrate with other tissue engineered organ systems such as liver or heart. It becomes viable to isolate systems

for the study of, for example, pharmaceutics and metabolism by kidney and liver; or the endocrine effects of kidney on the cardiovascular system.

By designing systems with a bottom-up approach, one can add capabilities as needed. For example, imaging can be a part of the design constraints, which would necessitate the use of confocal compatible reactor housings. Engineering design allows us to overcome technical challenges, for instance, there are no layers of skin and fat to penetrate as required in imaging *in vivo*, merely optically transparent plastics. Perhaps stretch or compression is required in the study, and these capabilities are easily added to bioreactor design. These are only a few examples of interesting functionalities that can be added to *in vitro* tissue engineered cell culture systems. While tissue engineered systems are not meant to completely supplant *in vivo* studies, they can recapitulate biological processes of interest, and actually work in complement with animal models for better understanding.

We have taken these tissue engineering approaches and applied them to the study of ADPKD. Using standard molecular biology techniques, we silenced the expression of *PKD1* and *PKD2*, the genes of interest in ADPKD. We can see the possible early effects of silencing on proliferation, apoptosis, and the cell cycle. But we can extend our studies with engineering techniques. We have placed cells in a relevant 3D collagen and Matrigel environment and utilized silk to prevent excessive gel contraction. Silk also confers benefits to handling of the gel, allowing for ease of imaging or for long-term bioreactor cultures. We can use these engineered 3D systems for studying morphological effects, or matrix mediated effects, or even pharmaceutical tests. The net result is that we have melded molecular biology techniques with engineering design to overcome technical obstacles in biomedical research.

Our tissue engineered system is not limited only to the study of ADPKD. As ADPKD is one of many genetic diseases in the cystic kidney disease group, the logical extension is to silence relevant genes for other diseases. For example, we could model Autosomal Recessive Polycystic Kidney Disease by silencing *PKHD1*, or Nephronophthisis by silencing *NEK8*. Nor are we limited only to lentivirus mediated DNA manipulation for loss or gain of function. Cutting edge DNA therapies such as triplex forming peptide nucleic acids (PNA) could be delivered by nanoparticles (153) to isolated cystic cells. PNA technology allows

for functional genes to replace faulty genes through site-specific recombination, thus, it would be possible to test gene correction in a model system.

Non-genetic perturbations such as pharmaceutical drugs can also be applied to the kidney tissue system. There are many pharmaceutical agents that have nephrotoxic side effects, such as cisplatin, a chemotherapy agent; gentamicin, an antibiotic against Gram-negative bacteria; and lithium, used in the treatment of unipolar depression. Nephrotoxicity can be assessed with these agents, and the resulting data would provide valuable insight into optimizing therapeutic value while minimizing nephrotoxic side effects.

While tissue engineering offers the prospect of many interesting applications for the study of human pathologies or developmental biology, only towards the end of my graduate study have I begun to appreciate the full potential of tissue engineering: the study of the cell and its place in relation to surrounding layers of extracellular molecules and neighboring cells. In development, the cell is perfectly located in relation to its neighbors such that tissue, organs, and finally the human body is formed. In developmental pathologies, mislocalization of cells is one of many possibilities that disrupt tissue and organ formation. In the study of biomedical sciences, it is of utmost importance to consider the cell and its surroundings; and tissue engineering offers the tools to study the cell and its response to spatial and physicochemical effects.

Were I to start anew, I would focus on scaffold designs to localize individual cells into pre-defined locations. For kidney tissue engineering, this would provide more detail for the mechanism of ureteric bud and metanephric mesenchyme reciprocal induction. Determination of proper spatial characteristics and temporally controlled signaling molecules akin to *in vivo* embryology could offer further insights into correcting renal agenesis in developing embryos when the surgical tools of the future are developed. Perhaps a less ambitious project derived from the understanding of reciprocal induction would be kidney organogenesis. After all, it is reciprocal induction that generates the kidney, beginning from the ureter and ending in the millions of nephrons. Studies of branching morphogenesis could also extend to lung tissue or mammary gland development.

The cell and its response to the scaffold, or the substrate on which the cell lies, is also a very tantalizing subject. After all, mechanical forces have been shown to regulate many cell functions such as gene transcription and translation. Cell and nuclear architecture can also drive cell responses to signaling molecules

(154). For the study of ADPKD, the study of normal cells in an ADPKD extracellular matrix could elucidate further mechanisms of disease pathogenesis. If the response of normal cells in diseased matrix is also dedifferentiation and cystogenesis, then this would suggest a feed-forward loop for ADPKD cyst expansion. This could suggest new avenues for treatment, as instead of combating the altered signaling pathways, it would be wiser to study the surrounding architecture, or the "master switch" for cystogenesis.

For the study of tissue function, combining scaffold design with microfluidic design would offer structurally and functionally relevant tissue constructs. Microfluidic chips would introduce relevant laminar flow through the apical surface through a hollow tube, and cellular transport across apical and basolateral surfaces could be assessed. Microfluidics would offer the ability to study flow and its role in ADPKD cilia dysfunction. Designs could also include delivery of cyclic AMP elevating agents, or antidiuretic hormone which leads to cyclic AMP, as it is relevant to cystogenesis. Kidney tissue microfluidic design is not limited only to ADPKD, but could also be used for diagnostics as previously mentioned. The integration of flow with scaffold-influenced cell architecture would also paint a more complete picture for future work in normal tissue and disease modeling.

To conclude, tissue engineering is not a discipline with constricting limits and delineations. It does not demand that a problem be fit to clearly defined solution matrices. Rather, tissue engineering is a philosophy for approaching biomedical problems. Whether it is a top-down or bottom-up design, tissue engineering is about providing the platforms and sets of tools on which to expand the capabilities of traditional biomedical research. It is about overcoming technical challenges in order to effect changes and assess experimental outcomes. Tissue engineering is a relatively new discipline, but it is brimming with limitless potential. Just as cell culture techniques have evolved from 2D to 3D, tissue engineering has similarly expanded our ability to study the intricacies of basic science by another dimension. Indeed, there is more to come.

References

[1] M E Salem and G Eknoyan. **The kidney in ancient Egyptian medicine: where does it stand?** *Am J Nephrol*, **19**(2):140–7, 1999. 1

[2] G Maio. **The metaphorical and mythical use of the kidney in antiquity**. *Am J Nephrol*, **19**(2):101–6, 1999. 1

[3] Garabed Eknoyan. **The kidneys in the Bible: what happened?** *J Am Soc Nephrol*, **16**(12):3464–71, Dec 2005. 1

[4] G Eknoyan. **The origins of nephrology–Galen, the founding father of experimental renal physiology**. *Am J Nephrol*, **9**(1):66–82, 1989. 1

[5] Melonie Heron, Donna L Hoyert, Sherry L Murphy, Jiaquan Xu, Kenneth D Kochanek, and Betzaida Tejada-Vera. **Deaths: final data for 2006**. *Natl Vital Stat Rep*, **57**(14):1–134, Apr 2009. 3

[6] M Pohl, R O Stuart, H Sakurai, and S K Nigam. **Branching morphogenesis during kidney development**. *Annu Rev Physiol*, **62**:595–620, 2000. 7

[7] E N Liatsikos, P Perimenis, K Dandinis, E Kaladelfou, and G A Barbalias. **Mermaid and Potter's syndrome occurring simultaneously**. *Int Urol Nephrol*, **31**(3):277–81, 1999. 7

[8] D Brown, T Katsura, and C E Gustafson. **Cellular mechanisms of aquaporin trafficking**. *Am J Physiol*, **275**(3 Pt 2):F328–31, Sep 1998. 12

[9] Rinat Abramovitch, Einat Tavor, Jasmine Jacob-Hirsch, Evelyne Zeira, Ninette Amariglio, Orit Pappo, Gideon Rechavi, Eithan Galun, and Alik Honigman. **A pivotal role of cyclic AMP-responsive element binding protein in tumor progression**. *Cancer Res*, **64**(4):1338–46, Feb 2004. 12

[10] Nicolas Dumaz, Robert Hayward, Jan Martin, Lesley Ogilvie, Douglas Hedley, John A Curtin, Boris C Bastian, Caroline Springer, and Richard Marais. **In melanoma, RAS mutations are accompanied by switching signaling from BRAF to CRAF and disrupted cyclic AMP signaling**. *Cancer Res*, **66**(19):9483–91, Oct 2006. 12

[11] M J Stutts, C M Canessa, J C Olsen, M Hamrick, J A Cohn, B C Rossier, and R C Boucher. **CFTR as a cAMP-dependent regulator of sodium channels**. *Science*, **269**(5225):847–50, Aug 1995. 12

[12] L P Sullivan, D P Wallace, and J J Grantham. **Chloride and fluid secretion in polycystic kidney disease**. *J Am Soc Nephrol*, **9**(5):903–16, May 1998. 12

[13] I V Yannas and J F Burke. **Design of an artificial skin. I. Basic design principles**. *J Biomed Mater Res*, **14**(1):65–81, Jan 1980. 12

[14] J F Burke, I V Yannas, W C Quinby, Jr, C C Bondoc, and W K Jung. **Successful use of a physiologically acceptable artificial skin in the treatment of extensive burn injury**. *Ann Surg*, **194**(4):413–28, Oct 1981. 12

[15] L E Niklason, J Gao, W M Abbott, K K Hirschi, S Houser, R Marini, and R Langer. **Functional arteries grown in vitro**. *Science*, **284**(5413):489–93, Apr 1999. 13

[16] Ali Tavakkolizadeh, Urs V Berger, Antonia E Stephen, Byung S Kim, David Mooney, Matthias A Hediger, Stanley W Ashley, Joseph P Vacanti, and Edward E Whang. **Tissue-engineered neomucosa: morphology, enterocyte dynamics, and SGLT1 expression topography**. *Transplantation*, **75**(2):181–5, Jan 2003. 13

[17] Tracy C Grikscheit, Jennifer B Ogilvie, Erin R Ochoa, Eben Alsberg, David Mooney, and Joseph P Vacanti. **Tissue-engineered colon exhibits function in vivo**. *Surgery*, **132**(2):200–4, Aug 2002. 13

[18] Y Cao, J P Vacanti, K T Paige, J Upton, and C A Vacanti. **Transplantation of chondrocytes utilizing a polymer-cell construct to produce tissue-engineered cartilage in the shape of a human ear**. *Plast Reconstr Surg*, **100**(2):297–302; discussion 303–4, Aug 1997. 13

[19] Dongeun Huh, Benjamin D Matthews, Akiko Mammoto, Martín Montoya-Zavala, Hong Yuan Hsin, and Donald E Ingber. **Reconstituting organ-level lung functions on a chip**. *Science*, **328**(5986):1662–8, Jun 2010. 13

[20] Francesco Pampaloni, Emmanuel G Reynaud, and Ernst H K Stelzer. **The third dimension bridges the gap between cell culture and live tissue**. *Nat Rev Mol Cell Biol*, **8**(10):839–45, Oct 2007. 14

[21] Genee Y Lee, Paraic A Kenny, Eva H Lee, and Mina J Bissell. **Three-dimensional culture models of normal and malignant breast epithelial cells**. *Nat Methods*, **4**(4):359–65, Apr 2007. 14

[22] Kenna R Mills Shaw, Carolyn N Wrobel, and Joan S Brugge. **Use of three-dimensional basement membrane cultures to model oncogene-induced changes in mammary epithelial morphogenesis**. *J Mammary Gland Biol Neoplasia*, **9**(4):297–310, Oct 2004. 14

[23] F Wang, V M Weaver, O W Petersen, C A Larabell, S Dedhar, P Briand, R Lupu, and M J Bissell. **Reciprocal interactions between beta1-integrin and epidermal growth factor receptor in three-dimensional basement membrane breast cultures: a different perspective in epithelial biology**. *Proc Natl Acad Sci U S A*, **95**(25):14821–6, Dec 1998. 14

REFERENCES

[24] Matthew J Paszek, Nastaran Zahir, Kandice R Johnson, Johnathon N Lakins, Gabriela I Rozenberg, Amit Gefen, Cynthia A Reinhart-King, Susan S Margulies, Micah Dembo, David Boettiger, Daniel A Hammer, and Valerie M Weaver. **Tensional homeostasis and the malignant phenotype**. *Cancer Cell*, **8**(3):241–54, Sep 2005. 14

[25] Lucy Erin O'Brien, Mirjam M P Zegers, and Keith E Mostov. **Opinion: Building epithelial architecture: insights from three-dimensional culture models**. *Nat Rev Mol Cell Biol*, **3**(7):531–7, Jul 2002. 14

[26] R Montesano, K Matsumoto, T Nakamura, and L Orci. **Identification of a fibroblast-derived epithelial morphogen as hepatocyte growth factor**. *Cell*, **67**(5):901–8, Nov 1991. 14, 75

[27] Claudia C Ceresa, Alan J Knox, and Simon R Johnson. **Use of a three-dimensional cell culture model to study airway smooth muscle-mast cell interactions in airway remodeling**. *Am J Physiol Lung Cell Mol Physiol*, **296**(6):L1059–66, Jun 2009. 14

[28] Kota Watanabe, Masaya Nakamura, Hideyuki Okano, and Yoshiaki Toyama. **Establishment of three-dimensional culture of neural stem/progenitor cells in collagen Type-1 Gel**. *Restor Neurol Neurosci*, **25**(2):109–17, 2007. 14

[29] Shulamit Levenberg, Ngan F Huang, Erin Lavik, Arlin B Rogers, Joseph Itskovitz-Eldor, and Robert Langer. **Differentiation of human embryonic stem cells on three-dimensional polymer scaffolds**. *Proc Natl Acad Sci U S A*, **100**(22):12741–6, Oct 2003. 14

[30] Stephanie M Willerth and Shelly E Sakiyama-Elbert. **Approaches to neural tissue engineering using scaffolds for drug delivery**. *Adv Drug Deliv Rev*, **59**(4-5):325–38, May 2007. 14

[31] Paul Roach, David Eglin, Kirsty Rohde, and Carole C Perry. **Modern biomaterials: a review - bulk properties and implications of surface modifications**. *J Mater Sci Mater Med*, **18**(7):1263–77, Jul 2007. 14

[32] Gregory H Altman, Frank Diaz, Caroline Jakuba, Tara Calabro, Rebecca L Horan, Jingsong Chen, Helen Lu, John Richmond, and David L Kaplan. **Silk-based biomaterials**. *Biomaterials*, **24**(3):401–16, Feb 2003. 14

[33] Yongzhong Wang, Hyeon-Joo Kim, Gordana Vunjak-Novakovic, and David L Kaplan. **Stem cell-based tissue engineering with silk biomaterials**. *Biomaterials*, **27**(36):6064–82, Dec 2006. 14

[34] Jingsong Chen, Gregory H Altman, Vassilis Karageorgiou, Rebecca Horan, Adam Collette, Vladimir Volloch, Tara Colabro, and David L Kaplan. **Human bone marrow stromal cell and ligament fibroblast responses on RGD-modified silk fibers**. *J Biomed Mater Res A*, **67**(2):559–70, Nov 2003. 15

[35] Dongeun Huh, Geraldine A Hamilton, and Donald E Ingber. **From 3D cell culture to organs-on-chips**. *Trends Cell Biol*, **21**(12):745–54, Dec 2011. 15

[36] S Takayama, E Ostuni, P LeDuc, K Naruse, D E Ingber, and G M Whitesides. **Subcellular positioning of small molecules**. *Nature*, **411**(6841):1016, Jun 2001. 15

[37] Jamil El-Ali, Peter K Sorger, and Klavs F Jensen. **Cells on chips**. *Nature*, **442**(7101):403–11, Jul 2006. 15

[38] T D Brown. **Techniques for mechanical stimulation of cells in vitro: a review**. *J Biomech*, **33**(1):3–14, Jan 2000. 15, 81

[39] Ivan Martin, David Wendt, and Michael Heberer. **The role of bioreactors in tissue engineering**. *Trends Biotechnol*, **22**(2):80–6, Feb 2004. 15

[40] W H Fissell, J Kimball, S M MacKay, A Funke, and H D Humes. **The role of a bioengineered artificial kidney in renal failure**. *Ann N Y Acad Sci*, **944**:284–95, Nov 2001. 15

[41] H David Humes, William H Fissell, William F Weitzel, Deborah A Buffington, Angela J Westover, Sherrill M MacKay, and Jorge M Gutierrez. **Metabolic replacement of kidney function in uremic animals with a bioartificial kidney containing human cells**. *Am J Kidney Dis*, **39**(5):1078–87, May 2002. 16

[42] Kyung-Jin Jang and Kahp-Yang Suh. **A multi-layer microfluidic device for efficient culture and analysis of renal tubular cells**. *Lab Chip*, **10**(1):36–42, Jan 2010. 16

[43] Kyung-Jin Jang, Hye Sung Cho, Do Hyun Kang, Won Gyu Bae, Tae-Hwan Kwon, and Kahp-Yang Suh. **Fluid-shear-stress-induced translocation of aquaporin-2 and reorganization of actin cytoskeleton in renal tubular epithelial cells**. *Integr Biol (Camb)*, **3**(2):134–41, Feb 2011. 16

[44] Peter Igarashi and Stefan Somlo. **Genetics and pathogenesis of polycystic kidney disease**. *J Am Soc Nephrol*, **13**(9):2384–98, Sep 2002. 17, 70

[45] G G Germino, D Weinstat-Saslow, H Himmelbauer, G A Gillespie, S Somlo, B Wirth, N Barton, K L Harris, A M Frischauf, and S T Reeders. **The gene for autosomal dominant polycystic kidney disease lies in a 750-kb CpG-rich region**. *Genomics*, **13**(1):144–51, May 1992. 18

[46] M C Schneider, A M Rodriguez, H Nomura, J Zhou, C C Morton, S T Reeders, and S Weremowicz. **A gene similar to PKD1 maps to chromosome 4q22: a candidate gene for PKD2**. *Genomics*, **38**(1):1–4, Nov 1996. 18

[47] J Milutinovic, P F Rust, P J Fialkow, L Y Agodoa, L A Phillips, T G Rudd, and S Sutherland. **Intrafamilial phenotypic expression of autosomal dominant polycystic kidney disease**. *Am J Kidney Dis*, **19**(5):465–72, May 1992. 18

[48] S Rossetti, L Strmecki, V Gamble, S Burton, V Sneddon, B Peral, S Roy, A Bakkaloglu, R Komel, C G Winearls, and P C Harris. **Mutation analysis of the entire PKD1 gene: genetic and diagnostic implications**. *Am J Hum Genet*, **68**(1):46–63, Jan 2001. 19, 26

[49] C C Deltas. **Mutations of the human polycystic kidney disease 2 (PKD2) gene**. *Hum Mutat*, **18**(1):13–24, 2001. 19

[50] F Qian, T J Watnick, L F Onuchic, and G G Germino. **The molecular basis of focal cyst formation in human autosomal dominant polycystic kidney disease type I**. *Cell*, **87**(6):979–87, Dec 1996. 19

[51] M Koptides, R Mean, K Demetriou, A Pierides, and C C Deltas. **Genetic evidence for a trans-heterozygous model for cystogenesis in autosomal dominant polycystic kidney disease**. *Hum Mol Genet*, **9**(3):447–52, Feb 2000. 19, 25

[52] T Watnick, N He, K Wang, Y Liang, P Parfrey, D Hefferton, P St George-Hyslop, G Germino, and Y Pei. **Mutations of PKD1 in ADPKD2 cysts suggest a pathogenic effect of trans-heterozygous mutations**. *Nat Genet*, **25**(2):143–4, Jun 2000. 19, 25

[53] J Hughes, C J Ward, B Peral, R Aspinwall, K Clark, J L San Millán, V Gamble, and P C Harris. **The polycystic kidney disease 1 (PKD1) gene encodes a novel protein with multiple cell recognition domains**. *Nat Genet*, **10**(2):151–60, Jun 1995. 19, 21

[54] O Ibraghimov-Beskrovnaya, N O Bukanov, L C Donohue, W R Dackowski, K W Klinger, and G M Landes. **Strong homophilic interactions of the Ig-like domains of polycystin-1, the protein product of an autosomal dominant polycystic kidney disease gene, PKD1**. *Hum Mol Genet*, **9**(11):1641–9, Jul 2000. 19

[55] T Mochizuki, G Wu, T Hayashi, S L Xenophontos, B Veldhuisen, J J Saris, D M Reynolds, Y Cai, P A Gabow, A Pierides, W J Kimberling, M H Breuning, C C Deltas, D J Peters, and S Somlo. **PKD2, a gene for polycystic kidney disease that encodes an integral membrane protein**. *Science*, **272**(5266):1339–42, May 1996. 19

[56] K Hanaoka, F Qian, A Boletta, A K Bhunia, K Piontek, L Tsiokas, V P Sukhatme, W B Guggino, and G G Germino. **Co-assembly of polycystin-1 and -2 produces unique cation-permeable currents**. *Nature*, **408**(6815):990–4, 2000. 19

[57] F Qian, F J Germino, Y Cai, X Zhang, S Somlo, and G G Germino. **PKD1 interacts with PKD2 through a probable coiled-coil domain**. *Nat Genet*, **16**(2):179–83, Jun 1997. 19, 25, 59

[58] Feng Qian, Alessandra Boletta, Anil K Bhunia, Hangxue Xu, Lijuan Liu, Ali K Ahrabi, Terry J Watnick, Fang Zhou, and Gregory G Germino. **Cleavage of polycystin-1 requires the receptor for egg jelly domain and is disrupted by human autosomal-dominant polycystic kidney disease 1-associated mutations**. *Proc Natl Acad Sci U S A*, **99**(26):16981–6, Dec 2002. 19

[59] Anil Kumar Bhunia, Klaus Piontek, Alessandra Boletta, Lijuan Liu, Feng Qian, Pei Ning Xu, F Joseph Germino, and Gregory G Germino. **PKD1 induces p21(waf1) and regulation of the cell cycle via direct activation of the JAK-STAT signaling pathway in a process requiring PKD2**. *Cell*, **109**(2):157–68, Apr 2002. 19, 21, 68

[60] Veronique Chauvet, Xin Tian, Herve Husson, David H Grimm, Tong Wang, Thomas Hiesberger, Thomas Hieseberger, Peter Igarashi, Anton M Bennett, Oxana Ibraghimov-Beskrovnaya, Stefan Somlo, and Michael J Caplan. **Mechanical stimuli induce cleavage and nuclear translocation of the polycystin-1 C terminus**. *J Clin Invest*, **114**(10):1433–43, Nov 2004. 19

[61] Seng Hui Low, Shivakumar Vasanth, Claire H Larson, Sambuddho Mukherjee, Nikunj Sharma, Michael T Kinter, Michelle E Kane, Tomoko Obara, and Thomas Weimbs. **Polycystin-1, STAT6, and P100 function in a pathway that transduces ciliary mechanosensation and is activated in polycystic kidney disease**. *Dev Cell*, **10**(1):57–69, Jan 2006. 19, 20

[62] Claudia A Bertuccio, Hannah C Chapin, Yiqiang Cai, Kavita Mistry, Veronique Chauvet, Stefan Somlo, and Michael J Caplan. **Polycystin-1 C-terminal cleavage is modulated by polycystin-2 expression**. *J Biol Chem*, **284**(31):21011–26, Jul 2009. 20

[63] Gregory J Pazour, Jovenal T San Agustin, John A Follit, Joel L Rosenbaum, and George B Witman. **Polycystin-2 localizes to kidney cilia and the ciliary level is elevated in orpk mice with polycystic kidney disease**. *Curr Biol*, **12**(11):R378–80, Jun 2002. 20

[64] Bradley K Yoder, Xiaoying Hou, and Lisa M Guay-Woodford. **The polycystic kidney disease proteins, polycystin-1, polycystin-2, polaris, and cystin, are co-localized in renal cilia**. *J Am Soc Nephrol*, **13**(10):2508–16, Oct 2002. 20

[65] H A Praetorius and K R Spring. **Bending the MDCK cell primary cilium increases intracellular calcium**. *J Membr Biol*, **184**(1):71–9, Nov 2001. 20

[66] P F Davies. **Flow-mediated endothelial mechanotransduction**. *Physiol Rev*, **75**(3):519–60, Jul 1995. 21

[67] Surya M Nauli, Francis J Alenghat, Ying Luo, Eric Williams, Peter Vassilev, Xiaogang Li, Andrew E H Elia, Weining Lu, Edward M Brown, Stephen J Quinn, Donald E Ingber, and Jing Zhou. **Polycystins 1 and 2 mediate mechanosensation in the primary cilium of kidney cells**. *Nat Genet*, **33**(2):129–37, Feb 2003. 21

[68] Jing Zhou. **Polycystins and primary cilia: primers for cell cycle progression**. *Annu Rev Physiol*, **71**:83–113, 2009. 21

[69] Hannah C Chapin and Michael J Caplan. **The cell biology of polycystic kidney disease**. *J Cell Biol*, **191**(4):701–10, Nov 2010. 21

[70] Mark Lal, Xuewen Song, Jennifer L Pluznick, Valeria Di Giovanni, David M Merrick, Norman D Rosenblum, Veronique Chauvet, Cara J Gottardi, York Pei, and Michael J Caplan. **Polycystin-1 C-terminal tail associates with beta-catenin and inhibits canonical Wnt signaling**. *Hum Mol Genet*, **17**(20):3105–17, Oct 2008. 21

[71] Evelyne Fischer, Emilie Legue, Antonia Doyen, Faridabano Nato, Jean-François Nicolas, Vicente Torres, Moshe Yaniv, and Marco Pontoglio. **Defective planar cell polarity in polycystic kidney disease**. *Nat Genet*, **38**(1):21–3, Jan 2006. 21, 73

REFERENCES

[72] Matias Simons, Joachim Gloy, Athina Ganner, Axel Bullerkotte, Mikhail Bashkurov, Corinna Krönig, Bernhard Schermer, Thomas Benzing, Olga A Cabello, Andreas Jenny, Marek Mlodzik, Bozena Polok, Wolfgang Driever, Tomoko Obara, and Gerd Walz. **Inversin, the gene product mutated in nephronophthisis type II, functions as a molecular switch between Wnt signaling pathways**. *Nat Genet*, **37**(5):537–43, May 2005. 21

[73] Xiaogang Li, Ying Luo, Patrick G Starremans, Coleen A McNamara, York Pei, and Jing Zhou. **Polycystin-1 and polycystin-2 regulate the cell cycle through the helix-loop-helix inhibitor Id2**. *Nat Cell Biol*, **7**(12):1202–12, Dec 2005. 21, 68

[74] M Kondo, E Cubillo, K Tobiume, T Shirakihara, N Fukuda, H Suzuki, K Shimizu, K Takehara, A Cano, M Saitoh, and K Miyazono. **A role for Id in the regulation of TGF-beta-induced epithelial-mesenchymal transdifferentiation**. *Cell Death Differ*, **11**(10):1092–101, Oct 2004. 21

[75] Tamara Roitbak, Christopher J Ward, Peter C Harris, Robert Bacallao, Scott A Ness, and Angela Wandinger-Ness. **A polycystin-1 multiprotein complex is disrupted in polycystic kidney disease cells**. *Mol Biol Cell*, **15**(3):1334–46, Mar 2004. 21

[76] Stephen C Parnell, Brenda S Magenheimer, Robin L Maser, Christopher A Zien, Anna-Maria Frischauf, and James P Calvet. **Polycystin-1 activation of c-Jun N-terminal kinase and AP-1 is mediated by heterotrimeric G proteins**. *J Biol Chem*, **277**(22):19566–72, May 2002. 21

[77] U Weber, N Paricio, and M Mlodzik. **Jun mediates Frizzled-induced R3/R4 cell fate distinction and planar polarity determination in the Drosophila eye**. *Development*, **127**(16):3619–29, Aug 2000. 21

[78] E Martin-Blanco, J C Pastor-Pareja, and A Garcia-Bellido. **JNK and decapentaplegic signaling control adhesiveness and cytoskeleton dynamics during thorax closure in Drosophila**. *Proc Natl Acad Sci U S A*, **97**(14):7888–93, Jul 2000. 21

[79] E Kleymenova, O Ibraghimov-Beskrovnaya, H Kugoh, J Everitt, H Xu, K Kiguchi, G Landes, P Harris, and C Walker. **Tuberin-dependent membrane localization of polycystin-1: a functional link between polycystic kidney disease and the TSC2 tumor suppressor gene**. *Mol Cell*, **7**(4):823–32, Apr 2001. 22

[80] Ken Inoki, Yong Li, Tianquan Zhu, Jun Wu, and Kun-Liang Guan. **TSC2 is phosphorylated and inhibited by Akt and suppresses mTOR signalling**. *Nat Cell Biol*, **4**(9):648–57, Sep 2002. 22

[81] Jonathan M Shillingford, Noel S Murcia, Claire H Larson, Seng Hui Low, Ryan Hedgepeth, Nicole Brown, Chris A Flask, Andrew C Novick, David A Goldfarb, Albrecht Kramer-Zucker, Gerd Walz, Klaus B Piontek, Gregory G Germino, and Thomas Weimbs. **The mTOR pathway is regulated by polycystin-1, and its inhibition reverses renal cystogenesis in polycystic kidney disease**. *Proc Natl Acad Sci U S A*, **103**(14):5466–71, Apr 2006. 22, 27, 30

[82] J J Grantham, J L Geiser, and A P Evan. **Cyst formation and growth in autosomal dominant polycystic kidney disease**. *Kidney Int*, **31**(5):1145–52, May 1987. 22

[83] T Nadasdy, Z Laszik, G Lajoie, K E Blick, D E Wheeler, and F G Silva. **Proliferative activity of cyst epithelium in human renal cystic diseases**. *J Am Soc Nephrol*, **5**(7):1462–8, Jan 1995. 22

[84] Ayumi Takakura, Leah Contrino, Alexander W Beck, and Jing Zhou. **Pkd1 inactivation induced in adulthood produces focal cystic disease**. *J Am Soc Nephrol*, **19**(12):2351–63, Dec 2008. 22

[85] Irma S Lantinga-van Leeuwen, Wouter N Leonhard, Annemieke van der Wal, Martijn H Breuning, Emile de Heer, and Dorien J M Peters. **Kidney-specific inactivation of the Pkd1 gene induces rapid cyst formation in developing kidneys and a slow onset of disease in adult mice**. *Hum Mol Genet*, **16**(24):3188–96, Dec 2007. 22

[86] T Yamaguchi, J C Pelling, N T Ramaswamy, J W Eppler, D P Wallace, S Nagao, L A Rome, L P Sullivan, and J J Grantham. **cAMP stimulates the in vitro proliferation of renal cyst epithelial cells by activating the extracellular signal-regulated kinase pathway**. *Kidney Int*, **57**(4):1460–71, Apr 2000. 23

[87] K Hanaoka and W B Guggino. **cAMP regulates cell proliferation and cyst formation in autosomal polycystic kidney disease cells**. *J Am Soc Nephrol*, **11**(7):1179–87, Jul 2000. 23, 29, 61

[88] K Hanaoka, O Devuyst, E M Schwiebert, P D Wilson, and W B Guggino. **A role for CFTR in human autosomal dominant polycystic kidney disease**. *Am J Physiol*, **270**(1 Pt 1):C389–99, Jan 1996. 23, 30

[89] Vicente E Torres, Lise Bankir, and Jared J Grantham. **A case for water in the treatment of polycystic kidney disease**. *Clin J Am Soc Nephrol*, **4**(6):1140–50, Jun 2009. 23

[90] Dominique Joly, Viviane Morel, Aurélie Hummel, Antonella Ruello, Patrick Nusbaum, Natacha Patey, Laure-Hélène Noël, Patricia Rousselle, and Bertrand Knebelmann. **Beta4 integrin and laminin 5 are aberrantly expressed in polycystic kidney disease: role in increased cell adhesion and migration**. *Am J Pathol*, **163**(5):1791–800, Nov 2003. 23

[91] Dominique Joly, Sophie Berissi, Amélie Bertrand, Laetitia Strehl, Natacha Patey, and Bertrand Knebelmann. **Laminin 5 regulates polycystic kidney cell proliferation and cyst formation**. *J Biol Chem*, **281**(39):29181–9, Sep 2006. 24

[92] Steve Mangos, Pui-ying Lam, Angela Zhao, Yan Liu, Sudha Mudumana, Aleksandr Vasilyev, Aiping Liu, and Iain A Drummond. **The ADPKD genes pkd1a/b and pkd2 regulate extracellular matrix formation**. *Dis Model Mech*, **3**(5-6):354–65, 2010. 24

[93] F G Giancotti and E Ruoslahti. **Integrin signaling**. *Science*, **285**(5430):1028–32, Aug 1999. 24

[94] N Hateboer, M A v Dijk, N Bogdanova, E Coto, A K Saggar-Malik, J L San Millan, R Torra, M Breuning, and D Ravine. **Comparison of phenotypes of polycystic kidney disease types 1 and 2. European PKD1-PKD2 Study Group**. *Lancet*, **353**(9147):103–7, Jan 1999. 24

[95] Jared J Grantham, Sumanth Mulamalla, and Katherine I Swenson-Fields. **Why kidneys fail in autosomal dominant polycystic kidney disease.** *Nat Rev Nephrol*, **7**(10):556–566, Oct 2011. 24

[96] Peter C Harris, Kyongtae T Bae, Sandro Rossetti, Vicente E Torres, Jared J Grantham, Arlene B Chapman, Lisa M Guay-Woodford, Bernard F King, Louis H Wetzel, Deborah A Baumgarten, Philip J Kenney, Mark Consugar, Saulo Klahr, William M Bennett, Catherine M Meyers, Qin Jean Zhang, Paul A Thompson, Fang Zhu, and J. Philip Miller. **Cyst number but not the rate of cystic growth is associated with the mutated gene in autosomal dominant polycystic kidney disease.** *J Am Soc Nephrol*, **17**(11):3013–3019, Nov 2006. 24, 25

[97] Arlene B Chapman, Lisa M Guay-Woodford, Jared J Grantham, Vicente E Torres, Kyongtae T Bae, Deborah A Baumgarten, Philip J Kenney, Bernard F King, James F Glockner, Louis H Wetzel, Marijn E Brummer, W. Charles O'Neill, Michelle L Robbin, William M Bennett, Saulo Klahr, Gladys H Hirschman, Paul L Kimmel, Paul A Thompson, J. Philip Miller, and Consortium for Radiologic Imaging Studies of Polycystic Kidney Disease cohort. **Renal structure in early autosomal-dominant polycystic kidney disease (ADPKD): The Consortium for Radiologic Imaging Studies of Polycystic Kidney Disease (CRISP) cohort.** *Kidney Int*, **64**(3):1035–1045, Sep 2003. 24

[98] Jared J Grantham, Vicente E Torres, Arlene B Chapman, Lisa M Guay-Woodford, Kyongtae T Bae, Bernard F King, Louis H Wetzel, Deborah A Baumgarten, Phillip J Kenney, Peter C Harris, Saulo Klahr, William M Bennett, Gladys N Hirschman, Catherine M Meyers, Xiaoling Zhang, Fang Zhu, John P Miller, and C. R. I. S. P. Investigators. **Volume progression in polycystic kidney disease.** *N Engl J Med*, **354**(20):2122–2130, May 2006. 24

[99] J. J. Grantham, L. T. Cook, V. E. Torres, J. E. Bost, A. B. Chapman, P. C. Harris, L. M. Guay-Woodford, and K. T. Bae. **Determinants of renal volume in autosomal-dominant polycystic kidney disease.** *Kidney Int*, **73**(1):108–116, Jan 2008. 24, 25

[100] Sandro Rossetti, Vickie J Kubly, Mark B Consugar, Katharina Hopp, Sushmita Roy, Sharon W Horsley, Dominique Chauveau, Lesley Rees, T Martin Barratt, William G van't Hoff, Patrick Niaudet, W Patrick Niaudet, Vicente E Torres, and Peter C Harris. **Incompletely penetrant PKD1 alleles suggest a role for gene dosage in cyst initiation in polycystic kidney disease**. *Kidney Int*, **75**(8):848–55, Apr 2009. 25

[101] T. J. Watnick, V. E. Torres, M. A. Gandolph, F. Qian, L. F. Onuchic, K. W. Klinger, G. Landes, and G. G. Germino. **Somatic mutation in individual liver cysts supports a two-hit model of cystogenesis in autosomal dominant polycystic kidney disease.** *Mol Cell*, **2**(2):247–251, Aug 1998. 25

[102] G. Wu, V. D'Agati, Y. Cai, G. Markowitz, J. H. Park, D. M. Reynolds, Y. Maeda, T. C. Le, H. Hou, R. Kucherlapati, W. Edelmann, and S. Somlo. **Somatic inactivation of Pkd2 results in polycystic kidney disease.** *Cell*, **93**(2):177–188, Apr 1998. 25

[103] Guanqing Wu, Xin Tian, Sayoko Nishimura, Glen S Markowitz, Vivette D'Agati, Jong Hoon Park, Lili Yao, Li Li, Lin Geng, Hongyu Zhao, Winfried Edelmann, and Stefan Somlo. **Trans-heterozygous Pkd1 and Pkd2 mutations modify expression of polycystic kidney disease.** *Hum Mol Genet*, **11**(16):1845–1854, Aug 2002. 26

[104] Sandro Rossetti, Sarah Burton, Lana Strmecki, Gregory R. Pond, Joe L. San Milln, Klaus Zerres, T Martin Barratt, Seza Ozen, Vicente E. Torres, Erik J. Bergstralh, Christopher G. Winearls, and Peter C. Harris. **The position of the polycystic kidney disease 1 (PKD1) gene mutation correlates with the severity of renal disease.** *J Am Soc Nephrol*, **13**(5):1230–1237, May 2002. 26, 27

[105] Sandro Rossetti, Dominique Chauveau, Vickie Kubly, Jeffrey M. Slezak, Anand K. Saggar-Malik, York Pei, Albert C M. Ong, Fiona Stewart, Michael L. Watson, Erik J. Bergstralh, Christopher G. Winearls, Vicente E. Torres, and Peter C. Harris. **Association of mutation position in polycystic kidney disease 1 (PKD1) gene and development of a vascular phenotype.** *Lancet*, **361**(9376):2196–2201, Jun 2003. 26

[106] T. Watnick, B. Phakdeekitcharoen, A. Johnson, M. Gandolph, M. Wang, G. Briefel, K. W. Klinger, W. Kimberling, P. Gabow, and G. G. Germino. **Mutation detection of PKD1 identifies a novel mutation common to three families with aneurysms and/or very-early-onset disease.** *Am J Hum Genet*, **65**(6):1561–1571, Dec 1999. 26

[107] D. A. O'Sullivan, V. E. Torres, P. A. Gabow, S. N. Thibodeau, B. F. King, and E. J. Bergstralh. **Cystic fibrosis and the phenotypic expression of autosomal dominant polycystic kidney disease.** *Am J Kidney Dis*, **32**(6):976–983, Dec 1998. 27

[108] Fangming Lin, Thomas Hiesberger, Kimberly Cordes, Angus M Sinclair, Lawrence S B Goldstein, Stefan Somlo, and Peter Igarashi. **Kidney-specific inactivation of the KIF3A subunit of kinesin-II inhibits renal ciliogenesis and produces polycystic kidney disease.** *Proc Natl Acad Sci U S A*, **100**(9):5286–5291, Apr 2003. 27

[109] Mira Kyttl, Jonna Tallila, Riitta Salonen, Outi Kopra, Nicolai Kohlschmidt, Paulina Paavola-Sakki, Leena Peltonen, and Marjo Kestil. **MKS1, encoding a component of the flagellar apparatus basal body proteome, is mutated in Meckel syndrome.** *Nat Genet*, **38**(2):155–157, Feb 2006. 27

[110] Ursula M Smith, Mark Consugar, Louise J Tee, Brandy M McKee, Esther N Maina, Shelly Whelan, Neil V Morgan, Erin Goranson, Paul Gissen, Stacie Lilliquist, Irene A Aligianis, Christopher J Ward, Shanaz Pasha, Rachaneekorn Punyashthiti,

REFERENCES

Saghira Malik Sharif, Philip A Batman, Christopher P Bennett, C. Geoffrey Woods, Carole McKeown, Martine Bucourt, Caroline A Miller, Phillip Cox, Lihadh Algazali, Richard C Trembath, Vicente E Torres, Tania Attie-Bitach, Deirdre A Kelly, Eamonn R Maher, Vincent H Gattone, Peter C Harris, and Colin A Johnson. **The transmembrane protein meckelin (MKS3) is mutated in Meckel-Gruber syndrome and the wpk rat.** *Nat Genet*, **38**(2):191–196, Feb 2006. 27

[111] M. Tieder, M. Levy, M. C. Gubler, M. F. Gagnadoux, and M. Broyer. **Renal abnormalities in the Bardet-Biedl syndrome.** *Int J Pediatr Nephrol*, **3**(3):199–203, Sep 1982. 27

[112] **PKD Foundation Autosomal Dominant Polycystic Kidney Disease: Mutation Database [online]**, 2012. 27

[113] Sandro Rossetti, Mark B Consugar, Arlene B Chapman, Vicente E Torres, Lisa M Guay-Woodford, Jared J Grantham, William M Bennett, Catherine M Meyers, Denise L Walker, Kyongtae Bae, Qin Jean Zhang, Paul A Thompson, J. Philip Miller, Peter C Harris, and C. R. I. S. P. Consortium. **Comprehensive molecular diagnostics in autosomal dominant polycystic kidney disease.** *J Am Soc Nephrol*, **18**(7):2143–2160, Jul 2007. 27

[114] **Critical Path Institute - Polycystic Kidney Disease Outcomes Consortium**, 2012. 27

[115] Arlene B Chapman, Vicente E Torres, Ronald D Perrone, Theodore I Steinman, Kyongtae T Bae, J. Philip Miller, Dana C Miskulin, Frederic Rahbari Oskoui, Amirali Masoumi, Marie C Hogan, Franz T Winklhofer, William Braun, Paul A Thompson, Catherine M Meyers, Cass Kelleher, and Robert W Schrier. **The HALT polycystic kidney disease trials: design and implementation.** *Clin J Am Soc Nephrol*, **5**(1):102–109, Jan 2010. 27

[116] Vicente E Torres, Arlene B Chapman, Ronald D Perrone, K. Ty Bae, Kaleab Z Abebe, James E Bost, Dana C Miskulin, Theodore I Steinman, William E Braun, Franz T Winklhofer, Marie C Hogan, Frederic R Oskoui, Cass Kelleher, Amirali Masoumi, James Glockner, Neil J Halin, Diego R Martin, Erick Remer, Nayana Patel, Ivan Pedrosa, Louis H Wetzel, Paul A Thompson, J. Philip Miller, Catherine M Meyers, and Robert W Schrier. **Analysis of baseline parameters in the HALT polycystic kidney disease trials.** *Kidney Int*, **81**(6):577–585, Mar 2012. 28

[117] Ronald D Perrone, Kaleab Z Abebe, Robert W Schrier, Arlene B Chapman, Vicente E Torres, James Bost, Diana Kaya, Dana C Miskulin, Theodore I Steinman, William Braun, Franz T Winklhofer, Marie C Hogan, Frederic Rahbari-Oskoui, Cass Kelleher, Amirali Masoumi, James Glockner, Neil J Halin, Diego Martin, Erick Remer, Nayana Patel, Ivan Pedrosa, Louis H Wetzel, Paul A Thompson, J. Philip Miller, K. Ty Bae, H. A. L. T. PKD Study Group, and Catherine M Meyers. **Cardiac magnetic resonance assessment of left ventricular mass in autosomal dominant polycystic kidney disease.** *Clin J Am Soc Nephrol*, **6**(10):2508–2515, Oct 2011. 28

[118] R. D. Perrone, R. Ruthazer, and N. C. Terrin. **Survival after end-stage renal disease in autosomal dominant polycystic kidney disease: contribution of extrarenal complications to mortality.** *Am J Kidney Dis*, **38**(4):777–784, Oct 2001. 28

[119] Ping Xie, Qihua Xiong, Ying Fang, Quan Qing, and Charles M Lieber. **Local electrical potential detection of DNA by nanowire-nanopore sensors.** *Nat Nanotechnol*, **7**(2):119–125, Feb 2012. 28

[120] Jonathan M Rothberg, Wolfgang Hinz, Todd M Rearick, Jonathan Schultz, William Mileski, Mel Davey, John H Leamon, Kim Johnson, Mark J Milgrew, Matthew Edwards, Jeremy Hoon, Jan F Simons, David Marran, Jason W Myers, John F Davidson, Annika Branting, John R Nobile, Bernard P Puc, David Light, Travis A Clark, Martin Huber, Jeffrey T Branciforte, Isaac B Stoner, Simon E Cawley, Michael Lyons, Yutao Fu, Nils Homer, Marina Sedova, Xin Miao, Brian Reed, Jeffrey Sabina, Erika Feierstein, Michelle Schorn, Mohammad Alanjary, Eileen Dimalanta, Devin Dressman, Rachel Kasinskas, Tanya Sokolsky, Jacqueline A Fidanza, Eugeni Namsaraev, Kevin J McKernan, Alan Williams, G. Thomas Roth, and James Bustillo. **An integrated semiconductor device enabling non-optical genome sequencing.** *Nature*, **475**(7356):348–352, Jul 2011. 28

[121] Lisa M Guay-Woodford. **Murine models of polycystic kidney disease: molecular and therapeutic insights**. *Am J Physiol Renal Physiol*, **285**(6):F1034–49, Dec 2003. 28, 29

[122] Cathy Cogswell, Sarah J Price, Xiaoying Hou, Lisa M Guay-Woodford, Lorraine Flaherty, and Elizabeth C Bryda. **Positional cloning of jcpk/bpk locus of the mouse**. *Mamm Genome*, **14**(4):242–9, Apr 2003. 28

[123] L Flaherty, E C Bryda, D Collins, U Rudofsky, and J C Montogomery. **New mouse model for polycystic kidney disease with both recessive and dominant gene effects**. *Kidney Int*, **47**(2):552–8, Feb 1995. 28

[124] A Atala, M R Freeman, J Mandell, and D R Beier. **Juvenile cystic kidneys (jck): a new mouse mutation which causes polycystic kidneys**. *Kidney Int*, **43**(5):1081–5, May 1993. 29

[125] Shanming Liu, Weining Lu, Tomoko Obara, Shiei Kuida, Jennifer Lehoczky, Ken Dewar, Iain A Drummond, and David R Beier. **A defect in a novel Nek-family kinase causes cystic kidney disease in the mouse and in zebrafish**. *Development*, **129**(24):5839–46, Dec 2002. 29

[126] Edgar A Otto, Melissa L Trapp, Ulla T Schultheiss, Juliana Helou, Lynne M Quarmby, and Friedhelm Hildebrandt. **NEK8 mutations affect ciliary and centrosomal localization and may cause nephronophthisis**. *J Am Soc Nephrol*, **19**(3):587–92, Mar 2008. 29

[127] Eisei Sohara, Ying Luo, Jingjing Zhang, Danielle K Manning, David R Beier, and Jing Zhou. **Nek8 regulates the expression and localization of polycystin-1 and polycystin-2**. *J Am Soc Nephrol*, **19**(3):469–76, Mar 2008. 29

[128] S Nagao, T Watanabe, N Ogiso, T Marunouchi, and H Takahashi. **Genetic mapping of the polycystic kidney gene, pcy, on mouse chromosome 9**. *Biochem Genet*, **33**(11-12):401–12, Dec 1995. 29

[129] H Omran, K Häffner, S Burth, C Fernandez, B Fargier, A Villaquiran, H G Nothwang, S Schnittger, H Lehrach, D Woo, M Brandis, R Sudbrak, and F Hildebrandt. **Human adolescent nephronophthisis: gene locus synteny with polycystic kidney disease in pcy mice**. *J Am Soc Nephrol*, **12**(1):107–13, Jan 2001. 29

[130] P G Starremans, X Li, P E Finnerty, L Guo, A Takakura, E G Neilson, and J Zhou. **A mouse model for polycystic kidney disease through a somatic in-frame deletion in the 5' end of Pkd1**. *Kidney Int*, **73**(12):1394–405, Jun 2008. 29

[131] A Boletta, F Qian, L F Onuchic, A K Bhunia, B Phakdeekitcharoen, K Hanaoka, W Guggino, L Monaco, and G G Germino. **Polycystin-1, the gene product of PKD1, induces resistance to apoptosis and spontaneous tubulogenesis in MDCK cells**. *Mol Cell*, **6**(5):1267–73, Nov 2000. 29

[132] Surya M Nauli, Sandro Rossetti, Robert J Kolb, Francis J Alenghat, Mark B Consugar, Peter C Harris, Donald E Ingber, Mahmoud Loghman-Adham, and Jing Zhou. **Loss of polycystin-1 in human cyst-lining epithelia leads to ciliary dysfunction**. *J Am Soc Nephrol*, **17**(4):1015–25, Apr 2006. 29

[133] Balajikarthick Subramanian, Darya Rudym, Chris Cannizzaro, Ronald Perrone, Jing Zhou, and David L Kaplan. **Tissue-engineered three-dimensional in vitro models for normal and diseased kidney**. *Tissue Eng Part A*, **16**(9):2821–31, Sep 2010. 29, 49, 50, 62

[134] Andreas L Serra, Diane Poster, Andreas D Kistler, Fabienne Krauer, Shagun Raina, James Young, Katharina M Rentsch, Katharina S Spanaus, Oliver Senn, Paulus Kristanto, Hans Scheffel, Dominik Weishaupt, and Rudolf P Wüthrich. **Sirolimus and kidney growth in autosomal dominant polycystic kidney disease**. *N Engl J Med*, **363**(9):820–9, Aug 2010. 30

[135] Vincent H Gattone, 2nd, Xiaofang Wang, Peter C Harris, and Vicente E Torres. **Inhibition of renal cystic disease development and progression by a vasopressin V2 receptor antagonist**. *Nat Med*, **9**(10):1323–6, Oct 2003. 30

[136] Baoxue Yang, Nitin D Sonawane, Dan Zhao, Stefan Somlo, and A S Verkman. **Small-molecule CFTR inhibitors slow cyst growth in polycystic kidney disease**. *J Am Soc Nephrol*, **19**(7):1300–10, Jul 2008. 30

[137] Shizuko Nagao, Kazuhiro Nishii, Makoto Katsuyama, Hiroki Kurahashi, Tohru Marunouchi, Hisahide Takahashi, and Darren P Wallace. **Increased water intake decreases progression of polycystic kidney disease in the PCK rat**. *J Am Soc Nephrol*, **17**(8):2220–7, Aug 2006. 30

[138] Nikolay O Bukanov, Laurie A Smith, Katherine W Klinger, Steven R Ledbetter, and Oxana Ibraghimov-Beskrovnaya. **Long-lasting arrest of murine polycystic kidney disease with CDK inhibitor roscovitine**. *Nature*, **444**(7121):949–52, Dec 2006. 30

[139] Lorenzo Battini, Salvador Macip, Elena Fedorova, Steven Dikman, Stefan Somlo, Cristina Montagna, and G Luca Gusella. **Loss of polycystin-1 causes centrosome amplification and genomic instability**. *Hum Mol Genet*, **17**(18):2819–33, Sep 2008. 33, 70

[140] Douglas A Rubinson, Christopher P Dillon, Adam V Kwiatkowski, Claudia Sievers, Lili Yang, Johnny Kopinja, Dina L Rooney, Mingdi Zhang, Melanie M Ihrig, Michael T McManus, Frank B Gertler, Martin L Scott, and Luk Van Parijs. **A lentivirus-based system to functionally silence genes in primary mammalian cells, stem cells and transgenic mice by RNA interference**. *Nat Genet*, **33**(3):401–6, Mar 2003. 33

[141] T Dull, R Zufferey, M Kelly, R J Mandel, M Nguyen, D Trono, and L Naldini. **A third-generation lentivirus vector with a conditional packaging system**. *J Virol*, **72**(11):8463–71, Nov 1998. 40

[142] L Tsiokas, E Kim, T Arnould, V P Sukhatme, and G Walz. **Homo- and heterodimeric interactions between the gene products of PKD1 and PKD2**. *Proc Natl Acad Sci U S A*, **94**(13):6965–70, Jun 1997. 59

[143] Lorenzo Battini, Elena Fedorova, Salvador Macip, Xiaohong Li, Patricia D Wilson, and G Luca Gusella. **Stable knockdown of polycystin-1 confers integrin-alpha2beta1-mediated anoikis resistance**. *J Am Soc Nephrol*, **17**(11):3049–58, Nov 2006. 62

[144] G Koopman, C P Reutelingsperger, G A Kuijten, R M Keehnen, S T Pals, and M H van Oers. **Annexin V for flow cytometric detection of phosphatidylserine expression on B cells undergoing apoptosis**. *Blood*, **84**(5):1415–20, Sep 1994. 62

[145] I Vermes, C Haanen, H Steffens-Nakken, and C Reutelingsperger. **A novel assay for apoptosis. Flow cytometric detection of phosphatidylserine expression on early apoptotic cells using fluorescein labelled Annexin V**. *J Immunol Methods*, **184**(1):39–51, Jul 1995. 62

[146] M L Agarwal, A Agarwal, W R Taylor, and G R Stark. **p53 controls both the G2/M and the G1 cell cycle checkpoints and mediates reversible growth arrest in human fibroblasts**. *Proc Natl Acad Sci U S A*, **92**(18):8493–7, Aug 1995. 68

[147] J R Nevins. **E2F: a link between the Rb tumor suppressor protein and viral oncoproteins**. *Science*, **258**(5081):424–9, Oct 1992. 68

[148] Charles J Sherr. **Principles of tumor suppression**. *Cell*, **116**(2):235–46, Jan 2004. 70

[149] M Reyes-Reyes, N Mora, A Zentella, and C Rosales. **Phosphatidylinositol 3-kinase mediates integrin-dependent NF-kappaB and MAPK activation through separate signaling pathways**. *J Cell Sci*, **114**(Pt 8):1579–89, Apr 2001. 70

[150] Melina Silberberg, Audra J Charron, Robert Bacallao, and Angela Wandinger-Ness. **Mispolarization of desmosomal proteins and altered intercellular adhesion in autosomal dominant polycystic kidney disease**. *Am J Physiol Renal Physiol*, **288**(6):F1153–63, Jun 2005. 73

[151] Laura Perin, Stefano Da Sacco, and Roger E De Filippo. **Regenerative medicine of the kidney**. *Adv Drug Deliv Rev*, **63**(4-5):379–87, Apr 2011. 81

[152] Hoi Ting H Au, Irene Cheng, Mohammad F Chowdhury, and Milica Radisic. **Interactive effects of surface topography and pulsatile electrical field stimulation on orientation and elongation of fibroblasts and cardiomyocytes**. *Biomaterials*, **28**(29):4277–93, Oct 2007. 81

[153] Nicole A McNeer, Joanna Y Chin, Erica B Schleifman, Rachel J Fields, Peter M Glazer, and W Mark Saltzman. **Nanoparticles deliver triplex-forming PNAs for site-specific genomic recombination in CD34+ human hematopoietic progenitors**. *Mol Ther*, **19**(1):172–80, Jan 2011. 82

[154] D E Ingber. **The riddle of morphogenesis: a question of solution chemistry or molecular cell engineering?** *Cell*, **75**(7):1249–52, Dec 1993. 84